AN IMPROVED PERTURBATION AND OBSERVATION MAXIMUM POWER POINT TRACKING ALGORITHM FOR PV PANELS

Liu Xuejun

A Thesis

In

The Department

Of

Electrical and Computer Engineering

Presented in Partial Fulfillment of the Requirements
For the Degree of Master of Applied Science at
Concordia University
Montréal, Québec, Canada

June 2004

Your file Votre référence
ISBN: 0-612-94705-X
Our file Notre référence
ISBN: 0-612-94705-X

ABSTRACT

AN IMPROVED PERTURBATION AND OBSERVATION MAXIMUM POWER POINT TRACKING ALGORITHM FOR PV PANELS

Liu Xuejun

Photovoltaic (PV) energy presents great potential for applications in distributed power systems. However, it still presents a low energy conversion rate even at the Maximum Power Point (MPP). For instance, the maximum efficiency for crystalline silicon cell technology is around 18%. The rest of the incident solar energy either becomes heat or is reflected back to the atmosphere. The actual average efficiency can be even lower if the operating point is allowed to drift according to uncontrolled load and atmospheric conditions variations. In order to maximize the energy conversion, power electronics converters controlled with Maximum Power Point Tracking (MPPT) algorithms that consider the nonlinear output characteristics of PV panels should be used.

Various MPPT algorithms have been proposed in the literature. Despite some drawbacks, Perturbation and Observation (P&O) MPPT algorithms are widely used in PV generating systems because of the ease of implementation and capability to compensate for variations in the solar irradiation level and temperature.

This thesis proposes a different implementation of a P&O MPPT algorithm that can mitigate/reduce the main drawbacks commonly related to the P&O method. This is achieved with Peak Current Control and Instantaneous Sampling methods. The operating principles of the proposed control scheme are discussed. Experimental results for a dc-dc converter controlled with a DSP system are presented to validate the analysis and verify the performance of the proposed control scheme. They are carried out with both a Solar Array Simulator (SAS) and a real PV panel.

ACKNOWLEDGMENTS

The author would like to express his sincere gratitude to his supervisor, Dr. Luiz A. C. Lopes for his invaluable guidance, advice, friendship and financial support throughout the course of this study.

The author would also like to thank his colleagues in the P. D. Ziogas Power Electronics Laboratory. A lot of technical support is from Mr. Joseph Woods. Smart suggestions from and helpful discussions with Zhixiang Luo, Huili Sun, Su Chen, and Neil D'Souza are unforgettable.

The author would also like to thank Stephen, and his mechanics, for providing access to the 13th floor of the Hall building of the Concordia University to conduct experiment of the MPPT system with real solar panels.

Last but not least, the author is very grateful towards his family whose constant support made it possible to finish the project.

To my wife and daughter

TABLE OF CONTENTS

LIST OF FIGURES

LIST OF TABLES

LIST OF ACRONYMS

A/D	Analog to Digital
CCS	Controlled Current Source
CS	Current Sensor
CVS	Controlled Voltage Source
DSP	Digital Signal Processing
IncCond	Incremental Conductance
MPP	Maximum Power Point
MPPT	Maximum Power Point Tracking
PC	Power Circuit
PCC	Peak Current Control
PI	Proportional and Integrated
P&O	Perturbation and Observation
PPC	PowerPC processor
PV	Photovoltaic
PWM	Pulse Width Modulation
RC	Resistor and Capacitor
SAS	Solar Array Simulator

LIST OF PRINCIPAL SYMBOLS

ΔE The marginal error;

τ The time constant of system;

ω_n The natural angle frequency;

ζ The damping ratio;

A The p-n junction ideality factor;

di/dv The incremental panels conductance;

D The duty ratio of the MPPT converter;

D_{max} The maximum duty ratio;

D_{min} The minimum duty ratio;

E_G The band-gap energy of the semiconductor;

f_{SW} The switching frequency;

I/V The instantaneous panels conductance;

i_{error} The error between I_{ref} and i_{PV};

I_j The current though the nonlinear impedance of p-n junction;

i_L The inductor current;

I_{MPP} The PV output current at the MPP;

I_{off} The current at switching off point;

I_{on} The current at switching on point;

I_{ph} PV cell photocurrent;

i_{PV} The PV panels output instantaneous current;

i_{PV_sense} The sensed value of PV panels output instantaneous current;

I_{PV} The PV panels output DC current;

$I_{PV}(k)$ The current sampling at the present cycle;

$I_{PV}(K)$ The present current sampling and holding block;

I_{ref} The current reference;

I_{ripple} The maximum current ripple;

I_{rr} The reverse saturation current at T_r;

I_{rs} The PV cell reverse saturation current;

I_{SC} The short-circuit current of PV panels;

I_{scr} The PV cell short-circuit current at reference temperature and irradiation;

I_{step} The perturbation current step size;

i_{VS} The current though CVS;

k Boltzmann's constant, which is 1.38×10^{-23}(eV/K);

k_j The short-circuit current temperature coefficient;

L The inductor of the MPPT converter;

m_{off} Off-state current slope;

m_{on} On-state current slope;

m_r The slope of compensation ramp;

n_p The number of PV modules connected in parallel;

n_s The number of PV cells connected in series;

P_{MPP} The PV output power at the MPP;

p_{PV} PV panels output instantaneous power;

P_{PV} PV panels output DC power;

$P_{PV}(k)$ The PV output power at the sampling point of the present cycle;

$P_{PV}(K)$ The present power sampling and holding block;

q The charge of an electron, which is 1.9×10^{-19}(C);

R_j The nonlinear impedance of p-n junction;

R_o The resistance load of the PV cell;

R_s The intrinsic series resistance of PV cell;

R_{sh} The intrinsic shunt resistance of PV cell;

S The solar solar irradiation in mW/cm^2;

T The cell temperature (K);

T_r The PV cell reference temperature;

T_{sw} The switching period;

T_{settle} The settling time of the MPPT system;

V_b The battery voltage;

V_{DS} The voltage across the switching component of converter;

V_{in} The input voltage of the boost converter;

V_{MPP} The PV output voltage at MPP (Maximum Power Point);

V_{OC} The open circuit voltage of PV panels;

V_{out} The output voltage of the boost converter;

v_{PV} The PV panels output instantaneous voltage;

V_{PV} The PV panels output DC voltage;

$V_{PV}(k)$ The PV output voltage at the sampling point of the present cycle;

$V_{PV(min)}$ The minimum PV panels output voltage;

V_{ref} The voltage reference;

CHAPTER 1

INTRODUCTION

1.1 BACKGROUND

In later years, the problem of energy crunch is more and more aggravating. People are much concerned with the fossil fuel exhaustion and the environmental problems caused by the conventional power generation. Significant research work on new power energy sources is underway around the world. As a result, the cost of renewable energy sources such as Photovoltaic (PV) panels and wind-generators is dropping and their performance is improving. To date, the main applications of PV systems are battery charging, water pumping, home power supply and satellite power systems. The major advantages of PV systems are being clean, maintenance- and pollution-free and supplied by an inexhaustible source, the sun.

PV systems are designed around the PV cell. Since a typical PV cell produces less than 2 watts at approximately 0.5 volt dc, cells must be connected in series-parallel configurations to produce enough power for high power applications. Cells first are configured into modules. Then modules are connected as panels. PV cells represent the fundamental power conversion unit of a PV system. They are made from semiconductors, and have much in common with other solid-state electronic devices, such as diodes, transistors and integrated circuits [1].

1.2 THE OUTPUT CHARACTERISTICS OF PV PANELS

1.2.1 The Equivalent Circuit of a PV Cell

The building block of PV panels is the solar cell, which is basically a *p-n* semiconductor junction that directly converts light energy into electricity. It has the equivalent circuit shown in Fig.1.1 [2]. The current source I_{ph} represents the cell photocurrent originated by photovoltaic conversion; R_j is used to represent the nonlinear impedance of the *p-n* junction; R_{sh} and R_s are the intrinsic shunt and series resistance of the cell, respectively. Usually the value of R_{sh} is very large and that of R_s is very small, hence they may be neglected to simplify the analysis.

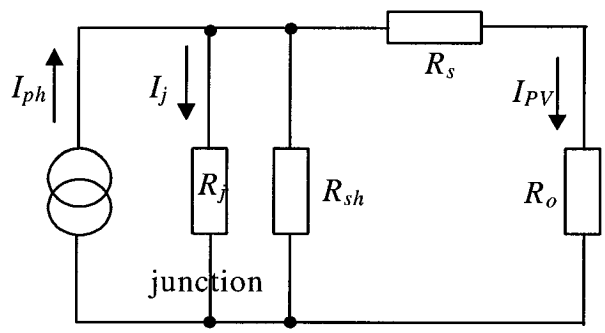

Fig. 1.1 The equivalent circuit of a solar cell

1.2.2 Mathematical Model of PV panels

A mathematical model for a PV panel can be described by the following set of equations [2]:

$$I_{PV} = n_p I_{ph} - n_p I_{rs}[\exp(\frac{q}{kTA}\frac{V_{PV}}{n_s}) - 1] \tag{1.1}$$

where I_{PV} is the PV panels output current (A); V_{PV} is the PV panels output voltage (V); n_s is the number of cells connected in series; n_p is the number of modules connected in parallel; q is the charge of an electron, which is $1.9\text{x}10^{-19}$(C); k is Boltzmann's constant, which is $1.38\text{x}10^{-23}$(eV/K); A is the p-n junction ideality factor; T is the cell temperature (K); and I_{rs} is the cell reverse saturation current. The factor A in Eq. (1.1) determines the cell deviation from the ideal p-n junction characteristics; it ranges between 1 and 5, 1 being the ideal value.

The cell reverse saturation current I_{rs} varies with temperature according to the following equation:

$$I_{rs} = I_{rr}[\frac{T}{T_r}]^3 \exp(\frac{qE_G}{kA}[\frac{1}{T_r} - \frac{1}{T}]) \tag{1.2}$$

where T_r is the cell reference temperature, I_{rr} is the reverse saturation current at T_r, and E_G is the band-gap energy of the semiconductor used in the cell. The photocurrent I_{ph} depends on the solar irradiation level and the cell temperature as follows:

$$I_{ph} = [I_{scr} + k_i(T - T_r)]\frac{S}{100} \tag{1.3}$$

where I_{scr} is the cell short-circuit current at reference temperature and irradiation, k_i is the short-circuit current temperature coefficient, and S is the irradiation level in mW/cm^2.

1.2.3 Output Characteristic Curves of PV panels

From the mathematical equations above, the output characteristics of PV panels can be computed in terms of the corresponding parameters. Fig. 1.2 shows the output curves of PV panels computed from the following parameters under different solar irradiation levels and temperatures with MATLAB software, which is shown in Appendix A1.

$$I_{ph} = 0.546 \text{ A}, I_{rr} = 2.54\text{E-}09 \text{ A}, A = 1, E_G = 1.13 \text{ eV}, n_p = 10, n_s = 200$$

Fig. 1.2(a) and (b) show the curves of output current and power *vs.* output terminal voltage under different solar irradiation levels and temperatures, respectively. The output curves of PV panel output power *vs.* output current are also shown in Fig. 1.2(c).

From the curves shown, it is apparent that the output characteristics of PV panels are nonlinear, that change with different atmospheric conditions such as environmental temperature and solar irradiation level, and other factors such as wind, which affects the output characteristics by changing the module temperature. It is also known from the curves of PV output power *vs.* voltage or current that there is one unique Maximum Power Point (MPP) under a certain atmospheric condition. The MPP changes with different solar irradiation levels, temperature and wind, which means that the operating point of PV panels must be adjusted by controlling v_{PV} or i_{PV}, to output the corresponding maximum power under certain conditions. Since other factors affect the output characteristics by changing the irradiation levels or temperature around the PV panels, only the irradiation levels and temperature are considered in the following discussion.

From Fig. 1.2(a), the curves of the PV panels output current *vs.* output voltage, it can be seen that the short-circuit current is approximately a linear function of solar irradiation

level and the open circuit voltage has negative temperature coefficient. In other words, variation of solar irradiation level mainly affects the short-circuit current, while changing of ambient temperature of PV panels mainly affects the open circuit voltage.

There maybe two or more peak points with regard to output power on the output curves of PV panels because of partial shading on the panels or other reasons, it is out of scope of this thesis.

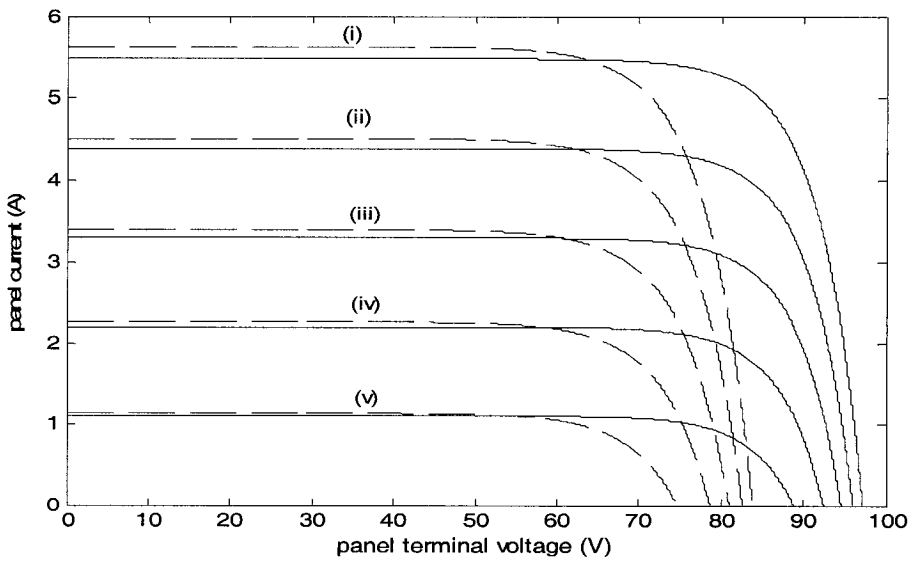

(a)

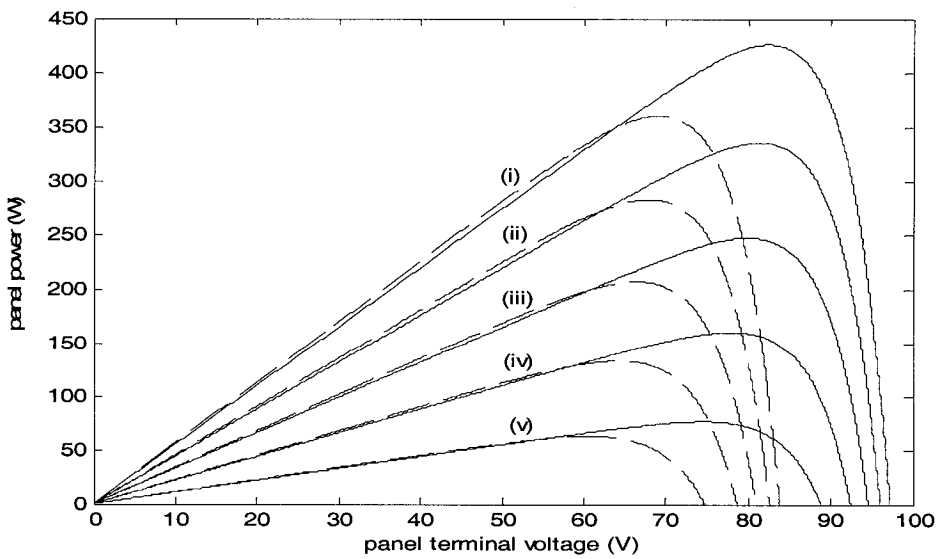

(b)

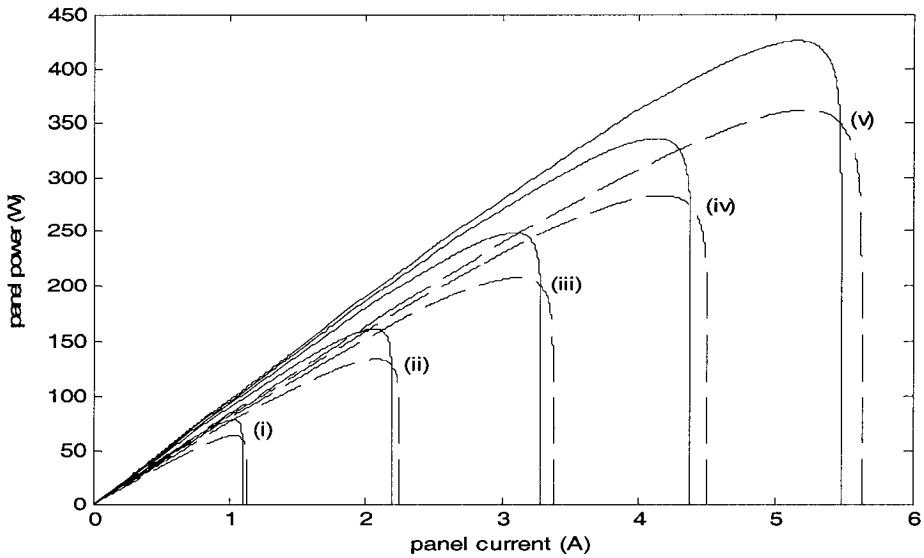

(c)

Fig. 1.2 Output characteristic curves of PV panels

(a) PV output current *vs.* output voltage;

(b) PV output power *vs.* output voltage;

(c) PV output power *vs.* PV output current;

___ 28°C ---- 56°C

(i) solar irradiation = 100mW/cm^2;

(ii) solar irradiation = 80mW/cm^2;

(iii) solar irradiation = 60mW/cm^2;

(iv) solar irradiation = 40mW/cm^2;

(v) solar irradiation = 20mW/cm^2;

1.3 PROBLEM STATEMENT AND LITERATURE REVIEW

From the output characteristics of PV panels, one sees that the output of PV panels is a function of solar irradiation and temperature, and it presents nonlinear characteristics of PV panel output power (p_{PV}) *vs.* output current or voltage (i_{PV} or v_{PV}). It is desirable to extract the highest possible power at all times. This can be done by controlling, with a power electronics converter, the PV current or voltage so that the PV panels operate at the maximum power point (MPP) at all times. Since the MPP varies with the atmospheric conditions, the reference value for the PV current or voltage has to be changed according to the atmospheric conditions which is done by a Maximum Power Point Tracking (MPPT) algorithm.

Different techniques to maximize PV power to various loads have been reported [2-22]. Of these, P&O MPPT algorithms [3-8] and their variations [9, 10] are widely used because of their simple structure and easy of implementation. However, there are some drawbacks with P&O algorithm such as oscillation around the MPP, slow response speed [11], and even tracking in wrong direction under rapidly changing atmospheric conditions [2]. The Incremental Conductance (IncCond) MPPT algorithm can, in principle, overcome the drawbacks of the P&O algorithms [2]. However, its implementation with analog circuitry is more complex and the refresh rate for digital implementation is lower because it needs to process two division operations (*di/dv* and *I/V*) while P&O algorithm require only one multiplication.

In traditional MPPT algorithm implementations, the aim is usually to control the average value of the PV output current or voltage [12]. The actual value is compared with

the reference value, the error goes to a *PI* controller, whose output is PWM modulated to regulate the duty ratio of the power switch in order to minimize the error. The response of a typical dc-dc converter with a linear controller is of an underdamped second-order system with a damping ratio between 0.4~0.6 for 25%~10% overshoot. The settling time for a 2% band is given by

$$T_{settle} = 4\tau = \frac{4}{\zeta\omega_n} \tag{1.4}$$

In practical systems the bandwidth of the system ($\approx \omega_n$) is commonly selected as 10% of the switching frequency of the power converter, resulting in a settling time of roughly 12 switching cycles. Therefore, if one wants the actual current or voltage of the PV panels to successfully follow a reference signal, the refresh or update rate (tracking cycle) of this reference signal, that is calculated by the MPPT, should not be bigger than the settling cycle of the dc-dc converter. That is the main factor in the relatively slow response speed of traditional MPPT algorithms.

In the proposed approach, one controls the PV current with peak current control, which presents a tracking cycle equal to the switching frequency of the power converter, thus improving the speed of response of the MPPT system. This scheme does not allow a precise control of the average PV current but this is not relevant since the PV current ripple is relatively small and the actual reference current is changed in every switching cycle.

Both analog implementation and digital implementation of the P&O algorithms can be found in the literature. They usually provide an average reference PV current, or PV voltage, which is varied according to the values of the previous and actual PV power. For analog implementation [3], the response speed is usually slower because of the RC

circuits required to filter out the switching harmonics in the PV current and voltage. The structure is also relatively complex compared to the digital implementation. For most digital implementations presented in the literature [4, 5, 7-10], the MPPT function block in MPPT system outputs an average voltage reference and a *PI* controller is employed to control the average value of the PV current or voltage. The calculation of the average values can be done by averaging the values sampled in a switching cycle. Even with implementations based on DSP systems, the time from start-up to the MPP is still long, from a few milliseconds to seconds [10]. In [7], the tracking speed is improved by increasing the sampling frequency. However, the tracking speed cannot be increased enough because of the delay introduced by the filters required to obtain the average values of output voltage and current.

1.4 Scope and Contributions of this Thesis

Ref. [13] mentioned that PV panels may present several *local* maximum output power points on the p x i or p x v curves of the PV panels while it is operated under non-uniform solar irradiation due to shadowing of some modules. However, most papers propose MPPT algorithms considering that there is only one unique global maximum point and no suboptimal local maxima along the output characteristic curves of the PV panels. Likewise, the analysis of MPPT algorithms for PV arrays that present more than one maximum output point on the p x i or p x v curves of the PV panels is out of the scope of this thesis. In essence, this thesis focuses on improving the existing P&O algorithms and reducing their drawbacks.

The main contributions of this thesis are the following:

1. Proposes some modifications on the existing P&O MPPT algorithms that can mitigate/reduce the main drawbacks commonly related to the P&O algorithm such as slow speed of response, oscillation around the Maximum Power Point (MPP), and even tracking in wrong direction under rapidly changing atmospheric conditions.
2. The PV panel output current is regulated with peak current control method, which does away with the need for average values and RC low pass filters, thus increasing the speed of response of the MPPT system.
3. Analyzes the effect of the sampling instant, with PV current increasing or decreasing, on the performance of the MPPT algorithm. The P&O algorithms oscillate the operating point around but do not stay at the MPP in steady-state, which makes the MPPT system lose some power. Because PV output power falls rapidly after the MPP, it is preferred that the operating point be on the left side rather than right side of the MPP for the same oscillating range. The sample on the switching off point (PV current decreasing) can move the range of operating point of the MPPT system to the left side corresponding to the MPP and reduce the power loss in steady-state.

1.5 THESIS OUTLINE

The contents of this thesis are organized as follows:

In Chapter 2, a classification of the MPPT algorithms is presented. The MPPT algorithms can be classified as On-line or Off-line methods, where On-line methods

include Perturbation and Observation (P&O) and Incremental Conductance (IncCond) algorithms, which are commonly used in medium or large power capacity PV systems. They are described in detail in this chapter. The Off-line methods are also briefly discussed here.

Chapter 3 presents *the proposed MPPT algorithm.* It is a P&O MPPT algorithm with different implementation, peak current control and instantaneous sampling values. The operating principles are presented and the design of the power electronics converter is also shown in this chapter.

Chapter 4 presents the simulation and experimental results, and analysis. The effects of the sampling instants on the overall performance of the MPPT system are shown and analyzed. A DSP system (dSPACE) is employed to construct the control system required for the MPPT system and the Peak Current Control method. The practical limitations of the dSPACE system are also discussed here.

Chapter 5 summarizes the work carried out in this thesis and the conclusions. Suggestions for future work on this topic are presented.

CHAPTER 2

REVIEW OF THE MPPT ALGORITHMS

2.1 INTRODUCTION

MPPT system is a power conversion system with a suitable control algorithm that allows extracting the maximum power from a PV panel independently of the operating conditions (temperature, solar irradiation, and aging). The maximization of the delivered power can be achieved by regulating the current drawn from the panels or the voltage across it to yield operation at or close to the Maximum Power Point (MPP).

Many different MPPT techniques have been reported in the literature [2-22]. They can be classified as either on-line or off-line methods. On-line methods include algorithms that calculate the actual power delivered by the PV panels, compare with previous values and adjust a reference signal that leads towards the actual MPP. Off-line methods are those which provide a reference signal based on detailed prior knowledge of the PV array and measurements of parameters such as solar irradiation level, module temperature, short-circuit current or open circuit voltage of sample PV panels.

In the MPPT algorithms proposed in the literature,

On-line methods include:

1. Perturbation and Observation (P&O) algorithm,
2. Incremental Conductance (IncCond) algorithm.

Off-line methods include:

1. Constant voltage,
2. Short-circuit current.

Once again, all algorithms here assume that there is only one unique global maximum power point and there is no sub-optimal maxima on the p x i or p x v curves of PV panels.

2.2 P&O ALGORITHM

A frequently used class of MPPT algorithms operates by continuously changing the operating point of the PV panels and detecting the corresponding variation in the output power in order to determine the next variation that leads to the MPP; therefore they are known as 'Perturbation and Observation' algorithms. P&O algorithms are widely used in MPPT systems because of their simple structure and easy implementation.

2.2.1 The Principle of P&O Algorithm

In P&O algorithms, the perturbation variable can be the reference value for the PV panel terminal voltage, PV panel output current, or the duty cycle of the MPPT converter. As shown in Fig. 2.1, if the output voltage of the PV panels is perturbed and $dp/dv > 0$, it is known that the operating point is on the left side of the MPP. The P&O algorithms would then increase the PV panel reference voltage to move the operating point towards the MPP. If $dp/dv < 0$, then it is known that the operating point is on the right side of the MPP. The P&O algorithms would then decrease the PV panel reference voltage.

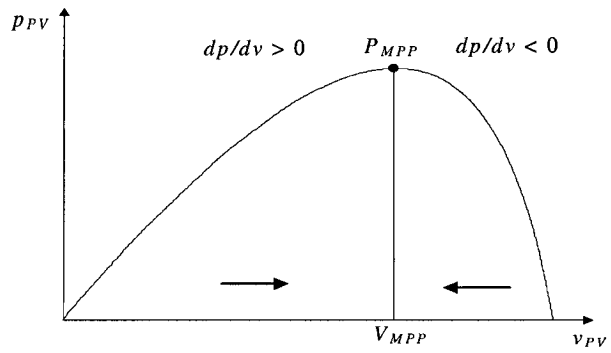

Fig. 2.1 The operating region on the curve of p_{PV} x i_{PV}

If the perturbation variable is current, then the perturbation in the PV output power is accomplished by periodically changing (either increasing or decreasing) the reference current by a small value. Hence, determination of the perturbation direction is the key function in the Perturbation and Observation algorithms.

Fig. 2.2 illustrates the flow chart for implementing P&O MPPT algorithms [5]. Here the PV output current is used as a control variable. First of all, the terminal voltage, v_{PV} and current, i_{PV}, of panels are sensed. The output power of PV panels, p_{PV}, can be obtained from the product of v_{PV} and i_{PV}. If PV output power increases with increasing PV current, the reference current is increased by one perturbation step size; otherwise the reference current is decreased by one perturbation step size. If the PV output power decreases with increasing PV current, the reference current is decreased by one perturbation step size; otherwise the reference current is increased by one perturbation step size. For example, if the output power and the current of PV panels with a perturbation are found to be:

$$P_{PV}(k-1) < P_{PV}(k) \tag{2.1}$$

and

$$I_{PV}(k-1) > I_{PV}(k) \tag{2.2}$$

where parameters k-1 and k indicate the corresponding measured quantities before and after the perturbation, respectively, (2.1) and (2.2) imply that this perturbation leads to an increased p_{PV} with decreased i_{PV}. It can be determined from the flow chart shown in Fig.2.2 that the next perturbation direction is to decrease the reference current I_{ref}.

In P&O algorithms, if the power is increasing, the perturbation will continue in the same direction in the next cycle, otherwise the perturbation direction will be reversed. So the P&O algorithm is also known as hill-climbing algorithm. With the continuous process above, the operating point of PV panels can be moved towards the maximum power points corresponding to different temperature and solar irradiation.

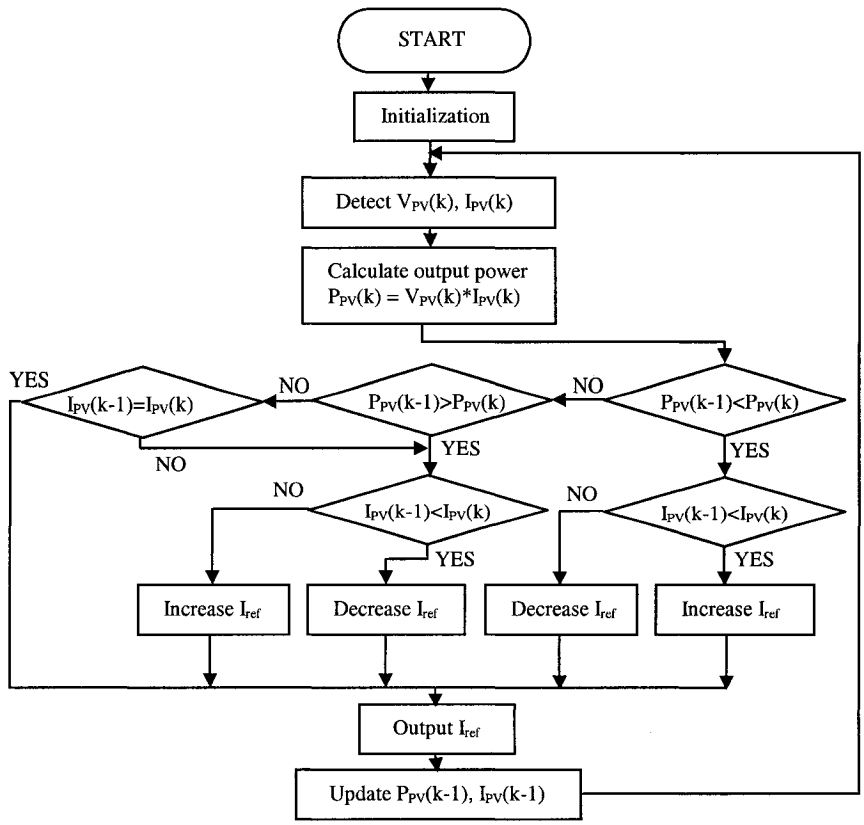

Fig. 2.2 The flow chart of the P&O MPPT algorithm

2.2.2 The Advantages and Disadvantages of P&O Algorithm

P&O MPPT algorithms are easily implemented by digital circuits. From Section 2.2.1, we know that only terminal voltage and current of PV panels are sampled to compute the output power of PV panels and the result is compared with the previous one to determine the direction of the next perturbation depending on the comparison results, which can be easily done with digital circuits [7-9].

The P&O methods have desirable adaptability to slowly fluctuating solar irradiation, temperature, and even variation of the PV panels' own characteristics, but have a drawback in terms of the response speed to seek the optimum operating point where the maximum output power can be obtained. In general, the P&O MPPT algorithms are slow since systems make a clocked perturbation of the electrical characteristic and have to wait the effect of the perturbation. Especially in most implementations, the perturbation methods use average voltage, power, or current to provide information about the derivatives, which also make the process relatively slow. The literature shows that the common P&O MPPT systems follow the MPP at time scales of a few tens of milliseconds or even longer [10].

The continuous use of perturbations to seek the MPP means that the operating point of the PV panels will be perturbed even after the MPP is reached. Therefore, the P&O systems oscillate around the MPP resulting in a loss of PV power in the steady-state conditions.

Another drawback of P&O algorithms is clearly described in [2]. In cases of rapidly changing atmospheric conditions, the P&O MPPT algorithms may actually deviate the operating point from the MPP momentarily. This can be explained by considering the

change in solar irradiation level as shown in Fig. 2.3. Assume that initially the panels' operating voltage, point (1), coincides with the MPP when a perturbation is made towards point (2). Now, an increase in the PV power will be measured because the solar irradiation has increased from S1 to S2. For the P&O algorithm, it means that the operating point is on the left side of the MPP when the power increases with increasing perturbation. However, the MPP, i.e. point (4), has already been passed. In the following perturbation the P&O algorithm will increase the PV reference voltage further right, to point (3), and again an increase in the PV power will be measured because the solar irradiation has increased from S2 to S3 with a new MPP, point (5). In this way, the reference voltage obtained from the P&O algorithm will further deviate the operating point from the actual MPP with a corresponding power loss. The P&O algorithm will bring the operating point back to the final MPP, point (5), after the transient process due to the atmospheric conditions, but some PV power was lost during the process.

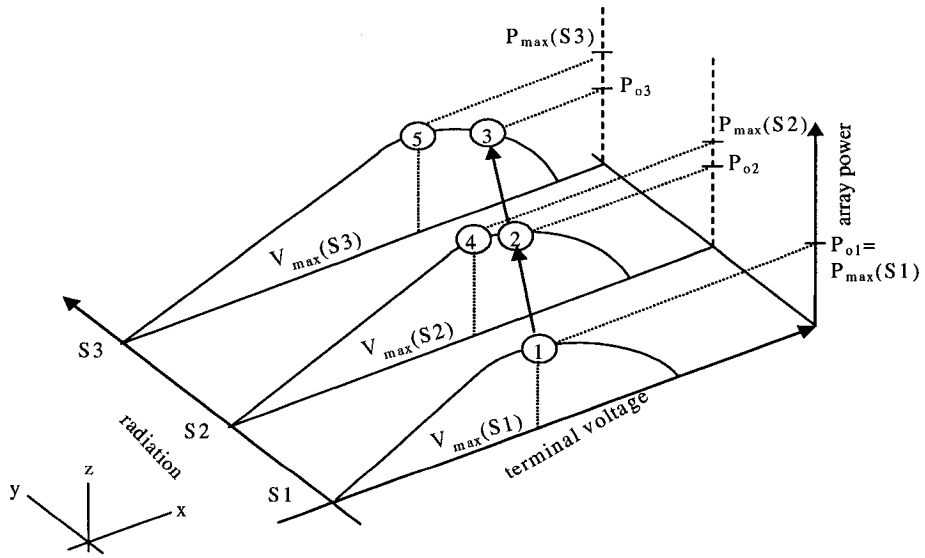

$P_{03} > P_{02} > P_{01}$, but $P_{03} < P_{max}(S3)$, $P_{02} < P_{max}(S2)$

Fig. 2.3 Deviation of the P&O algorithm from the MPP [2]

P&O algorithms assume that variations in the output power are essentially a result of perturbation. They cannot identify sudden variations in the atmospheric conditions from the measured values and that keeping the direction of the perturbation, that increased the output power, can result in moving away from the MPP. Therefore, the tracking in the wrong direction cannot be prevented. However, its duration and loss of power can be reduced with faster tracking cycles.

2.3 INCREMENTAL CONDUCTANCE (INCCOND) ALGORITHM

It has been shown in section 2.2.2 that P&O MPPT algorithms have some drawbacks. These would in principle be overcome by the Incremental Conductance algorithms, which locate the maximum power point by comparing the incremental conductance with the instantaneous static conductance as described in the following sections.

2.3.1 The Principle of IncCond Algorithm

The basic idea of the IncCond algorithms [14] is that, at the MPP, the derivative of the power with respect to the voltage or current becomes zero because the MPP is the maximum point of the power curve, as shown in Fig. 1.2(b) and (c). Here the output characteristics of p x v are analyzed. We note in Fig. 1.2(b) that in the left side of the MPP the power increases with the voltage, i.e. $dp/dv > 0$, and it decreases with voltage in the right side of the MPP, i.e. $dp/dv < 0$. This can be rewritten in the following simple equations:

$$dp/dv = 0 \text{ at the MPP} \tag{2.3}$$

$$dp/dv > 0 \text{ to the left of the MPP} \tag{2.4}$$

$$dp/dv < 0 \text{ to the right of the MPP} \tag{2.5}$$

These relations can further be written in terms of the panels' current and voltage using

$$dp/dv = d(iv)/dv = I + Vdi/dv \tag{2.6}$$

$$\frac{1}{V} dp/dv = \frac{I}{V} + di/dv \tag{2.7}$$

Hence, the PV panels terminal voltage can be adjusted relative to the MPP voltage by measuring the incremental and instantaneous panels conductance (di/dv and I/V, respectively) and making use of the equations above. The detailed operation of the IncCond algorithms can be followed with reference to the flow chart of Fig. 2.4 [2].

The algorithm starts its cycle by obtaining the present values of *I(k)* and *V(k)*, then using the corresponding values stored at the end of the preceding cycle, *I(k-1)* and *V(k-1)*, the incremental change is approximated as: $di \approx I(k) - I(k-1)$, and $dv \approx V(k) - V(k-1)$. The main check is carried out by comparing *di/dv* against *–I/V*, and according to the result of this check, the control reference signal V_{ref} will be adjusted in order to move the panels' terminal voltage towards the MPP voltage. At the MPP, *di/dv = -I/V*, no control action is needed; therefore the adjustment stage will be bypassed, which means the reference does not change, and the operating point remains at the MPP. The algorithm updates the stored parameters at the end of the cycle as usual. Two other checks are included in the algorithm to detect whether a control action is required (Here the buck converter is employed as MPPT converter and a large capacitor is used in parallel with

the PV panels [2]) when the panels was operating at the MPP in the preceding cycle (dv = 0); in this case the change in the atmospheric conditions is detected using ($di \neq 0$). Now the control signal V_{ref} adjustment will depend on whether di is positive or negative, as shown in the flow chart.

However, because of the approximation made in the calculation of di and dv the condition $dp/dv = 0$ (or $di/dv = -I/V$) seldom occurs, that is, the reference is seldom kept constant in the steady-state. This condition can be detected by allowing a small marginal error (ΔE) in the above comparisons, i.e. $dp/dv = \pm \Delta E$ and the value of ΔE depends on the required sensitivity of MPPT [2].

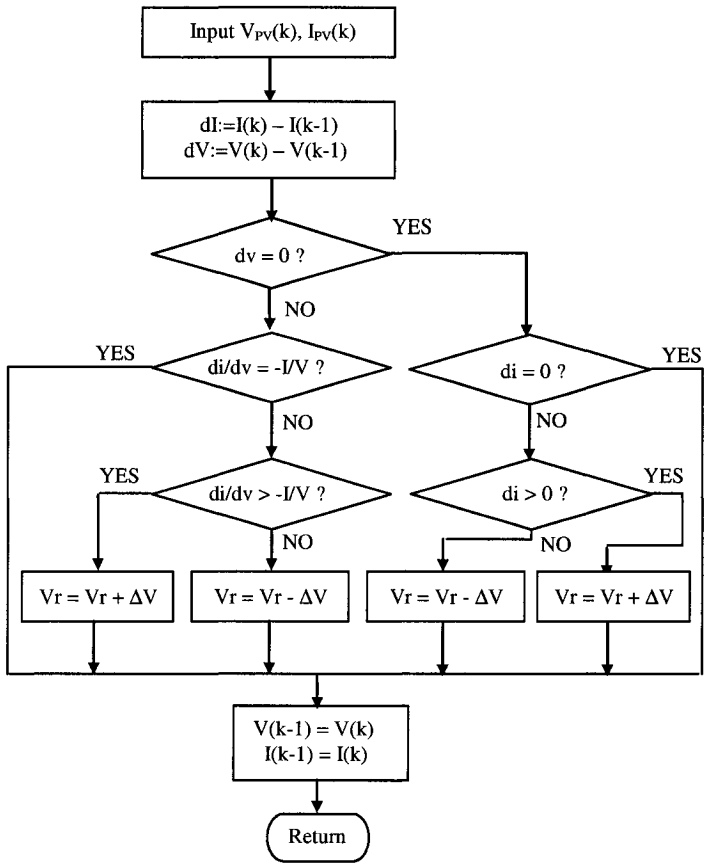

Fig. 2.4 Flow chart of the IncCond MPPT algorithms

2.3.2 The Advantages and Disadvantages of IncCond Algorithm

First of all, IncCond algorithms can in principle avoid the oscillation around the MPP when it is reached. From the flow chart one sees that when the condition *di/dv* = *-I/V* is satisfied, which means that the MPP is reached, the operating point should remain there. If this condition is not met, the direction, in which operating point of the MPPT system must be changed, can be determined using the relationship between *di/dv* and *–I/V*. This relationship is derived from the fact that *dp/dv* is negative when operation point is to the right of the MPP and positive when it is to the left of the MPP.

Second, IncCond algorithms can track the MPP even in the case of rapidly changing atmospheric conditions. IncCond algorithm uses *di/dv* = *-I/V* (also *dp/dv* = 0) as the determining condition to determine that the operating point is on the left or right side of MPP. In any circumstances, if the differential of operating point, *dp/dv*, is greater than zero, which means *di/dv* > *-I/V*, the operating point is on the left of the MPP; and if *dp/dv* is smaller than zero, which means *di/dv* < *-I/V*, the operating point is on the right of the MPP. So in principle, the algorithm can move the operating point towards the MPP no matter how rapidly the atmospheric conditions change.

However, the Incremental Conductance algorithm has the disadvantage that the control circuit complexity results in a higher system cost. It also requires a fast computation for the incremental conductance *di/dv*. Usually *di/dv* is approximated by

$$\frac{di}{dv} = \frac{I(k) - I(k-1)}{V(k) - V(k-1)} \tag{2.8}$$

If the speed of computation is slow, under the rapid changing atmospheric conditions, the approximation of *di/dv* is not valid, the advantage that IncCond algorithms can move

the operating point towards the MPP no matter how rapidly the atmospheric conditions change can not be guaranteed and a problem similar to the P&O algorithm that deviates from the MPP under rapidly changing atmospheric conditions arises.

2.4 Constant Voltage and Current Methods

The constant voltage control method is a simple control method which uses the fact that the operating voltage at MPP of PV panels (V_{MPP}) is linearly proportional to the open circuit voltage of PV panels (V_{OC}) with varying solar irradiation level. The ratio of V_{MPP}/V_{OC} depends on the solar cell parameters, but a commonly used value is around 76% [15, 16].

2.4.1 The Principle of Constant Voltage Method

The principle of Constant Voltage algorithm is that, for crystalline PV cell structures, the operating point, where maximum power is obtained, is always close to a fixed percentage of its open-circuit voltage (within ±2%). Production spread, temperature, and solar irradiation levels cause the position of the maximum power point to vary within this 2% tolerance band [16]. In this method, the MPPT system momentarily sets the PV panels current to zero and allows a measurement of the panels' open-circuit voltage. Alternatively an extra sample PV module or cell is employed to measure the panels' open-circuit voltage. Then, the reference voltage is set at around 76% of the measured open-circuit voltage and is kept in a hold circuit until the next sampling instant.

2.4.2 The Advantages and Disadvantages of Constant Voltage Method

The advantage of this method is its simplicity and low cost. No costly multipliers or digital controllers are needed.

This control method results in a quasi-maximum power point tracker. The controller does not constantly seek the true maximum point of the power *versus* voltage curve, but rather rests on pre-knowledge of where the maximum power point is. The main shortcomings of this algorithm are the waste of energy during the open-circuit period or the need for a sample PV module or cell that should be subject to the same solar irradiation level and temperature as that of the main PV panels.

2.4.3 Principle of the Short-Current Circuit Method

The Short-Circuit Current method is similar to the Constant Voltage method and utilizes the fact that the current corresponding to the MPP is approximately proportional to the short-circuit current under various solar irradiation levels.

Ref. [17] showed that the current of PV panels at MPP (I_{MPP}) is proportional to the short-circuit current (I_{SC}) under various solar irradiation levels (S) as follows:

$$I_{MPP}(S) = kI_{SC}(S) \quad k = \textit{proportional constant} \tag{2.8}$$

This Eq.(2.8) shows that I_{MPP} can be determined instantaneously by detecting I_{SC} and the MPPT system can be achieved by giving a current reference command $I_{ref} = I_{MPP}$ to a current-controlled power converter. The relationship between I_{MPP} and I_{SC} is still proportional, even though the temperature varies. The generality of the relationship under various temperature and solar irradiation levels is confirmed with different PV panels

[17]. One implementation requires to monitor PV panels to measure the short-circuit current. Another implementation, which is similar to the Constant Voltage method, shorts the PV panels for a short period to obtain the short-circuit current in the sampling interval.

2.4.4 The Advantages and Disadvantages of Short-Current Method

The method is fast, simple, and of easy implementation.

However, the system requires a monitor PV panels to measure the short-circuit current; hence, there are several problems, such as system characteristic mismatch between the monitor PV panels and the main PV panels, or the system shorting the PV panels to obtain the short current in the sampling interval means that available energy is wasted.

For both ways to obtain the short-circuit current there is a problem with the variation of the proportional parameter which is normally regarded as a constant. Uneven solar irradiation distribution on the PV panels' surface due to the shades and dirt on the surface of the PV panels can alter the proportionality parameter.

2.5 CONCLUSIONS

In general, the off-line MPPT systems cannot track the MPP in time when the atmospheric conditions change until the next sampling time is reached and the off-line MPPT system obtains the new reference value corresponding to the new MPP. Usually the sampling time interval is very long compared to the switching cycle of the MPPT

converter to reduce energy loss during the sampling process. Besides, the off-line MPPT systems might not be able to track the MPP accurately because of the characteristic mismatch between the monitor PV panels and the main PV panels. However, the off-line MPPT methods are very simple to implement and are cost effective. They are considered suitable for small power (a few hundreds of watts) PV conversion systems where total cost is very low.

On the other hand, the On-line MPPT methods can track the MPP all the time, regardless of the atmospheric conditions, types of PV panels, and even aging of the PV panels. So they can track the MPP in time and more accurate than the Off-line MPPT methods. However, they increase the complexity and the cost of the PV generation systems. So usually the On-line MPPT methods are used in medium or large power level PV system. Although the On-line MPPT methods increase the cost of the PV generation systems, the added cost is relatively small compared to the total cost of the medium or large power level PV systems.

Among the On-line MPPT algorithms, the IncCond MPPT algorithms seem to be, in principle and for negligible PV panels' capacitance, the most prone to find and remain at the MPP, yielding higher power generation at the expense of a more complex control circuit. Conversely, the P&O MPPT algorithms allegedly present some intrinsic limitations such as oscillation around the MPP, slow response speed, and tracking in wrong direction under rapidly changing atmospheric conditions. The main goal of this thesis is to propose ways for minimizing these problems, making the P&O MPPT algorithms that are already widely used in PV systems, more effective.

CHAPTER 3

THE PROPOSED MPPT SYSTEM

3.1 BASIC ALGORITHM

P&O MPPT algorithms are easily implemented, less affected by the intrinsic capacitance of the PV panels, have desirable adaptability to slowly fluctuating solar irradiation, temperature and even variation of the PV's own characteristics. So they are widely used in PV generation systems. However, they usually present some drawbacks such as slow response speed, oscillation around the MPP, and sometimes moving the operating point away from the maximum power point instead of close to it during some transients.

The proposed MPPT algorithm is based on the conventional P&O algorithms, but some new functions are added to minimize the problems mentioned above that are related to the implementations of traditional P&O algorithms.

The principle of P&O algorithm has been introduced in Section 2.2.1. The P&O algorithm operates by periodically perturbing v_{PV} or i_{PV} and comparing the PV output power with that of the previous perturbation cycle. If the power increased, the perturbation will continue in the same direction in the next perturbation cycle (which is defined in Section 3.2), otherwise the perturbation direction will be reversed. This way, the operating point gradually moves towards the maximum power point. When the MPP is reached, the operating point will oscillate around it.

In most MPPT systems [7-10, 12], there is a large capacitor in parallel with the PV panels irrespective of the type of power converter (buck or boost) employed in the MPPT system. The capacitor works as a filter to reduce the ripple of the PV output current and voltage which are introduced by the switching of the power converter.

However, the capacitor as a filter reduces the response speed of the MPPT system and will not be used in the proposed MPPT system. The following analysis shows that the existence of voltage and current ripples does not affect the determination of the correct direction of the next perturbation.

3.2 Added Features

3.2.1 Definition of Terms

It is important to define some terms frequently used in the in the following discussion.

Perturbation cycle:

The time interval in which the reference outputted by the MPPT block is updated.

Tracking speed:

The actual variation of the PV output variables (current or voltage) in unit time interval (the unit is A/s or V/s for PV output current or voltage working as control variable, respectively).

Assuming that the actual variation of the control variable in one switching cycle is equal to perturbation step size, then the relationship among tracking speed, perturbation cycle, and the perturbation step size can be expressed as:

$$\text{tracking speed} = \frac{\text{perturbation step size}}{\text{perturbation cycle}} \tag{3.1}$$

So if perturbation step size is fixed, tracking speed is reciprocal to the perturbation cycle, which means, the smaller the perturbation cycle is, the faster is the tracking speed. If the tracking speed is fixed, the shorter the perturbation cycle becomes, the smaller the perturbation step size can be.

Tracking accuracy:

The tracking accuracy can be expressed as the actual average PV output power drawn by the MPPT converter divided by the maximum power at the MPP for a given atmospheric condition.

When the operating point oscillates around the MPP in the steady-state, the perturbation step size determines the oscillating range around the MPP. The bigger the perturbation step size is, the larger is the oscillating range around the MPP, which means more power loss and poorer tracking accuracy.

3.2.2 Instantaneous Sampling

In the proposed P&O MPPT algorithm implementation, a boost converter is employed as the MPPT converter, the PV output current is chosen as the control variable, and no capacitor is used in parallel with the PV panels.

Without the parallel capacitor there is a significant PV voltage ripple but the locus of the operating point should be on the p x i curves. Therefore, the comparison of any two instantaneous operating points can be used to determine correctly the direction of the next perturbation.

Let's first assume that the MPPT system operates on the left side of the MPP. In every switching cycle, the PV instantaneous current increases during switching on and decreases during switching off. The i_{PV} waveform in two cycles is shown in Fig. 3.1(a). If the sampling time instant in switching cycle T(k-1) is at point A and the sampling time instant in switching cycle T(k) is at point B; the instantaneous current at A, I_A, is less than the instantaneous current at B, I_B. It can be seen from Fig. 3.1(b) that the instantaneous power at A, P_A is less than the instantaneous power at B, P_B. From the P&O MPPT algorithm, the operating point is on the left side of the MPP. Therefore, the current reference I_{ref} should be increased. If the sampling time instant in switching cycle T(k) is at point C instead of point A and I_C is less than I_A. It is known from the p x i curve that the instantaneous power at C, P_C is less than P_A. So the operating point is also on the left side of the MPP. The current reference I_{ref} should be increased in order to increase the output power. From the discussion above, one concludes that the sampling time instant in the switching cycle can be arbitrary. The correct calculation of the direction of the next perturbation is not affected by the sampling time instants even if the variation of the instantaneous sampled values does not reflect the variation of the average current on corresponding switching cycles. The situation is similar when the operating point is on the right side of the MPP. Since I_{MPP} is usually very close to I_{SC}, that region of the curve is detailed for explanation as shown in Fig. 3.2. Assuming that the sampling time instant in the previous switching cycle T(j-1) is at point D and the sampling time instant in the present switching cycle T(j) is at point E, the instantaneous current at D, I_D, is greater than the instantaneous current at E, I_E. From the p x i curve, the instantaneous power at point D, P_D is less than the instantaneous power at E, P_E.

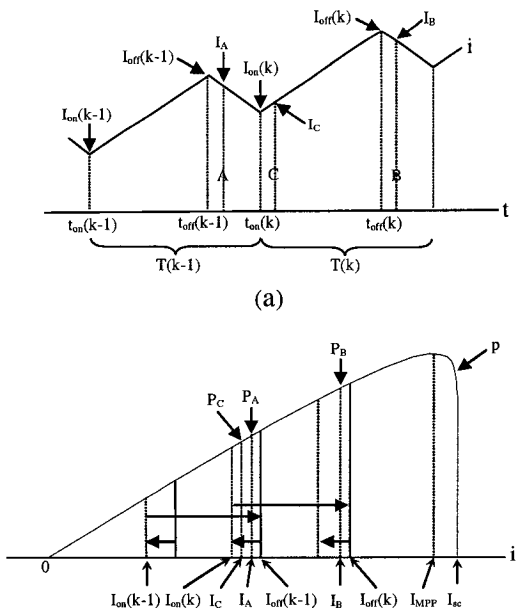

Fig. 3.1 Operating point on the left side of the MPP

(a) i_{PV} locus on p-i curve; (b) i_{PV} waveform in two switching cycles;

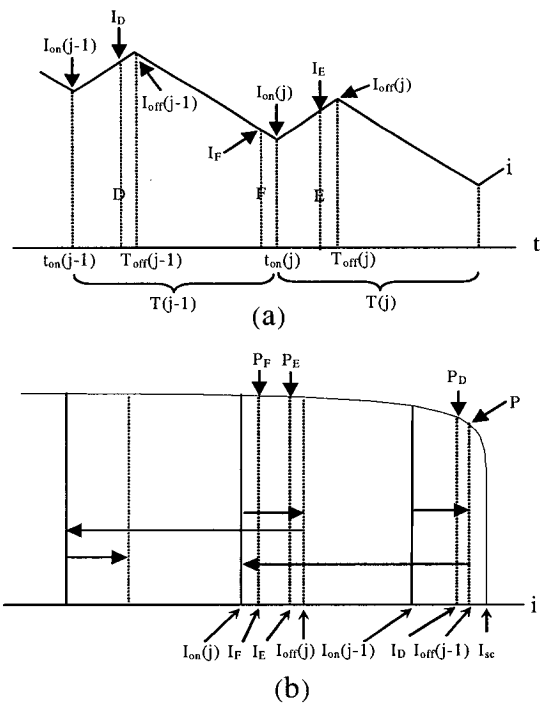

Fig.3.2 Operating point on the right side of the MPP.

(a) i_{PV} locus on p-i curve; (b) i_{PV} waveform in two switching cycles;

So power increases with decreasing current. From the P&O MPPT algorithm, the reference current, I_{ref}, should be decreased at the next perturbation.

If the sampling time instant in the previous switching cycle T(j-1) is at point F instead of point D and I_F is less than I_E. From the p x i curve, the instantaneous power at F, P_F is greater than the instantaneous power at E, P_E. The current reference, I_{ref}, should be decreased at the next perturbation due to that the output PV power decreases with increasing current. Again, the sampling time instant in the switching cycle can also be arbitrary and the correct calculation of the direction of the next perturbation is not affected by the sampling time instants even if the variation of the instantaneous sampled values do not correspond to the variation of the average current on corresponding switching cycles.

From the discussion above, only one instantaneous sampling is required in each switching cycle to compare with the instantaneous sampling in previous switching cycle and determine the perturbation direction of next perturbation cycle. Besides, the sampling instants do not need to be synchronized.

The switching frequency of the MPPT converter is usually made high (hundreds of kHz) for smaller filter components and faster transient response speed. Since one will employ a single instantaneous sampling per switching cycle, the perturbation cycle is equal to the switching period of the MPPT converter that is very small. From the analysis in the beginning of Section 3.2, for the same tracking speed, a smaller perturbation cycle permits smaller perturbation step size, which implies smaller power loss when the operating point oscillates around the MPP.

Even with a small perturbation step size, the tracking speed can be very fast because of the very short perturbation cycle. The high tracking speed implies that the MPPT system has very fast response speed to track the changing MPP due to varying atmospheric conditions.

As mentioned before, the traditional P&O MPPT algorithm has a problem that, under rapidly changing atmospheric conditions, it moves the operating point away from the MPP instead of close to it during a brief transient. This drawback has been clearly described in Section 2.2.2, which is because the P&O MPPT algorithm is based on the derivatives of two points on the same p x i (or p x v) curve. If the two points are not on the same curve due to a sudden variation on the solar irradiation level, the P&O algorithm leads to a wrong direction. This is shown in Fig. 3.3(a). When the perturbation cycle is large, the difference of PV panels output characteristics corresponding to the two consecutive sampling points will be very big under rapidly changing atmospheric conditions. One sees in Fig. 3.3(a) that an increase in the PV current ($I_2 > I_1$) might result in an increase in the output power ($P_2 > P_1$) what makes the P&O MPPT algorithm further increase I_{ref} leading the operating away from the MPP, instead of towards it.

In the proposed implementation of the P&O MPPT algorithm, because the perturbation cycle is very short, PV output characteristic changes very little between two consecutive sampling points even under very rapidly changing atmospheric conditions. The two consecutive sampling points can be approximated on the same p x i (or p x v) curve. This is shown in Fig. 3.3(b). $P_2 < P_1$, $I_2 > I_1$, I_{ref} is decreased in terms of the P&O MPPT algorithm. In fact, the operating point is on the right side of the MPP, I_{ref} should also be decreased. So the improved P&O MPPT algorithm can better deal with rapidly

changing atmospheric conditions. The possibility that the P&O MPPT algorithm moves the operating point far from the MPP under rapidly changing atmospheric conditions is reduced with the proposed implementation of the P&O MPPT algorithm.

In conclusion, the use of a single instantaneous sampling per switching cycle yields a short perturbation cycle, which reduces the two main dynamic drawbacks of the traditional P&O MPPT algorithm: slow response speed and tracking in wrong direction under rapidly changing atmospheric conditions. Besides, one can use a small perturbation step size what reduces the power loss when the operating point oscillates around the MPP.

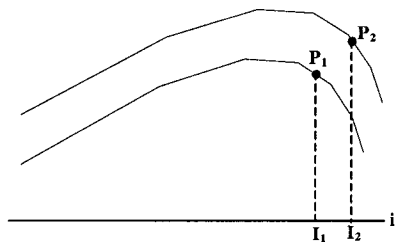

(a)

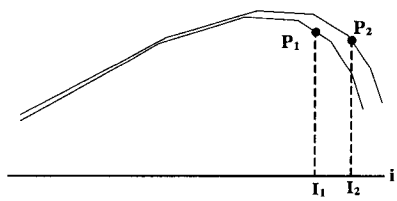

(b)

Fig. 3.3 the comparison between samplings for long and short perturbation cycle under rapidly changing atmospheric conditions

(a) sampling for long perturbation cycle

(b) sampling for short perturbation cycle

3.3 THE MPPT CONVERTER

3.3.1 The Choice of the MPPT Converter

The MPPT systems are usually as shown in the following scheme:

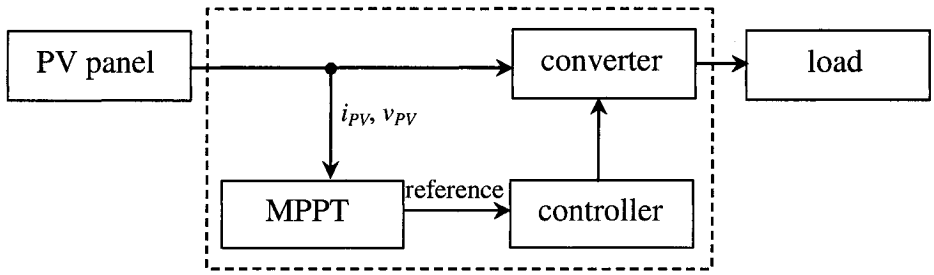

Fig. 3.4 the simple blocks of the MPPT system

The blocks in the dashed line box are considered in the analysis and design of the MPPT system.

In principle all DC/DC converters can be used as MPPT converter. However, the step-down [7-10] and boost converters [3, 12] are mostly used in MPPT systems because of their simple structure and high efficiency. If the desired output voltage of the MPPT system is lower than the PV panels' voltage a step-down buck converter is used, whereas a step-up boost converter is used to achieve output voltages higher than that of the PV panels. In this thesis a step-up converter is used as MPPT converter and the capacitor, which is usually in parallel with the PV panels in most MPPT systems to decrease the switching ripple introduced by the MPPT converter, is eliminated for fast transient response. The extra advantage of the step-up converter is that its input current is continuous and presents low ripple in most cases, which is very good for keeping i_{PV} close to I_{MPP}.

3.3.2 The Choice of the Control Variable

In MPPT systems, there are three possible variables that can be supplied by the MPPT block to the power converter in order to drive the operating point towards the MPP. They are the PV panels' terminal voltage (v_{PV}), the PV panels' output current (i_{PV}), and the duty ratio of the MPPT converter (D).

MPPT systems that employ the PV voltage as control variable usually employ a capacitor in parallel with the PV panels to reduce the voltage ripple [7-10, 12]. In such a case, the PV output current is not the same as the input current of the MPPT converter and there are some delays when the controller of the MPPT system regulates the PV output current through the MPPT converter. However, the PV output voltage is the same as the input voltage of the MPPT converter and the curve around the MPP on the p x v output characteristics is more flat than the counterpart on the p x i output characteristics. One disadvantage of using v_{PV} as the control variable is the difficulty in designing the controller.

Ref. [9] uses duty cycle of MPPT converter (D) as control variable. The output of MPPT block is duty ratio (D), which directly controls the "on" and "off" time of the power switch in the converter. However, D as control variable will make the transient process very long. For example, if we assume that the current at MPP (I_{MPP}) is 5A, the maximum inductor current increment is 0.1A under the maximum duty ratio, D_{max}, in each cycle. When the MPPT system starts up it needs 5/0.1 = 50 cycles to reach the MPP even the duty ratio in every switch cycle is D_{max}. If D is used as control variable, then D should increase gradually, which makes the transient process from 0A to I_{MPP} much longer and sometimes does not work properly.

In this thesis, the capacitor in parallel with the PV panels is not used and the PV output current is the same as the input current of the MPPT converter. It is easier to design a feedback control system with PV output current as control variable compared to that with PV output voltage as control variable. For example, if the output reference of MPPT block (I_{ref}) is greater than the actual PV output current (i_{PV}), the error between I_{ref} and i_{PV} ($i_{error} = I_{ref} - i_{PV}$) is positive, which goes to a controller to increase the duty ratio and increase correspondingly i_{PV} to reduce the error between I_{ref} and i_{PV}. An interesting control technique for applications that require fast response speed is the Peak Current Control method, which presents a one-cycle response time. Details of the Peak Current Control method are discussed in the following section.

3.3.3 The Choice of the Control Strategy: Peak Current Control

PWM control is very common in MPPT systems [7-10]. There, the reference signal for the average value of PV voltage or current and the actual signal are compared and the error is fed to a *PI* type controller. The output of the controller is compared to a fixed-frequency sawtooth producing a train of pulses with a variable duty cycle that is used to control the power switch and reduce the error. However, as discussed before, the MPPT system with a *PI* controller requires longer time (4τ, τ is the time constant of the MPPT system) to settle down, which slows the response speed of the MPPT system.

Peak Current Control scheme has very fast response speed (one-cycle response time) [23]. Because the ripple in the PV output current, which is the same as the inductor current of the MPPT converter, is a triangular waveform, just like a PWM carrier, it is possible to substitute the current for the carrier waveform if a triggering clock is provided

separately. The process is illustrated in Fig.3.5. In this arrangement, a short pulse from the clock causes the main switch to turn on by setting the latch. The inductor current begins to ramp up. The comparator tests the relationship between the current reference (I_{ref}) and the PV output current. The latch is reset and the switch turns off when the two signals match. This method is called Peak Current Control since the switch turn-off point determines the PV output peak current in the corresponding switching cycle.

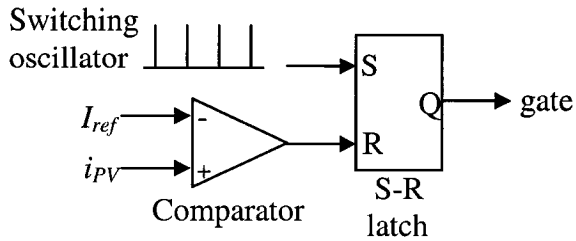

Fig. 3.5 Peak Current Control scheme [24]

In Peak Current Control scheme, it is not necessary to filter out the ripple in the inductor current. On the contrary, the ripple is utilized to substitute for the PWM carrier. The Peak Current Control has very fast transient process. So Peak Current Control scheme is used as the control scheme for the MPPT system in the thesis for its good operating properties and simplicity to implement.

3.3.4 Slope Compensation

One intriguing limitation of the Peak Current Control approach is a limit on the duty ratio. If D exceeds 50%, instability occurs [24]. This can be seen in Fig. 3.6. The figure shows an inductor current, compared to a fixed reference I_{ref} and the duty ratio is beyond 50%. Imagine what would happen if a disturbance current Δi is added beginning at time

t_0. The current will ramp up, and reach I_{ref} sooner than in the preceding cycle. In boost converter, the on-state slope is $m_{on} = V_{in} / L$, V_{in} is the input voltage of the boost converter, which is the PV output voltage v_{PV}; and the off-state slope is $m_{off} = (V_{in} - V_{out}) / L$, V_{out} is the output voltage of the boost converter. At the moment of turn-off, there is a change in the on-time $\Delta(DT_s)$ such that $m_{on} = \Delta i / \Delta(DT_s)$. The current then ramps down, and finishes the cycle at time $t_1 = t_0 + T_s$ with a value $i_0 - \Delta i_1$. The change Δi_1 is such that $m_{off} = \Delta i_1 / \Delta(DT_s)$. The ratio of the two current changes can be found as

$$\frac{\Delta i_1}{\Delta i} = -\frac{m_{off}}{m_{on}} \tag{3.2}$$

where the negative sign reflects the fact that m_{off} is negative. For stability, the disturbance must not grow with time. The ratio m_{off} / m_{on} was $-D/(1-D)$ before the disturbance. If D exceeds 0.5, then the ratio exceeds one, the magnitude of Δi_1 will exceed Δi. The disturbance will grow, and instability occurs.

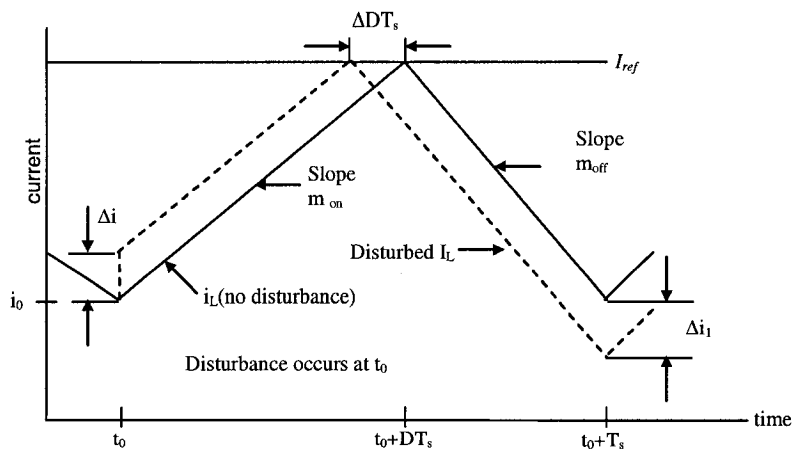

Fig. 3.6 Current waveform and I_{ref} for high duty ratio [24].

The operation is unstable because $\Delta i_1 > \Delta i$.

The instability can be avoided by altering the slopes. One approach is to use a ramp signal in place of the fixed current reference. In this case, a ramp oscillator output is subtracted from the current reference I_{ref}. The result is compared to the current waveform. This control signal is called a *stabilizing ramp*. This method is also called *slope compensation*.

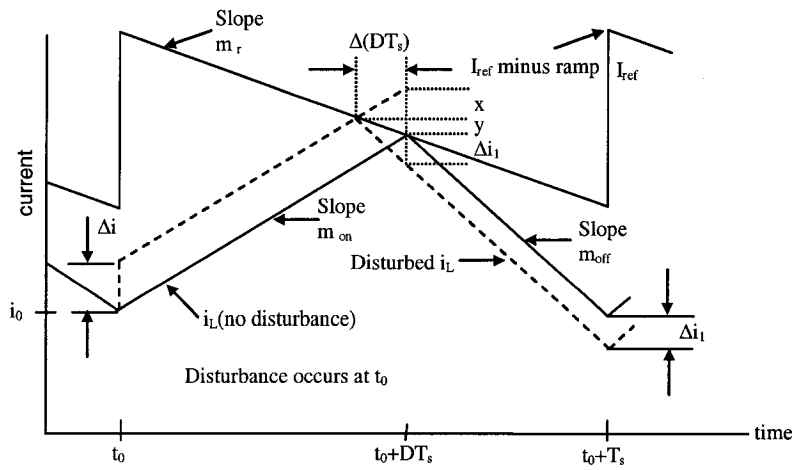

Fig. 3.7 Peak current control with a stabilizing ramp on I_{ref} [24]

The effect is shown in Fig.3.7. If m_r is the ramp slope, the condition to be met is as follows:

$$x = m_{on} \times \Delta(DTs) \tag{3.3}$$

$$y = -m_r \times \Delta(DTs) \tag{3.4}$$

$$\Delta i = x + y = (m_{on} - m_r) \times \Delta(DTs) \tag{3.5}$$

$$\Delta i_1 = -m_{off} \times \Delta(DTs) - y = -m_{off} \times \Delta(DTs) + m_r \times \Delta(DTs) \tag{3.6}$$

$$\frac{\Delta i_1}{\Delta i} = \frac{- m_{off} \times \Delta(DTs) + m_r \times \Delta(DTs)}{(m_{on} - m_r) \times \Delta(DTs)} = \frac{m_r - m_{off}}{m_{on} - m_r} < 1 \tag{3.7}$$

in which $m_{on} > 0$, m_r, $m_{off} < 0$.

The choice $m_r = m_{off}$ will guarantee stability for all possible duty ratio values, which is sometimes called the *optimum stabilizing ramp*.

3.3.5 The Calculations of the Power Circuit Components

1. Determination of the switching frequency

For a certain output power and different applications, the PV modules can be connected in series or in parallel to get high terminal voltage and high output current, respectively. For low voltage applications, MOSFETs are usually employed as switches in the dc-dc power converter. A switching frequency of 100 kHz or more should be reasonable for MOSFETs. While in higher voltage applications, IGBTs are usually used. A switching frequency of 20~50 kHz should be reasonable. In this thesis, the PV output voltage is only a few tens volts, so power MOSFETs are used and a switching frequency of 100 kHz is selected.

2. MOSFET ratings

The maximum current that the power switch carries is the PV short-circuit current, I_{SC}. For high reliability, the rated current of MOSFET should be 1.2~1.5 I_{SC}.

The maximum voltage that the switch stands is the output voltage of boost converter, V_{out}. For high reliability, the rated voltage of MOSFET should be 1.5 V_{out}.

3. Diode ratings

The maximum current that the diode carries is also I_{SC}. For high reliability, the rated current of the diode should also be 1.2~1.5 I_{SC}.

The maximum voltage that the diode blocks is V_{out}. For high reliability, the rated voltage of diode should be 1.5 V_{out}.

4. Ratings of the Output Capacitor

The selection of the output capacitor depends on the requirement of output voltage ripple [25]. Because it is assumed that the MPPT will charge a battery, the determination of the output capacitor is not important for MPPT converter here.

5. Perturbation Current Step Size

The choice of the perturbation step size (I_{step}) is very important in the P&O algorithm. I_{step} influences the tracking accuracy and tracking speed in inverse proportion. Because P&O algorithm oscillates around the MPP when it is reached, larger I_{step} results in larger power loss, whereas it needs fewer steps to reach the MPP during start up. This implies faster response speed. However, the tracking speed depends not only on I_{step} but also on the perturbation cycle.

Because the fluctuation of the MPP of a PV panel relative to the ambient change is commonly slow (~ milliseconds), tracking speed does not have to be very fast. Moreover, the perturbation cycle is very short (same as the switching cycle, which is 10us in simulation and 100us in experiment because of the limitation of dSPACE system) in the proposed P&O algorithm. So theoretically, I_{step} can be very small. However, there is a factor to limit the minimum I_{step}.

The proposed P&O algorithm works based on the signs of current difference ΔI and the corresponding power difference ΔP in two consecutive sampling points. Because of the digital implementation of the proposed algorithm in the thesis, i_{PV} and v_{PV} are sensed and converted to digital variables by A/D converters. The minimum current increment or decrement that can be reflected by the A/D converters is limited by their resolution. For example, if the maximum PV output current is 10A, and 12 bits A/D converters are used, the minimum changing of i_{PV} that can be shown by the A/D converters should be greater than $10/2^{12} \approx 2.5mA$. Otherwise the A/D converter outputs the same digital values for two current samplings with difference less than 2.5 mA.

So the minimum step size I_{step} must be greater than the resolution of A/D converters. Hence the minimum I_{step} is chosen to be bigger than two times the resolution of the A/D converter.

The maximum step size will be chosen so that the PV output power in the steady-state while oscillating around the MPP is always bigger than 90% of the power at the MPP.

From the p x i curve of the PV panels' simulation model in Fig. 4.4 and 4.5, one obtains the following data:

P_{MPP} = 61.32W, I_{MPP} = 3.267A, I_{SC} = 3.452A; $90\%P_{MPP}$ = 55.188W, and the current corresponding to $90\%P_{MPP}$ at the right side of the MPP, $I(90\%P_{MPP})$ = 3.43A; because the ratio of ($I(90\%P_{MPP})$ - I_{MPP}) to (I_{SC} - I_{MPP}) can show the position of the point of $90\%P_{MPP}$ relative to the MPP and short-circuit current point, the ratio, instead of the actual data, is used in the following discussion. Here the ratio of ($I(90\%P_{MPP})$ - I_{MPP}) to (I_{SC} - I_{MPP}) is equal to $\frac{3.43-3.267}{3.452-3.267} \approx 0.9$.

The ratio of ($I(90\%P_{MPP})$ - I_{MPP}) to (I_{SC} - I_{MPP}) can vary with different types of PV panels. However, 0.9 of ratio of ($I(90\%P_{MPP})$ - I_{MPP}) to (I_{SC} - I_{MPP}) is used in this thesis for the following discussions. The relationships below can be derived again with different requirements and ratio of ($I(90\%P_{MPP})$ - I_{MPP}) to (I_{SC} - I_{MPP}) according to the following discussion.

Before the discussion of the determination of the maximum perturbation step size (I_{step}), some assumptions are made as follows.

1. Samples are taken at the switching off point.
2. The p x i curve is symmetrical around the MPP, that is, for small current variations (Δ), $P(I_{MPP} - \Delta) = P(I_{MPP} + \Delta)$.
3. $I_{ref}(k)$ is the current reference of the present perturbation cycle just before the MPP and $I_{ref}(k+1)$ is the current reference of next perturbation cycle, which is just after the MPP. So we have

$$I_{ref}(k+1) = I_{ref}(k) + I_{step} \tag{3.8}$$

The power corresponding to $I_{ref}(k)$, $P(k)$, can be larger, smaller than, or equal to the power corresponding to $I_{ref}(k+1)$, $P(k+1)$, depending on the positions of $I_{ref}(k)$ and $I_{ref}(k+1)$ as shown in Fig. 3.8.

In Fig. 3.8(a), $P(k)$ is smaller than $P(k+1)$, from the P&O algorithm, I_{ref} will be increased by another I_{step} to $I_{ref}(k+2)$. Then I_{ref} is decreased and $I_{ref}(k+2)$ is the maximum reference current in this case. So

$$\begin{aligned} I_{ref}(k+2) &= I_{ref}(k+1) + I_{step} \\ &= I_{ref}(k) + 2I_{step} \end{aligned} \tag{3.9}$$

Because $P(k)$ is smaller than $P(k+1)$, from assumption 3 we have

$$I_{MPP} - I_{ref}(k) > I_{ref}(k+1) - I_{MPP} \tag{3.10}$$

combines Eq.(3.9), (3.10), the following inequalities can be obtained

$$I_{MPP} - [I_{ref}(k+2) - 2I_{step}]) > [I_{ref}(k+2) - I_{step}] - I_{MPP} \tag{3.11}$$

$$\frac{3}{2} I_{step} > I_{ref}(k+2) - I_{MPP} \tag{3.12}$$

which means that the distance from the MPP to the point where I_{ref} is decreased will be less than 3/2 times I_{step}.

In Fig. (b), *P(k)* is equal to *P(k+1)*, from the implementation of P&O algorithm in Section 4.6.3, I_{ref} will also be increased by another I_{step} to $I_{ref}(k+2)$. Then I_{ref} is decreased. From assumption 3 we have

$$I_{MPP} - I_{ref}(k) = I_{ref}(k+1) - I_{MPP} \tag{3.13}$$

combines Eq.(3.9), (3.13), the following equalities can be obtained

$$I_{MPP} - [I_{ref}(k+2) - 2I_{step}]) = [I_{ref}(k+2) - I_{step}] - I_{MPP} \tag{3.14}$$

$$\frac{3}{2} I_{step} = I_{ref}(k+2) - I_{MPP} \tag{3.15}$$

which means that the distance from the MPP to the point where I_{ref} is decreased will be equal to 3/2 times I_{step}.

In Fig. (c), *P(k)* is larger than *P(k+1)*, from the P&O algorithm, I_{ref} will not be increased to $I_{ref}(k+2)$, but decreased from $I_{ref}(k+1)$. It is apparent that

$$I_{ref}(k+1) - I_{MPP} < I_{step} \tag{3.16}$$

which means that the distance from the MPP to the point where I_{ref} is decreased will be less than I_{step}.

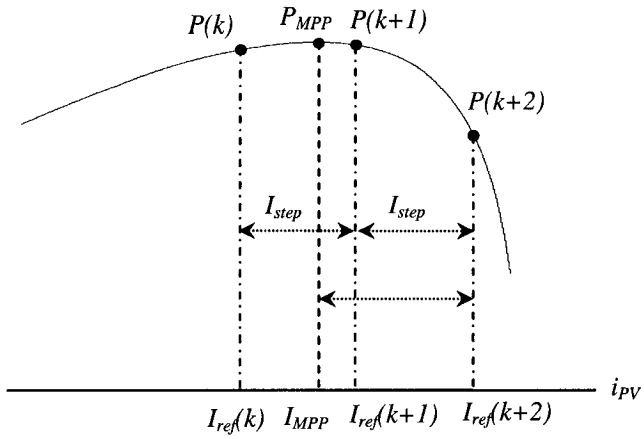

(a)

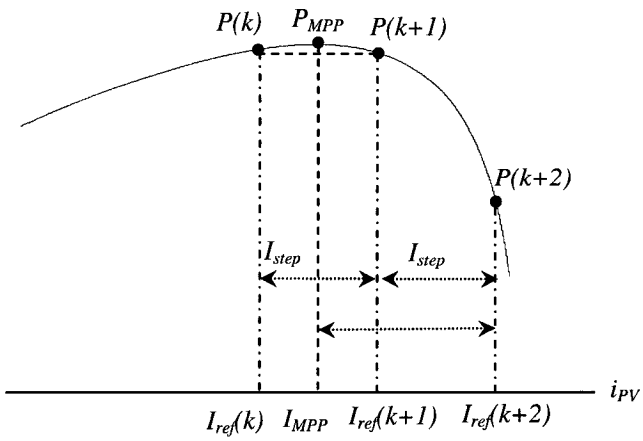

(b)

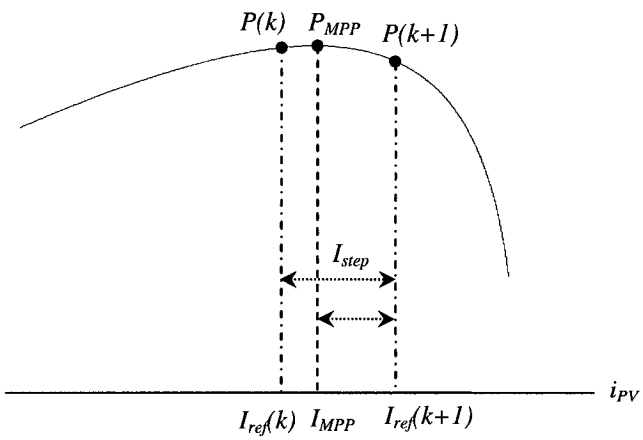

(c)

Fig. 3.8 The relationship of the two sampling points around the MPP

(a) $P(k) < P(k+1)$; (b) $P(k) = P(k+1)$; (c) $P(k) > P(k+1)$;

From the discussion above, it is known that the biggest distance from the MPP to the point that I_{ref} is decreased happens in Fig. 3.8 (b) which is equal to 3/2 times I_{step}. In order to prevent that the PV output power p_{PV} is less than $90\%P_{MPP}$ from happening, the biggest possible distance from the MPP to the point where I_{ref} is decreased should be less than the distance from the MPP to the point where the PV output power is $90\%P_{MPP}$ on the right side of the MPP, which is $0.9(I_{SC} - I_{MPP})$. So we have

$$\frac{3}{2} I_{step} < 0.9 \times (I_{SC} - I_{MPP}) \tag{3.17}$$

$$I_{step} < 0.6 \times (I_{SC} - I_{MPP}) \tag{3.18}$$

Therefore, I_{step} should range from two times the resolution of A/D converters to $0.6(I_{SC} - I_{MPP})$, which is expressed by the following inequality:

$$2 \textit{ times the resolution of } A/D \textit{ convterter} < I_{step} < 0.6 \times (I_{SC} - I_{MPP}) \tag{3.19}$$

6. Current Ripple and Inductor of the MPPT converter

Ideally, a pure dc current would be drawn from the PV panels. However, this is impossible for a switching mode converter connecting to the PV panels. Larger or smaller, current ripple exists in the output current of PV panels, which is also the same as the inductor current of converter here. A small current ripple is better for the PV panels, since it results in a small power loss, but requires a large inductor, what reduces the transient response of the MPPT system, increases MPPT system volume, weight, cost, and also leads to longer time from 0 to I_{MPP} during start-up.

In the determination of the inductor size, the requirement for the current increment in each switching cycle will be taken into consideration, which is that the current increment

under the maximum duty ratio in each switching cycle should be larger than the perturbation step size (I_{step}). Otherwise the changing of the actual PV output current can not follow the changing of I_{ref}.

Assuming that the voltage in the switching cycle around the MPP changes very little, from the discussion above that the current increment under the maximum duty ratio in each switching cycle should be larger than the perturbation step size. That is

$$\frac{V_{MPP}}{L} D_{\max} T_{sw} + \frac{V_{MPP} - V_b}{L}(1 - D_{\max})T_{sw} = \frac{V_{MPP}}{L} T_{sw} - \frac{V_b}{L}(1 - D_{\max})T_{sw} > I_{step} \qquad (3.20)$$

in which

V_{MPP}: the PV output voltage at the MPP;

V_b : the output voltage of the converter, which is assumed to be the rated value of the battery bank;

L : the inductance of the converter inductor;

D_{max} : the maximum duty ratio;

T_{sw} : the switching cycle;

I_{step} : the perturbation step size;

Neglecting the term $\frac{V_b}{L}(1 - D_{\max})T_{sw}$ for an approximate computation, the inequality becomes

$$\frac{V_{MPP}}{L} T_{sw} > I_{step} \qquad (3.21)$$

$$L < \frac{V_{MPP}}{I_{step}} T_{sw} \qquad (3.22)$$

Before the discussion of maximum possible ripple, some assumptions are made as follows.

1. Sampling values are obtained at the switching on point of each switching cycle.
2. The current at the switching on point of the next switching cycle ($I_{on}(k+1)$) is larger than the current at the switching on point of the present switching cycle ($I_{on}(k)$) by I_{step}. So $I_{on}(k+1) = I_{on}(k) + I_{step}$.
3. When the switching off point of the present cycle reaches the point of $90\%P_{MPP}$, the perturbation direction should be reversed and I_{ref} should be decreased.
4. The p x i curve is symmetrical around the MPP, that is, for small current variations (Δ), $P(I_{MPP} - \Delta) = P(I_{MPP} + \Delta)$.

From assumption 3, the PV power at the switching on point of the present cycle ($P(k)$) should be larger than the PV power at the switching on point of the next cycle ($P(k+1)$), then I_{ref} is decreased because of the decreasing power with increasing current. From Fig. 3.9 and assumption 4, if $I_{on}(k) = I_{MPP} - 0.5I_{step}$ and $I_{on}(k+1) = I_{MPP} + 0.5I_{step}$, $P(k) = P(k+1)$. If $I_{on}(k) < I_{MPP} - 0.5I_{step}$, then $P(k) < P(k+1)$. If $I_{on}(k) > I_{MPP} - 0.5I_{step}$, then $P(k) > P(k+1)$. So $I_{on}(k)$ should be larger than $I_{MPP} - 0.5I_{step}$ to make that $P(k) > P(k+1)$ and I_{ref} is decreased. Because the ratio of ($I(90\%P_{MPP})$ - I_{MPP}) to (I_{SC} - I_{MPP}) is 0.9, the current ripple from $I_{on}(k)$ to $I_{off}(k)$ should be smaller than

$$\frac{1}{2} I_{step} + 0.9(I_{SC} - I_{MPP}) \tag{3.23}$$

Assuming that the voltage around the MPP is constant and the maximum possible current ripple happens under the maximum duty ratio, which is $\frac{V_{MPP}}{L} D_{\max} T_{sw}$, one obtains

$$\frac{V_{MPP}}{L} D_{\max} T_{sw} < \frac{1}{2} I_{step} + 0.9(I_{SC} - I_{MPP}) \tag{3.24}$$

$$\frac{V_{MPP}}{\frac{1}{2} I_{step} + 0.9(I_{SC} - I_{MPP})} D_{\max} T_{sw} < L \tag{3.25}$$

Combining Eq. (3.22) and (3.24), L should be in the following range.

$$\frac{V_{MPP}}{\frac{1}{2}I_{step}+0.9(I_{SC}-I_{MPP})}D_{\max}T_{sw} < L < \frac{V_{MPP}}{I_{step}}T_{sw} \tag{3.26}$$

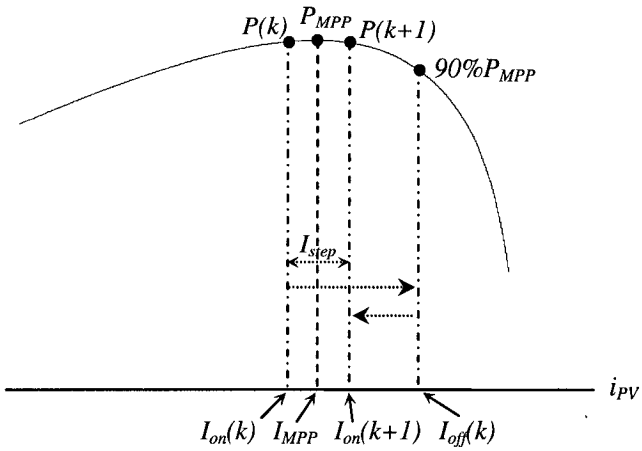

Fig. 3.9 The maximum possible ripple on the p x i curve

7. Maximum and Minimum Duty Ratio

It is mentioned in [23, 24] that a voltage controlled boost converter system has a large signal stability problem. From the output voltage characteristics as a function of duty ratio for a boost converter, one sees that there are two duty ratios for each output voltage when $V_{out} \geq V_{in}$. This happens because of the parasitic elements, that represent the losses associated with the inductor, the capacitor, the switch, and the diode [25]. The large signal instability in the boost converter can be avoided entirely by ensuring that duty ratio is limited. However, the stability problem does not exist if the inductor current is chosen as the control variable, as in the proposed MPPT. However, the power loss is still very large in the boost converter when it operates at high values of the duty ratio because of

the same parasitic elements. So the maximum duty ratio D_{max} is usually limited between 0.7 and 0.85.

The minimum duty ratio (D_{min}) should not be too large. Otherwise, the operating range of the duty ratio will be small, which reduces the response speed of the MPPT converter. For example, if the PV output current is to be decreased, the decreasing magnitude of the current in each switching cycle is limited by D_{min} if other conditions are fixed. However, D_{min} can not be too small for the design of the inductor. So D_{min} is determined as 0.1 based on the experience.

3.4 CONCLUSIONS

The implementation of a P&O algorithm with instantaneous sampling was proposed as a way to reduce the drawbacks of standard P&O algorithms. Because the locus of the PV output current is on the p x i curve no matter how the MPPT converter draws the PV current, any two consecutive sampling points can be used to determine the position of the instantaneous operating point, on the left or right side of the MPP, and the adequate perturbation direction.

One instantaneous, not averaged, sampling value of v_{PV} and i_{PV} is taken in each switching cycle to realize the P&O algorithm in the thesis, which makes the perturbation cycle equal to the switching cycle. Besides, the sampling instants do not need to be synchronized.

The combination of the One Instantaneous Sampling and Peak Current Control scheme makes that both inner current loop and outer MPPT loop have very fast response speed. So the proposed implementation of the P&O algorithm has very fast response

speed. That reduces the drawback of tracking in wrong direction under rapidly changing atmospheric conditions and the power loss of system oscillating around the MPP due to a relatively small perturbation step size.

The selection of various circuit components and algorithm parameters is discussed. The most relevant parameters were suitable ranges for the perturbation step size and inductor size. So that the actual PV current can follow the reference signal during transients and the instantaneous output power in steady-state does not fall below 90% of the maximum power at that solar irradiation level.

CHAPTER 4

THE SIMULATION AND DSP IMPLEMENTATION

4.1 THE SIMULATION SCHEMATICS

4.1.1 Schematic Diagram of the PV System

Fig.4.1 shows the schematic diagram of the PV system for the simulation with MATLAB/SIMULINK. The PV output current i_{PV} and voltage v_{PV} are measured and multiplied for instantaneous PV output power p_{PV}. The MPPT block processes i_{PV} and v_{PV} and outputs a current reference I_{ref}. The PCC (Peak Current Control) block outputs the PWM driving signal, according to I_{ref} and i_{PV}, to the PC (Power Converter) block to make i_{PV} follow I_{ref}.

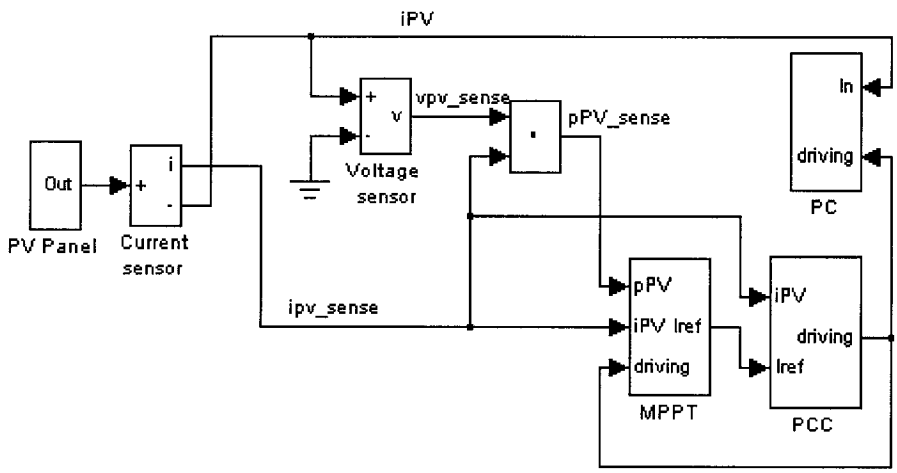

Fig. 4.1 Main Circuit Diagram of the simulation

4.1.2 PV Panels

The PV panel simulation model is based on a look up table and there are two possible approaches. In the first, shown in Fig. 4.2, the value of the output voltage is obtained from a look up table with data from the i_{PV} x v_{PV} curve of the PV according to the instantaneous value of the PV output current. Block CS is a current sensor and CVS a controlled voltage source. In this case, only one i x v curve is directly stored in the table, and the model can not be used to evaluate a MPPT system's dynamic behavior with respect to the variation of the solar solar irradiation levels.

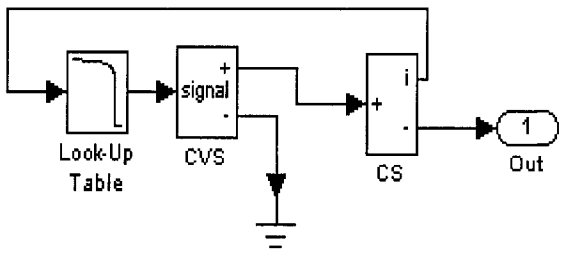

Fig.4.2 The simulation model of PV Panels with i x v curve in table

Another method is based on the model of the PV panels, which is shown in Fig. 1.1. The model of the PV panels is comprised of a current source in parallel with a voltage source. In the classical PV cell, the input current decreases when the solar irradiation level falls. Likewise, one can emulate a decrease in the solar irradiation level by decreasing the current of the current source [26]. So the simulation model of PV panels used in the thesis is constructed according to the second method, as shown in Fig. 4.3.

In the simulation model shown in Fig. 4.3, the elements to the right of block CS are related to the shunt branch of the PV panels' model. The output of the PV panels is the bus represented by the connector "Out1". The value of the PV output voltage is obtained

from a look up table with data from an i_{VS} x v_{PV} curve according to the actual value of the shunt current (i_{VS}). Variations in the solar solar irradiation level can be represented by increasing or decreasing the reference value for the controlled current source *CCS* which supplies the short-circuit current of the PV panels (I_{SC}). The relationship between the current in the PV model are shown below.

$$I_{SC} = i_{VS} + i_{PV} \tag{4.1}$$

$$i_{VS} = I_{SC} - i_{PV} \tag{4.2}$$

The data of i_{VS} and v_{PV} are shown in table 4.1.

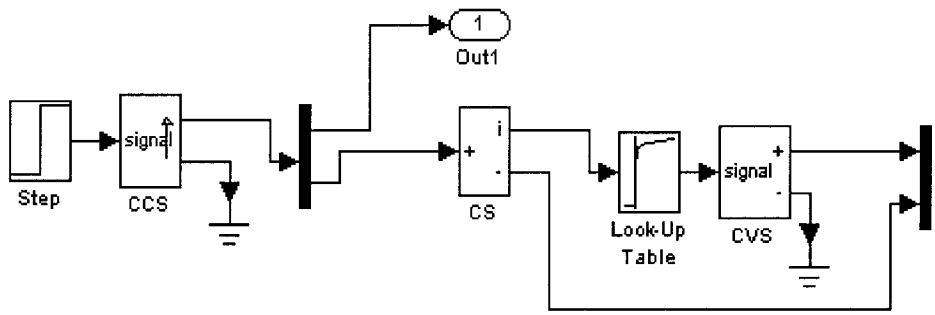

Fig. 4.3 The simulation model of PV Panels with i_{VS} x v_{PV} curve in table.

I_{VS}	0	0.002	0.004	0.022	0.028	0.071	0.115	0.146
V_{PV}	0	10	14.676	16.1	16.724	17.748	18.26	18.516
I_{VS}	0.164	0.175	0.184	0.185	0.188	0.191	0.197	0.209
V_{PV}	18.644	18.708	18.764	18.772	18.788	18.804	18.836	18.9
I_{VS}	0.236	0.3	0.485	1.268	3.435	3.452		
V_{PV}	19.028	19.284	19.796	20.82	21.881	21.886		

Table 4.1 i_{VS} and the corresponding v_{PV} in the table of PV simulation model

The curves corresponding to the different short-circuit currents are simulated with the above PV model and shown in the Fig. 4.4 and 4.5. Comparing these curves with the ones in Fig. 1.2, one sees that the simulation model of PV panels shown in Fig 4.3 can accurately represent the variation of the solar irradiation level by changing the short-circuit current of the current source. The model can be used to evaluate the dynamic response of the MPPT system in the simulation by variation of the short-circuit current of the current source. At rated solar irradiation and temperature, the following values are obtained: I_{SC} = 3.452A, V_{OC} = 21.886V, V_{MPP} = 18.771V, I_{MPP} = 3.267A, P_{MPP} = 61.32W.

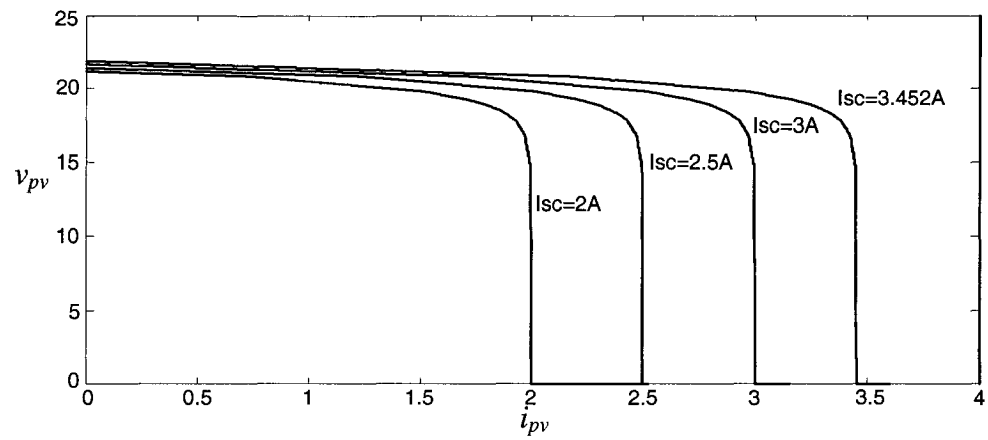

Fig.4.4 The output characteristics of PV simulation model, v_{PV} x i_{PV}

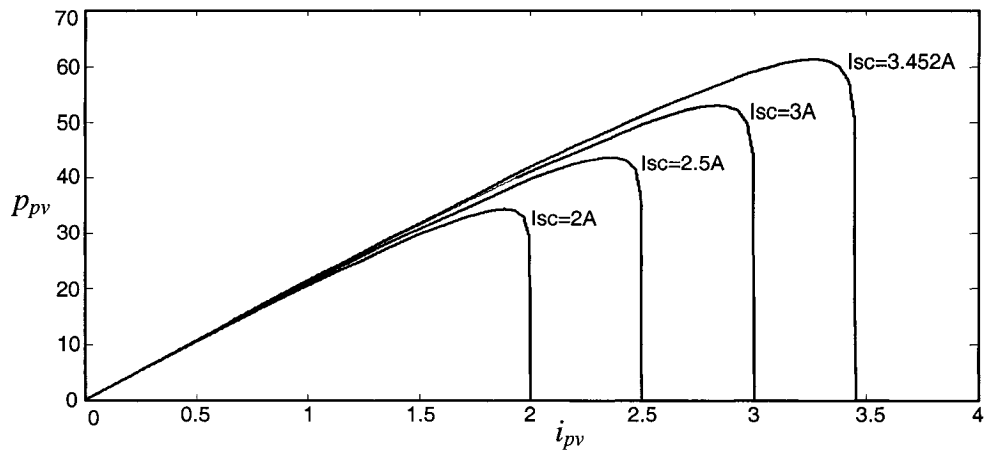

Fig. 4.5 The output characteristics of PV simulation model, p_{PV} x i_{PV}

4.1.3 Power Circuit (PC) Simulation Model and the PC Block

As discussed before, a boost converter is used as the MPPT converter in this thesis. Usually the output voltage of the converter is kept constant by a battery or another converter load.

In MPPT systems, the main parameters are the PV output current (i_{PV}) and voltage (v_{PV}), which are actually the input variables of the boost converter. From the boost converter in Fig. 4.6, we know that V_{DS} is zero when power switch *SW* is turned on and is V_{out} when power switch is off in continuous mode, which is considered in this case. Therefore, one can represent the power converter in the dashed line box of Fig. 4.6 with a controlled voltage source (*CVS1*) in series with a diode as shown in Fig. 4.7.

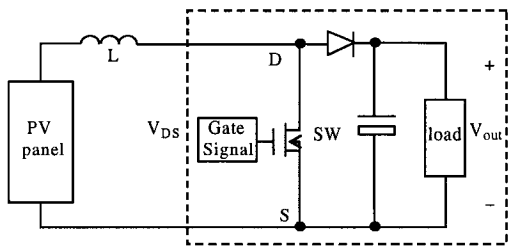

Fig.4.6 Power Circuit of MPPT Converter

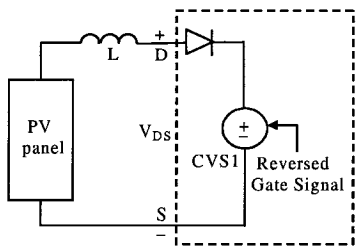

Fig.4.7 Simulation Model of Power Circuit

When the gate signal of the power switch (*SW*) in Fig. 4.6 is "high", the voltage V_{DS} across *SW* is zero. In the simulation model, *CVS1* is controlled to output 0V. On the other

hand, when the gate signal is "low", V_{DS} is equal to V_{out}. In the simulation model, *CVS1* is controlled to output V_{out}V. The inside of the Power Circuit block is shown in Fig. 4.8.

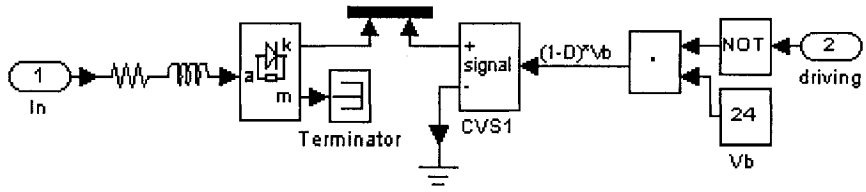

Fig. 4.8 The simulation model of PC block

4.1.4 MPPT Block

The MPPT block implements the MPPT algorithm with the proposed "Instantaneous Sampling" method. One set of samples of i_{PV} and p_{PV} is taken in each switching cycle and processed. I_{ref} is updated according to the perturbation direction calculated in each switching cycle.

In the MPPT block diagram shown in Fig. 4.9, P(K), P(K-1), I(K), and I(K-1) are triggered blocks of sampling & holding. The rising-edge of the driving signal determines the sampling instant in each switching cycle. The present $P_{PV}(k)$ sample from P(K) block subtracts the previous $P_{PV}(k-1)$ from P(K-1) block and the result passes through a Sign unit, where the output is "1" for positive input values, "-1" for negative input values, and "0" for zero input value. If the input of the sign unit is positive, which means that p_{PV} is increasing, the Sign unit outputs "1". If the input of the Sign unit is negative, which means that p_{PV} is decreasing, the sign unit outputs "-1"; otherwise the input of the Sign unit is 0, which means that p_{PV} is the same in the two switching cycles, the Sign unit outputs 0. Similar blocks are applied for the i_{PV} channel. The results of the two channels

are multiplied to determine the perturbation direction. If both current and power increased or decreased simultaneously, the product is 1, which means that I_{ref} should increase by one step, that can be obtained by multiplying the perturbation step size with the perturbation direction. If they change in opposite way, the product is -1, which means that I_{ref} should decrease by one step. This is the principle of the P&O algorithm. If the product is zero, I_{ref} keeps constant in that switching cycle. Because of the oscillation of the current reference I_{ref}, the samplings of two consecutive perturbation cycles on both PV output current and power are not equal to each other, and the product won't be zero in the simulation of steady-state.

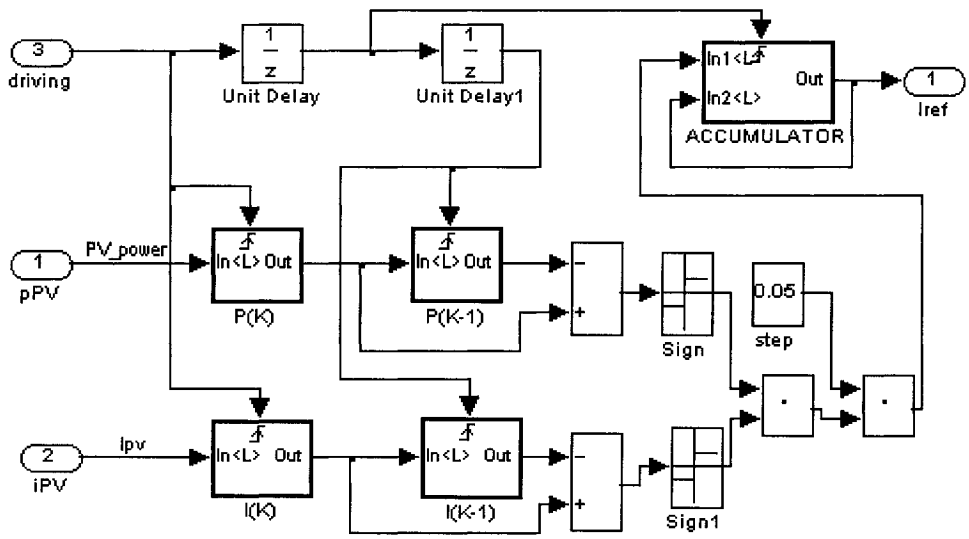

Fig.4.9 The simulation model of MPPT block

1. Accumulator

The Accumulator in the MPPT block shown in Fig 4.9 is a triggered block, which is executed one time when it is fired by the rising edge of the triggering signal. The inside of the accumulator, which is shown in Fig. 4.10, is a summer. One input of the summer is the signed perturbation step. The other input is its output. The triggering signal determines the instant that I_{ref} is updated, as well as the instant when the summing

operation is carried out, once per perturbation cycle. If the Accumulator is not a triggered block, the summing operation will be executed every simulation step size which is determined by Simulink itself, instead of for every perturbation cycle as described in the discussion of the implementation of the P&O algorithm.

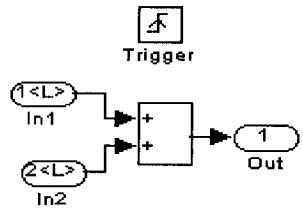

Fig. 4.10 The simulation model of ACCUMULATOR

4.1.5 PCC Block

The Peak Current Control scheme is realized in the PCC block, shown in Fig. 4.11. At the beginning of each switching cycle, a short pulse from the D_{min} block sets the output of the *OR* gate "1", which goes to the gate driver circuit to turn on the power switch and make the inductor current to ramp up. It also unlocks the *AND* gate to permit the output of the comparator to go through it. At the beginning of each cycle, the actual current i_{PV} is usually smaller than I_{ref} and the output of comparator is "1". So even after output of D_{min} block changes from "1" to "0" the output of *OR* will keep "1" until i_{PV} and I_{ref} match, or maybe i_{PV} can not reach I_{ref} in maximum duty ratio D_{max}, then D_{max} block will output "0" to force the *AND* block to output "0" and the *OR* block to output "0", turning off the power switch. So for the arrangement above, the power switch will be on for at least $D_{min}T_{SW}$ and at most $D_{max}T_{SW}$. During the minimum and maximum *ON* time interval, the switching off point depends on the relationship between I_{ref} and i_{PV}. When

i_{PV} reaches I_{ref} the *OR* gate outputs "0" to turn off the power switch and lock the *AND* gate. Once the power switch turns off, it cannot turn on again in the same cycle.

The unit delay is just required by Simulink to prevent the algebraic loop. A compensation ramp is also subtracted from the current reference I_{ref} by a summer.

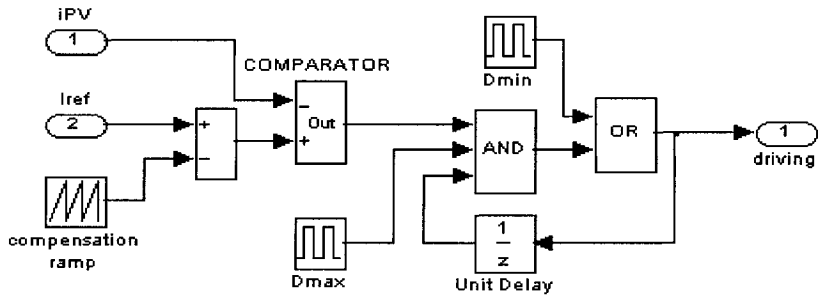

Fig. 4.11 The simulation model of the PCC block

1. Comparator Block

There is no comparator block in the Simulink library. So one comparator is implemented as in Fig. 4.12, where the upper and lower limits of the saturation block are 1 and 0, respectively. If "+" input is larger than "-" input, the summer outputs a positive value, and the sign block outputs 1. Because the upper limit of the saturation block is 1, so the comparator block outputs 1. Otherwise, if "+" input is equal to or less than "-" input, the summer outputs zero or a negative value, and the sign block outputs 0 or -1. Because the lower limit of the saturation block is 0, the comparator block outputs 0.

So if "+" input is larger than "-" input, the comparator block outputs 1, otherwise outputs 0, which is the same as the operation of a comparator.

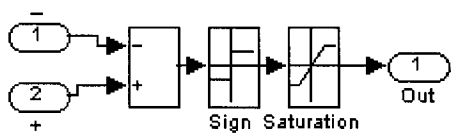

Fig. 4.12 The simulation model of the comparator

4.2 CALCULATION OF THE PARAMETERS FOR THE SIMULATION

The parameters of the PV panels' model under the rated solar irradiation level and temperature are shown below.

I_{SC} = 3.452A, V_{OC} = 21.886V, V_{MPP} = 18.771V, I_{MPP} = 3.267A, P_{MPP} = 61.32W.

From Section 3.3.5, the perturbation step size (I_{step}) can be calculated according to Eq. (3.19). For 12 bits A/D converter the resolution of the A/D converter in terms of current is

$$I_{SC} / 2^{12} = 3.452 / 2^{12} \approx 0.00085A\,(0.85mA)$$

$$2\ times\ the\ resolution\ of\ A/D\ convterter < I_{step} < 0.6 \times (I_{SC} - I_{MPP}) \tag{4.3}$$

$$2 \times 0.85mA < I_{step} < 0.6 \times (3.452 - 3.267) = 0.111A \tag{4.4}$$

I_{step} is chosen as 50mA.

The inductor (L) is also calculated according to Eq. (3.26).

$$\frac{V_{MPP}}{\frac{1}{2} I_{step} + 0.9(I_{SC} - I_{MPP})} D_{\max} T_{sw} < L < \frac{V_{MPP}}{I_{step}} T_{sw} \tag{4.5}$$

$$\frac{18.771}{\frac{1}{2} \times 0.05 + 0.9(3.452 - 3.267)} \times 0.75 \times 10 \times 10^{-6} < L < \frac{18.771}{0.05} \times 10 \times 10^{-6} \tag{4.6}$$

$$0.74mH < L < 3.75mH$$

Here the switching frequency f_{sw} is 100 kHz and the switching cycle is 10us. D_{max} is 0.75.

L is chosen as 1mH.

For the slope of the compensation ramp (m_r), it should satisfy the following inequality:

$$\frac{m_r - m_{off}}{m_{on} - m_r} < 1 \tag{4.7}$$

$$\begin{aligned} m_r &< \frac{m_{on} + m_{off}}{2} \\ &< \frac{\frac{V_{PV}}{L} + \frac{V_{PV} - V_{out}}{L}}{2} \\ &< \frac{2V_{PV} - V_{out}}{2L} \end{aligned} \tag{4.8}$$

Considering that the MPPT system is used to charge a battery bank, V_{out} is assumed to be 24V. The minimum possible value for the PV panels output voltage $V_{PV(min)}$ takes place for $D_{max} = 0.75$ and is calculated as:

$$\begin{aligned} V_{PV(\min)} &= (1 - D_{\max})V \\ &= (1 - 0.75) \times 24 \\ &= 6V \end{aligned} \tag{4.9}$$

So

$$\begin{aligned} m_r &< \frac{2V_{PV(\min)} - V_{out}}{2L} \\ &= \frac{2 \times 6 - 24}{2 \times 1 \times 10^{-3}} \\ &\approx -6 \times 10^3 A/S \end{aligned} \tag{4.10}$$

For the switching frequency of 100 KHz, the magnitude of compensation ramp at the end of each cycle can be computed as:

$$\begin{aligned} T_{SW} \times (-m_r) &= \frac{1}{100 \times 10^3} \times 6 \times 10^3 \\ &= 0.06A \end{aligned} \tag{4.11}$$

The minus sign means that the ramp is subtracted from the reference current (I_{ref}).

4.3 Simulation Results and Analysis

4.3.1 Sampling at the Switching On Point

The proposed system is simulated with MATLAB/Simulink. Fig. 4.13 shows the waveforms of PV output power (p_{PV}), reference current from the output of the MPPT block (I_{ref}), PV output current (i_{PV}) and voltage (v_{PV}) versus time during the start up process from 0 to the MPP under the rated solar irradiation level. There one can see that the start-up process is very short, about 0.7 ms from 0 to the MPP. Fig. 4.14 shows details of the previous waveforms and that the MPPT system operates around the MPP in steady-state.

Fig. 4.15 shows the response of the system when the solar irradiation level increases from 50% (1.7A) to the rated value (3.452A) in 10 ms, which is actually very fast compared to the variation of the practical solar irradiation. The waveforms show that the MPPT system can promptly adjust the operating point, increasing the reference current and the power drawn from the PV panels. From the detailed waveforms in Fig. 4.16, it can be seen that the current reference (I_{ref}) still oscillates, which is because the tracking speed is faster than the variation of the solar irradiation level (I_{SC}). Fig 4.17 shows the system response for a step variation of the solar irradiation level what although not a practical case, allows the assessment of the tracking speed of the MPPT system under "worst case conditions". In this case, I_{ref} goes up all the way until it reaches another steady-state. The response process from one steady-state to another steady-state is also very fast, less than 0.4 ms.

The MPPT system can also adjust to reductions on the solar irradiation as shown in Fig. 4.18, when the short current (I_{SC}) in the PV simulation model decreases from 3.452A

at t=1ms to 1.7A at t=11ms. Fig. 4.19 shows the detailed waveforms of the system response to the reduction on the solar irradiation.

However, as shown in the dashed-line ovals of Fig. 4.15, 4.16, and 4.18, 4.19 the PV output voltage and power fall to zero when the solar irradiation level is close to 1.7A. This is because when the solar irradiation level decreases the range from the MPP to the short-circuit current I_{SC} (I_{SC} - I_{MPP}) also decreases. These phenomena are explained with the help of Fig. 4.20. In Fig. 4.20, S is the solar irradiation level, $S_1 < S_2 < S_3 < S_4$.

$I_{on}(k-1)$, $I_{on}(k)$, $I_{on}(k+1)$, and $I_{on}(k+2)$ are the current samples at the switching on points of the $(k-1)^{th}$, k^{th}, $(k+1)^{th}$, and $(k+2)^{th}$ switching cycle, respectively. $I_{on}(j-1)$, $I_{on}(j)$, and $I_{on}(j+1)$ are the current samplings at the switching on points of the $(j-1)^{th}$, j^{th}, and $(j+1)^{th}$ switching cycle, respectively. $I_{ref}(k-2)$, $I_{ref}(k-1)$, $I_{ref}(k)$, and $I_{ref}(k+1)$ are the current references of the $(k-2)^{th}$, $(k-1)^{th}$, k^{th}, and $(k+1)^{th}$ switching cycle, respectively. $I_{ref}(j-2)$, $I_{ref}(j-1)$, and $I_{ref}(j)$ are the current references of the $(j-2)^{th}$, $(j-1)^{th}$, and j^{th} switching cycle, respectively.

$P_{S1}(k-1)$, $P_{S1}(k)$, and $P_{S1}(k+1)$ are the PV output power at the sampling points of the $(k-1)^{th}$, k^{th}, and $(k+1)^{th}$ switching cycle under the solar irradiation level S_1, respectively. $P_{S2}(k-1)$, $P_{S2}(k)$, and $P_{S2}(k+1)$ are the PV output power at the sampling points of the $(k-1)^{th}$, k^{th}, and $(k+1)^{th}$ switching cycle under the solar irradiation level S_2, respectively. $P_{S3}(k)$, $P_{S3}(k+1)$, and $P_{S3}(k+2)$ are the PV output power at the sampling points of the k^{th}, $(k+1)^{th}$, and $(k+2)^{th}$ switching cycle under the solar irradiation level S_3, respectively. $P(j-1)$, $P(j)$, and $P(j+1)$ are the PV output power at the sampling points of the $(j-1)^{th}$, j^{th}, and $(j+1)^{th}$ switching cycle under the solar irradiation level S_4, respectively. $I_{SC}(S_1)$ is the PV panels short-circuit current relative to solar irradiation level S_1.

Under solar irradiation level S_1, $P_{S1}(k) > P_{S1}(k-1)$. PV output power increases with increasing current. From the P&O algorithm, current reference I_{ref} will be increased to $I_{ref}(k)$. However, because the range from the MPP to $I_{SC}(S_1)$ is small under the lower solar irradiation level S_1, $I_{ref}(k)$ which is obtained by increasing $I_{ref}(k-1)$ by one perturbation step size I_{step} is larger than $I_{SC}(S_1)$. This is why the PV output power and voltage fall to zero. Then $P_{S1}(k) > P_{S1}(k+1)$. The PV output power decreases with increasing current. From the P&O algorithm, current reference I_{ref} will be decreased from $I_{ref}(k)$ to $I_{ref}(k-1)$.

Under solar irradiation level S_2, the situation is similar as solar irradiation level S_1. $P_{S2}(k) > P_{S2}(k-1)$. The PV output power increases with increasing current. The current reference I_{ref} will be increased to $I_{ref}(k)$. Then $P_{S2}(k) > P_{S2}(k+1)$. The PV output power decreases with increasing current. The current reference I_{ref} will be decreased from $I_{ref}(k)$ to $I_{ref}(k-1)$. So both oscillation ranges of I_{ref} under solar irradiation level S1 and S2 are the same. It is verified by the simulation results shown in the dotted oval of Fig. 4.16. It can be seen that the current reference I_{ref} oscillates around the same range in a period of time. Because $I_{ref}(k)$ is smaller than the PV panels short-circuit current relative to solar irradiation level S_2, $I_{SC}(S_2)$, the PV output power and voltage won't fall to zero. When the PV short-circuit current I_{SC}, which increases with rising solar irradiation level, is bigger than the maximum current reference in the oscillation range of I_{ref}, the PV output power and voltage won't fall to zero. This is why PV output power and voltage fall to zero first, and then it is corrected with the increasing solar irradiation level in the simulation results in Fig. 4.15. In Fig. 4.20, under solar irradiation level S_3, $P_{S3}(k) > P_{S3}(k-1)$. I_{ref} is increased from $I_{ref}(k-1)$ to $I_{ref}(k)$. However, because $P_{S3}(k) < P_{S3}(k+1)$, The current reference I_{ref} will not be decreased from $I_{ref}(k)$ to $I_{ref}(k-1)$ as under solar irradiation level

S1 and S2, but be increased to $I_{ref}(k+1)$. Because $I_{ref}(k+1)$ is larger than the PV panels short-circuit current ($I_{SC}(S_3)$) relative to solar irradiation level S_3, PV output current will be brought to $I_{SC}(S_3)$. This is why the PV output power and voltage fall to zero again. Then $P_{S3}(k+1) > P_{S3}(k+2)$. The PV output power decreases with increasing current. The current reference I_{ref} will be decreased from $I_{ref}(k+1)$ to $I_{ref}(k)$. From the simulation results in Fig. 4.16, it can be seen that the PV output power and voltage falling to zero happen again with rising solar irradiation level. However, it will never happen again when the solar irradiation level increases to big enough to satisfy the following discussion.

From Fig. 3.8(b), the maximum reference current happens when the PV output power values of the two consecutive sampling points which just locate before and after the MPP are equal under the certain solar irradiation level, and it is called $I_{ref}(max)$ here. If $I_{ref}(max)$ is smaller than the PV panels short-circuit current corresponding to the solar irradiation level, the PV output power and voltage won't fall to zero again under the increasing solar irradiation level.

In Fig. 4.20, under solar irradiation level S_4, $P(j-1)$ and $P(j)$ are the PV output power values of two consecutive sampling points which just locate before and after the MPP. They are almost equal to each other and I_{ref} is increased by I_{step} to the new current reference ($I_{ref}(j)$), which is less than I_{SC} under solar irradiation level S_4. So the PV output power and voltage won't fall to zero again under the solar irradiation levels larger than S_4, which is also verified by the simulation results under larger solar irradiation levels in Fig. 4.15.

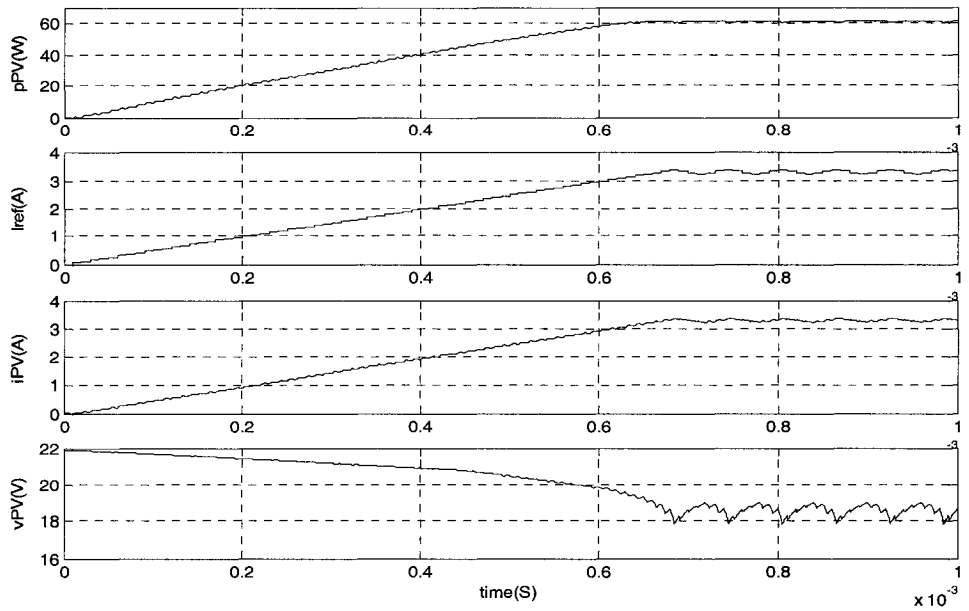

Fig. 4.13 The start up process of the MPPT system under rated ambient conditions

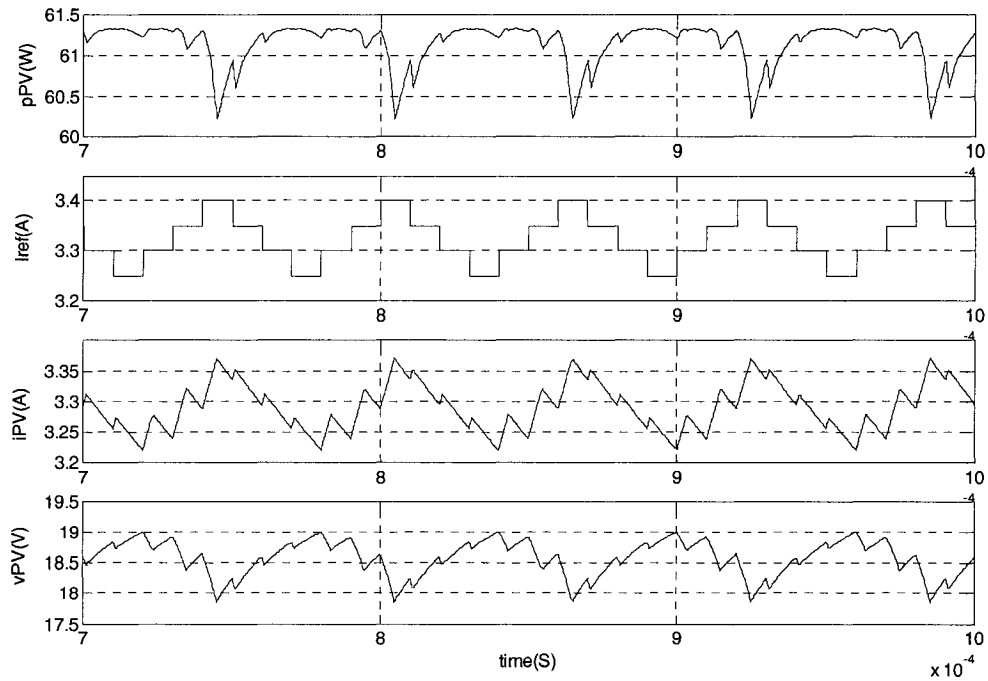

Fig. 4.14 The detailed steady-state waveforms

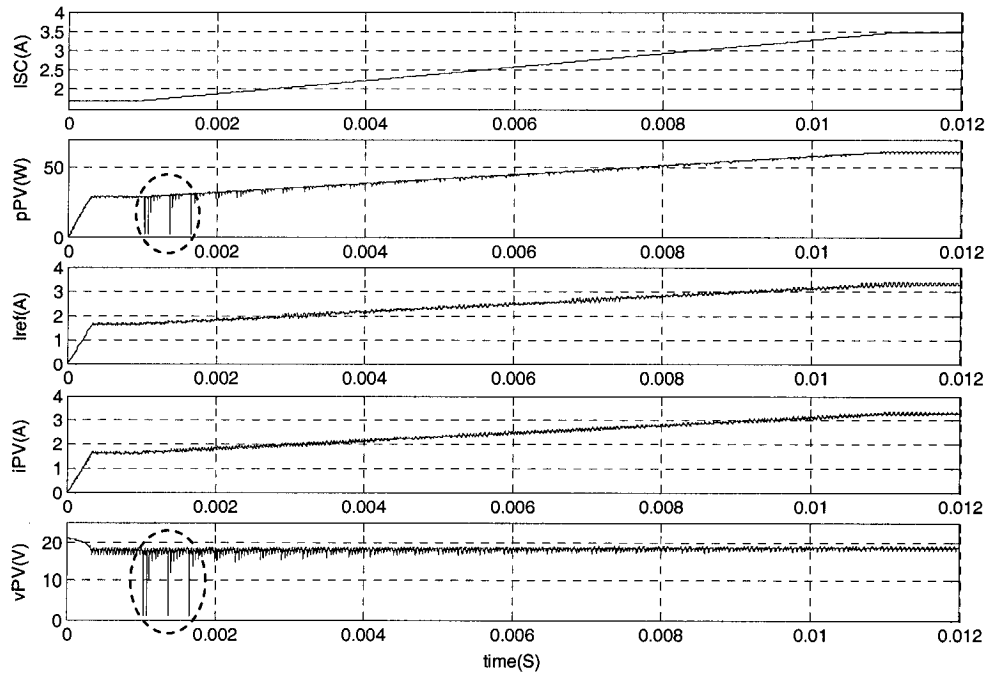

Fig. 4.15 The response when I_{SC} slowly increases from 1.7A to 3.452A in 10 ms.

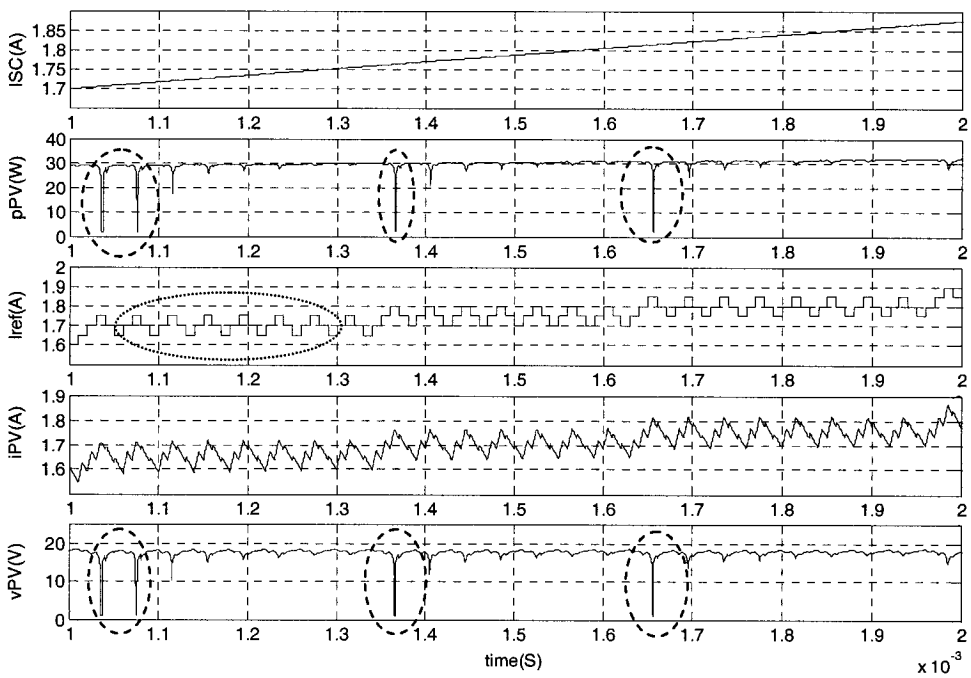

Fig. 4.16 The detailed waveforms when I_{SC} slowly increases

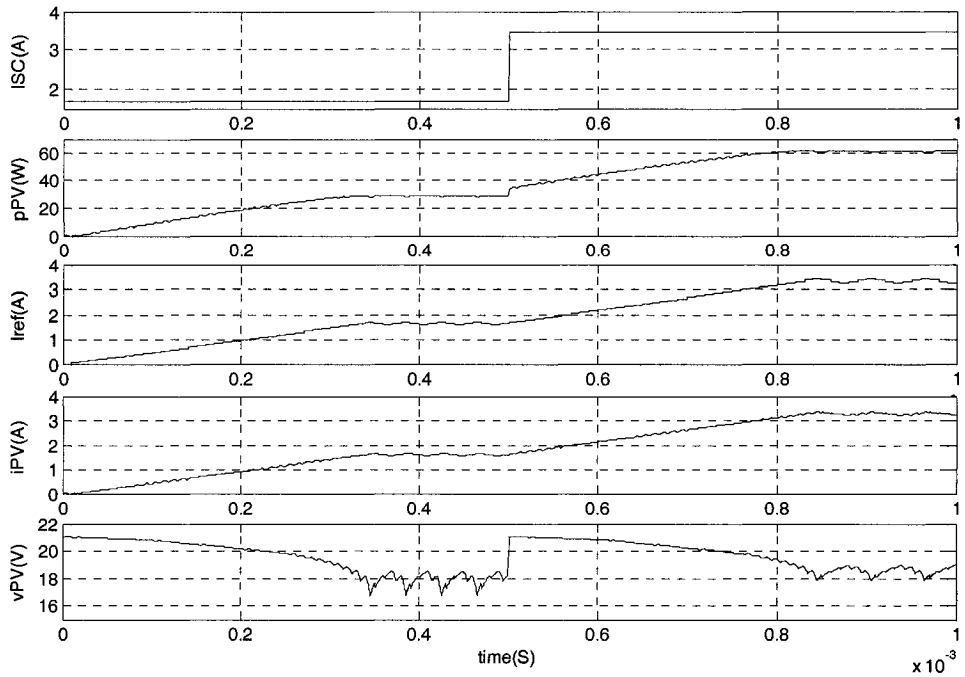

Fig. 4.17 The system response to the stepping up of I_{SC}

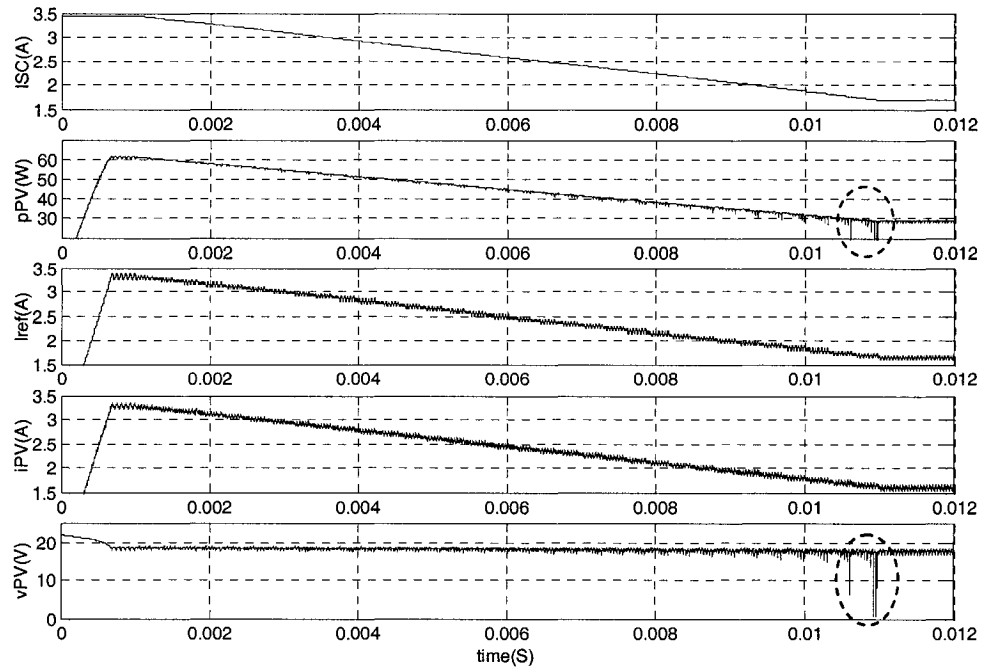

Fig. 4.18 The response when I_{SC} slowly decreases from 3.452A to 1.7A in 10 ms

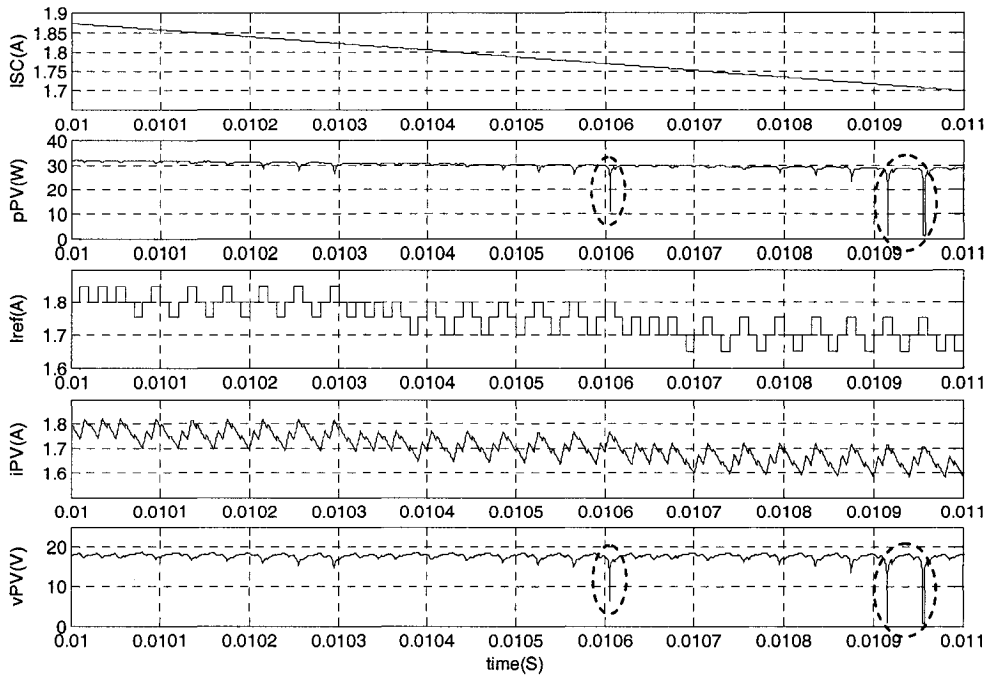

Fig. 4.19 The detailed waveforms when I_{SC} slowly decreases

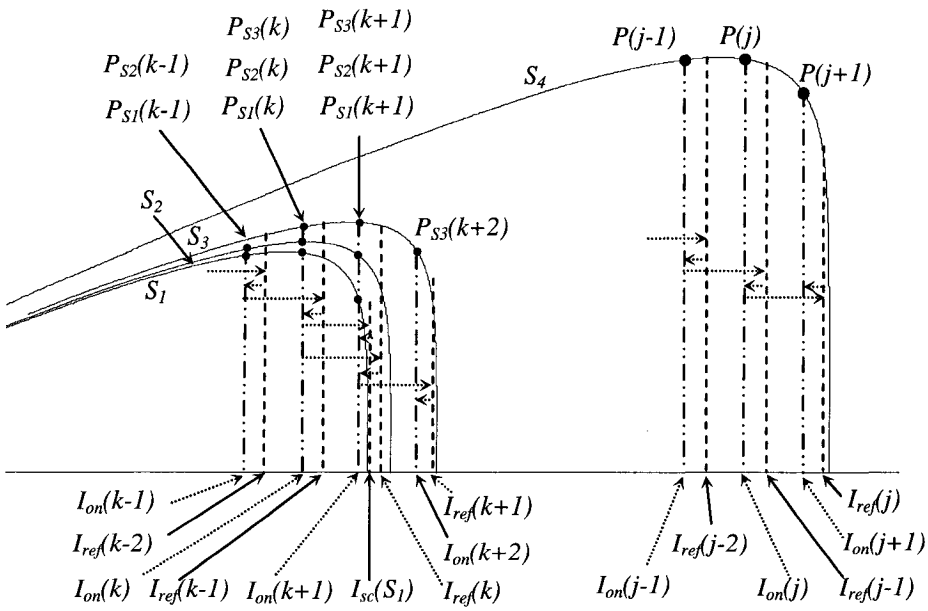

Fig. 4.20 Positions of the maximum I_{ref} relative to I_{SC} under different solar irradiation levels

Fig. 4.21 shows that the system response to a stepping down solar irradiation level. The process from one steady-state to another is very long. First, when I_{SC} steps down, I_{ref} fixes for a while then decreases. This can be explained as follows. When I_{SC} steps down and the PV output current (i_{PV}) is held by the inductor of the boost converter, the theoretical short-circuit current of PV panels is smaller than the inductor current of the MPPT converter (for example, here the new short-circuit current is 1.7A, but the actual inductor current slowly decreases from about 3.2A when I_{SC} steps down), the PV output voltage and power are both zero and the difference of the previous and present power (ΔP_{PV}) is zero during this period. From the diagram of the MPPT block, we know that the perturbation direction is zero. So there is no perturbation to I_{ref} and it keeps constant. Because PV output voltage (v_{PV}) is zero, i_{PV} decreases regardless the fact that I_{ref} is larger than i_{PV}. Then I_{ref} begins to decrease after i_{PV} falls around the new short current $I_{SC(new)}$ corresponding to the new solar irradiation level. That is because when i_{PV} falls below the new short current $I_{SC(new)}$, the PV output power is not zero any more. The MPPT algorithm learns that the PV output power increases with decreasing PV output current and reduces I_{ref}. However, because I_{ref} is bigger than the actual PV output current i_{PV}, the duty ratio is always D_{max} during this phase. i_{PV} falls below the new short current $I_{SC(new)}$ during the switching off period and then is increased to the new short current $I_{SC(new)}$ during the switching on period of each switching cycle. So i_{PV} oscillates around $I_{SC(new)}$ until I_{ref} decreases below $I_{SC(new)}$, and i_{PV} follows I_{ref} decreasing and operating around the new MPP.

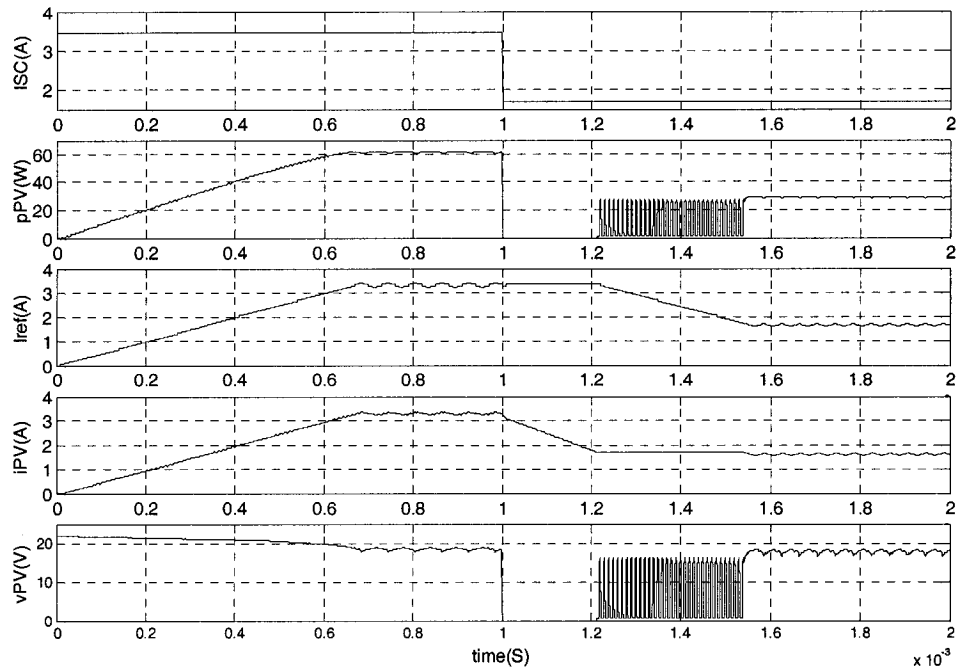

Fig. 4.21 System response to the stepping down I_{SC}

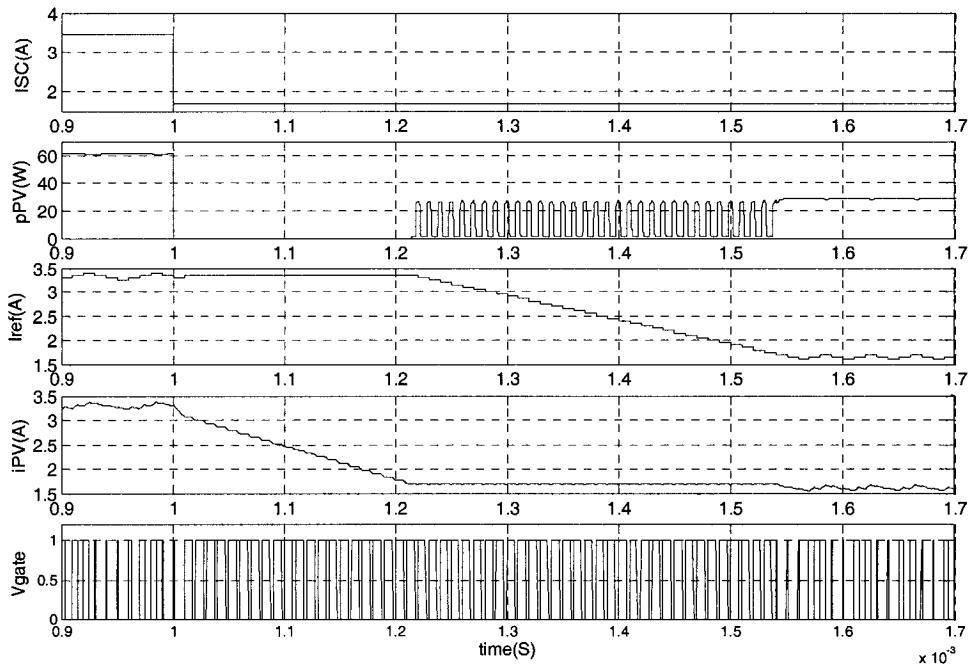

Fig. 4.22 Detailed system response to the stepping down I_{SC}

To solve this problem, a new block (*CS*) is added to the MPPT block, shown in Fig. 4.23, which utilizes the characteristics of PV panels that v_{PV} is zero when i_{PV} is equal to or larger than I_{SC}. If v_{PV} is zero, the current reference I_{ref} should always decrease. However, in practical implementation, even when the PV output terminals are shorted the PV output voltage maybe not zero because of the line resistance. So a constant is set to make that if v_{PV} is smaller than the preset value, it is known that i_{PV} is equal or close to I_{SC} and the current reference is forced to decrease. The constant is not hard to be determined. Actually once the PV output voltage v_{PV} is less than the voltage at the MPP (V_{MPP}), the operating point is on the right side of the MPP of the p x i curve and I_{ref} should be decreased. So it will be fine if the constant is less than the voltage at the MPP, V_{MPP}. Because V_{MPP} is much closer to the open-circuit voltage of PV panels (V_{OC}) than to the short-circuit voltage (0V) (as mentioned before, V_{MPP} is typically about 76% of the V_{OC}). The range of the preset constant can be very large.

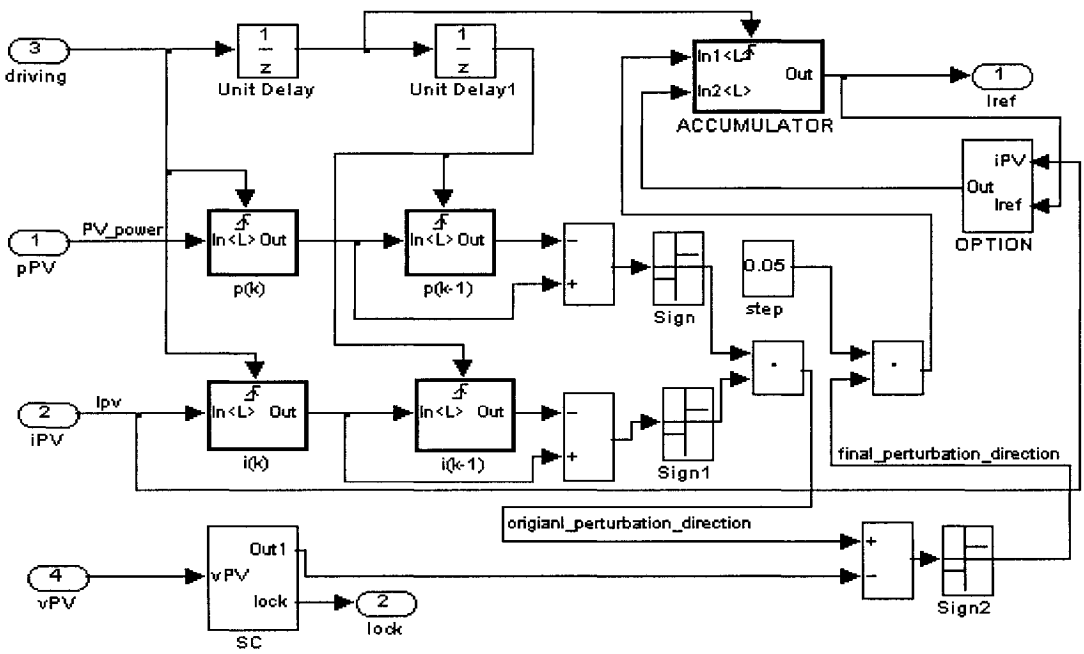

Fig. 4.23 The MPPT block with *SC* and *OPTION* block

In the *SC* block shown in Fig. 4.24, if v_{PV} is larger than a preset constant, which means the operating point is far away from (less than) I_{SC}, the comparator outputs zero. The final perturbation direction is the same as the original perturbation direction; the *SC* block has no effect on the MPPT block under this situation. If v_{PV} is less than the preset constant, which means i_{PV} operates on the right of the MPP, *SC* block outputs 2. Because the original perturbation direction has only three possible values, 1, 0, and -1, the final perturbation direction outputs -1, which means I_{ref} always decreases no matter what the original perturbation direction is. From the simulation waveforms in Fig. 4.23, we can see that I_{ref} begins to decrease when I_{SC} steps down. The transient process in Fig. 4.25 is faster than that in Fig. 4. 21.

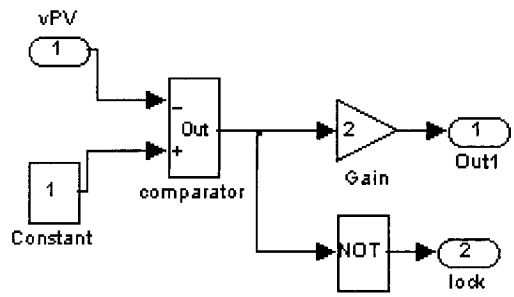

Fig. 4.24 The simulation model of *SC* block

Nevertheless, it is still slow. In Fig. 4.26, one sees that I_{ref} and i_{PV} decrease slowly. The duty cycle of the driving pulses is always max during that period. That is because I_{ref} decreases slowly, the driving pulses have to operate at D_{max} to make i_{PV} decrease slowly. In fact, during this period, because i_{PV} is larger than or close to the new short current $I_{SC(new)}$, which can be learnt from the fact that v_{PV} is less than the preset value, it is wished that the driving pulses operate at the minimum duty ratio to make i_{PV} decrease rapidly. So as shown in Fig. 4.27, there is another input (*lock*) from *SC* block which is "0" when v_{PV}

is smaller than the preset constant and sets the *AND* gate output as "0". The power switch is turned off to make i_{PV} decrease rapidly. Now I_{ref} can not follow the decrease of i_{PV}. To change this situation, another block (*OPTION*) shown in Fig. 4.28 is added in MPPT block. The idea is that when the difference between I_{ref} and i_{PV} is larger than a preset value, I_{ref} is replaced by the actual i_{PV} to add to the perturbation step in *ACCUMULATOR* block and output a refreshed I_{ref}. This preset value is determined according to the idea that the difference between I_{ref} and i_{PV} should not exceed the maximum possible current increment or decrement in each perturbation cycle (equal to the switching cycle here). If the difference between I_{ref} and i_{PV} exceeds the maximum possible current increment or decrement in one switching cycle the actual PV output current i_{PV} can not reach I_{ref} in that switching cycle. From the simulation waveforms in Fig. 4.29, the system response to the stepping down I_{SC} is less than 0.1ms, which is very fast, compared to the transient process without the extra blocks in Fig. 4.21.

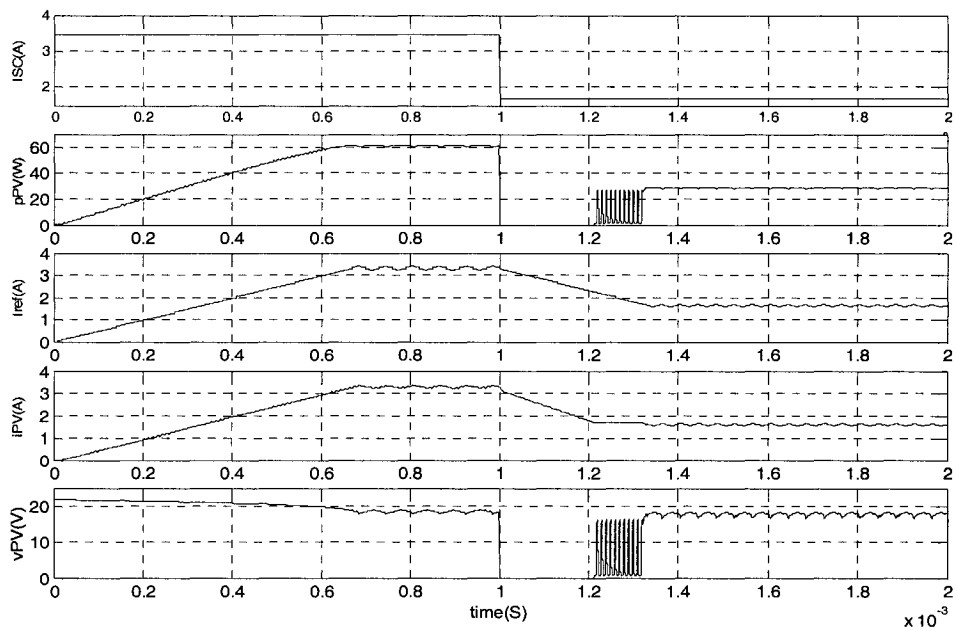

Fig. 4.25 System response to the stepping down of I_{SC} with *SC* block

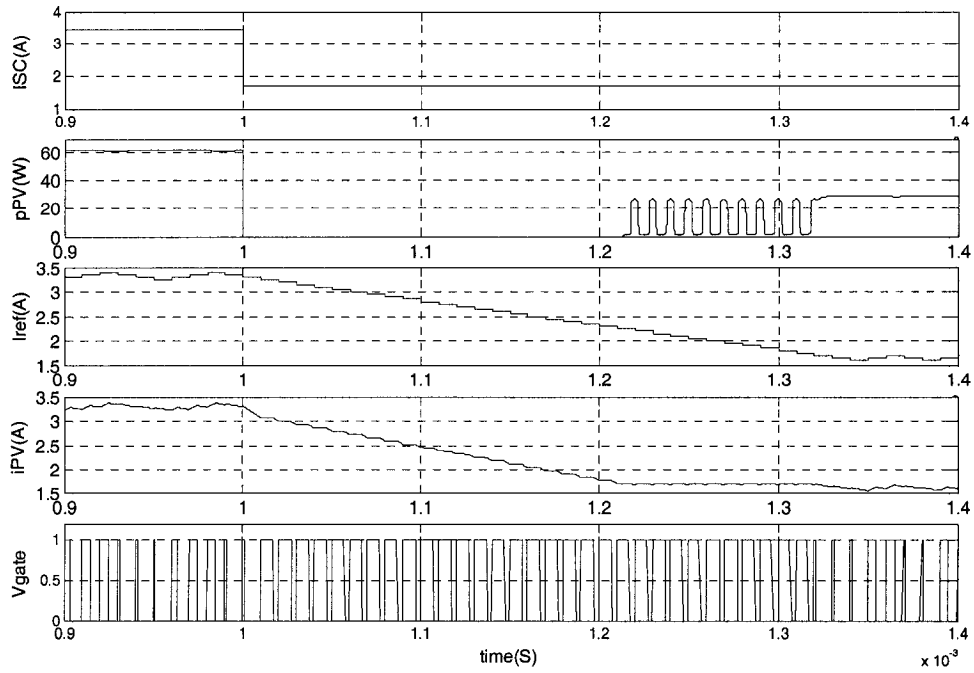

Fig. 4.26 Detailed system response with *SC* block

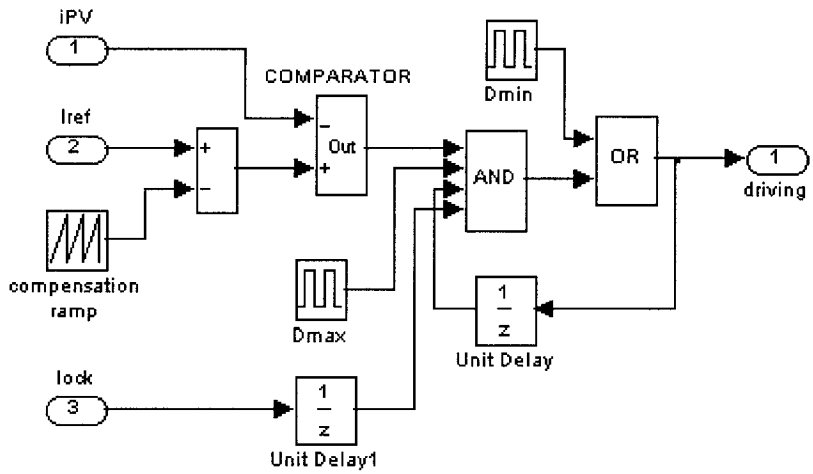

Fig. 4.27 The PCC block with *lock* input

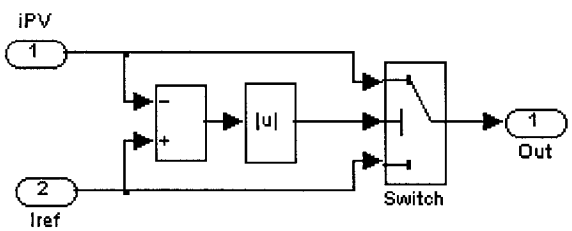

Fig. 4.28 *OPTION* block

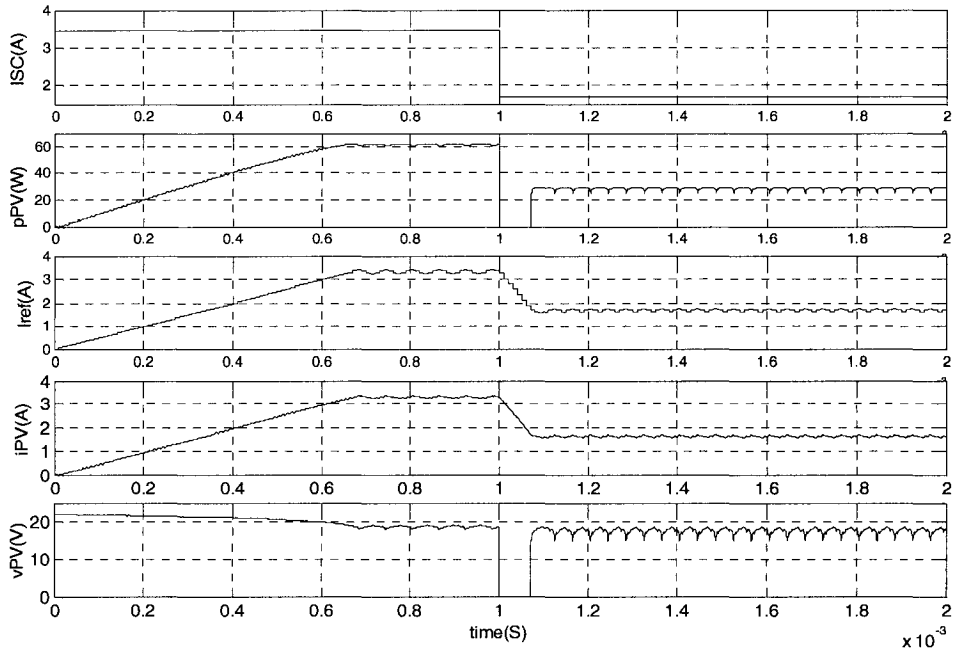

Fig. 4.29 The start-up process with both *SC* and *OPTION* block

4.3.2 Sampling at the Switching Off Point

The implementation of the sampling at the switching off point is very simple. It can be achieved by changing the triggering signal of the Sampling and Holding blocks, P(K), P(K-1), I(K), and I(K-1), and the ACCUMULATOR block in the MPPT block in Fig. 4.23 from rising edge to falling edge.

Fig. 4.30 shows the detailed waveforms of the system with sampling at switching off point in the steady-state. By comparing the steady-state waveforms of I_{ref} and p_{PV} in Fig. 4.30 and 4.14 it can be seen that the maximum value of I_{ref} of the MPPT system with sampling at the switching off point in the steady-state is less than its counterpart in the MPPT system with sampling at the switching on point. The PV output power of the

MPPT system with sampling at the switching off point is higher than that of the MPPT system with sampling at the switching on point. This can be explained as follows.

In the proposed implementation of the P&O algorithm, assuming that I_{ref} is to be decreased, the power in the present sampling point should be less than the power in the previous sampling point. From the p x i curve, it is known that the present sampling point must be on the right of the MPP. In Fig. 4.31, it is assumed that A and B are the previous and present sampling point, respectively, and the power at A, $P(A)$ is larger than the power at B, $P(B)$, which will make I_{ref} to be decreased in next perturbation cycle. Fig. 4.31(a) shows the situation with sampling at the switching on point. Because samples are taken at the switching on point in Fig. 4.31(a), the current at A and B, $I(A)$ and $I(B)$, are equal to the current at the switching on points of previous and present switching cycle, $I_{on}(k-1)$ and $I_{on}(k)$. In this thesis, a boost converter will be used as the MPPT converter, PV current i_{PV} increases during switching on interval and decreases during switching off interval in each switching cycle. The current at the off point is the highest in the corresponding switching cycle. So as shown in Fig. 4.31(a), in present switching cycle both $I_{on}(k-1)$ and $I_{on}(k)$ are less than the current at the off point $I_{off}(k)$, which is also the current reference of present cycle $I_{ref}(k)$.

If samples are taken at the switching off point as shown in Fig. 4.31(b), $I(A)$ and $I(B)$ are equal to the current at the switching off points of previous and present switching cycle, $I_{off}(k-1)$ and $I_{off}(k)$, and $I_{ref}(k)$ is also equal to $I(B)$. Comparing Fig. 4.31(a) and (b), it can be seen that the highest value for the current reference I_{ref} in MPPT system with sampling at switching on point is larger than I_{ref} in MPPT system with sampling at switching off point. This is also seen from the simulation results in Fig. 4. 14 and 30 that

the maximum I_{ref} in MPPT system with sampling at off point is 3.35A while the maximum I_{ref} in MPPT system with sampling at on point is 3.4A.

From the comparison between (a) and (b), MPPT system with sampling at switching on point brings i_{PV} further right side of the MPP, which leads to larger power loss because the PV output power reduces fast after the MPP, especially when i_{PV} is close to I_{SC}. From the simulation results shown in Fig. 4. 14 and 30, one can see that the PV output power of the MPPT system with sampling at the switching off point is larger than that of the MPPT system with sampling at the switching on point.

From the analysis above, comparing with the system with sampling at other points, the system with sampling at the switching off point can draw more power from the PV panels. So the switching off point is the best sampling point from the viewpoint of power loss. This conclusion will also be verified by the experimental results in 4.7.2.

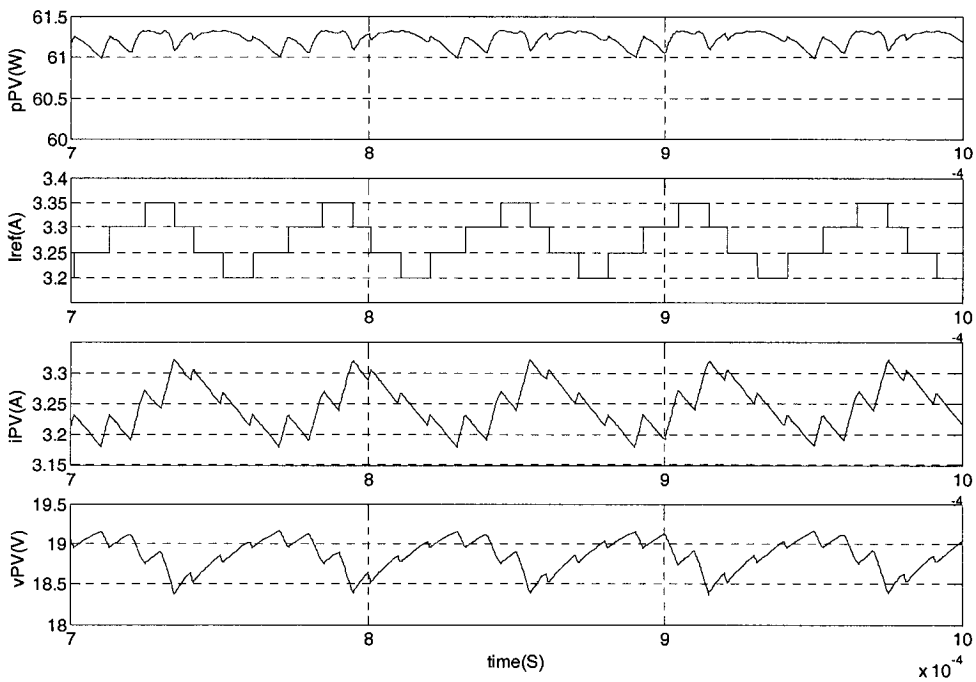

Fig. 4.30 The detailed steady-state waveforms with sampling at off point

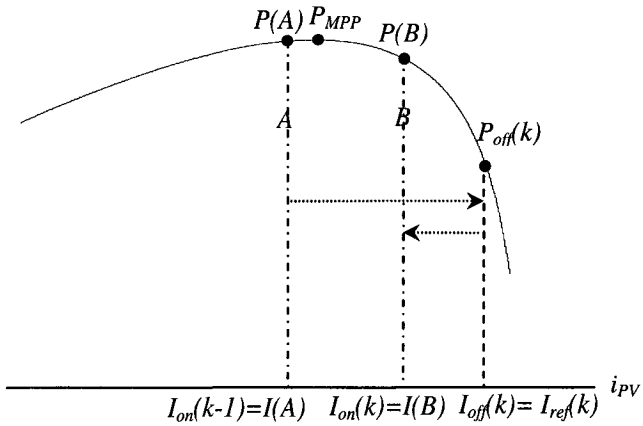

(a)

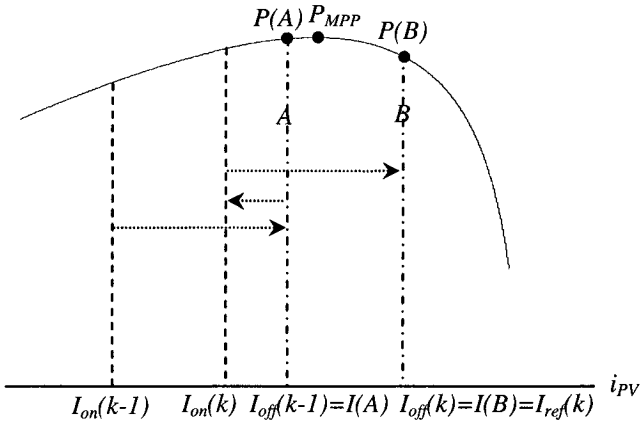

(b)

Fig. 4.31 The comparison of operating points between sampling at switching on and off points

a. sampling points at switching on point;

b. sampling points at switching off point

4.4 Introduction To The dSPACE System

An experiment is conducted to verify the performance of the new P&O MPPT algorithm proposed in this thesis. In the experiment, the MPPT algorithm and Peak Current Control are implemented with a DSP system from dSPACE. The PV panels' output current i_{PV} and voltage v_{PV} are sensed and processed by the DSP system. Then, PWM pulses are outputted to the driving circuit of the boost converter. So fully digital control is realized.

4.4.1 Introduction

The dSPACE system is a hardware architecture used for rapid prototyping of electrical control systems, which is comprised of DS1103 PPC controller board. It is equipped with a Motorola PowerPC 604e processor, whose computing power allows for the simulation of large-scale floating-point control algorithms in real-time. A full range of I/O devices including a TMS320F240 slave DSP is available on-board. Using the Real-Time Interface to Simulink, automatic code generation from block diagrams is possible. I/O functions are specified graphically as part of the simulation model.

4.4.2 Hardware Architecture

The DS1103 PPC Controller Board is equipped with a Motorola PowerPC 604e processor for fast floating-point calculation at 333MHz. This high-performance superscalar microprocessor has three integer execution units, one floating-point arithmetic unit, and a separate load/store unit for fast memory access. The on-chip cache

size is 32kByte for instruction and data. The processor's ability to execute instructions out-of-order leads to a performance improvement of about factor 2 for typical simulation models compared to strictly serial instruction flow.

A 2MByte local memory is used for program and data of the simulation model. The local memory is fully cached and cannot be accessed by the host PC in standard operation mode. For data buffering and exchange between PowerPC and the host, up to 128 MByte of non-cached global memory is available. The host interface of the board is used to perform board setups, program downloads, and runtime data transfer. It supports Plug&Play functionality for easy installation.

I/O Section

The board can be adapted to a wide range of closed-loop applications due to its large number of I/O devices. High-resolution A/D converters (16-bits and 12 bits) with a sampling time of 4us and 800 ns, respectively, are available, as well as D/A output channels with a resolution of 14-bit and a 5 us settling time. 32 digital I/O channels and a serial line interface complete the list of standard I/O units.

4.4.3 Real-Time Interface to Simulink

Using MATLAB and Simulink for modeling, analysis, design and offline simulation has become a de-facto standard for control system development. The Real-Time Interface enhances the Simulink block library with additional blocks, which provide the link between Simulink and the real-time hardware, as shown in Fig.4.32. To graphically specify an I/O channel the corresponding block icon has to be picked up from the I/O block library and attached to the Simulink controller model. I/O parameters, such as

voltage ranges or resolutions, can be set in appropriate dialog boxes. The Simulink model then is transferred into real-time code, using the Real-Time Workshop, state flow control, and the Real-Time Interface. Code generation includes the I/O channel specification and the multitasking setup, which are translated into appropriate function calls of the Real-Time Library. The library is a C function library providing a high-level programming interface to the hardware. The Real-Time Library also includes access functions for the slave DSP. These blocks cover the I/O functionality of the prototyping hardware.

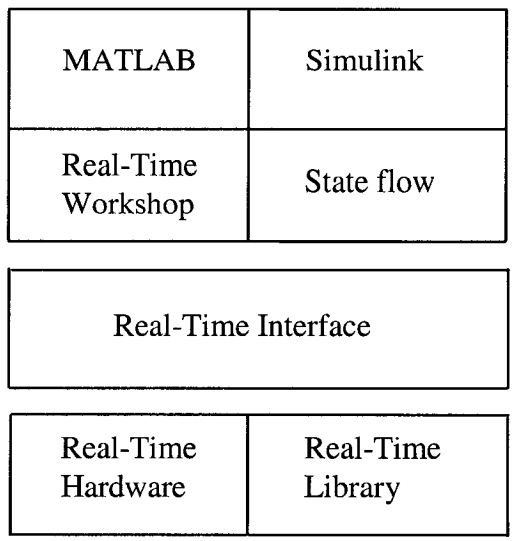

Fig.4.32 The Real-Time Interface in the MATLAB/Simulink environment

4.4.4 Simulink Block Library for DS1103

The block library for the DS1103 PowerPC Controller Board is subdivided into two major parts according to the two microprocessor units on the board. The library shown in Fig. 4.33 comprises all I/O units that are directly served by the PowerPC master processor. Block icons for the standard I/O channels such as A/D, D/A converters, and digital I/O are included as well as the more complex incremental encoder blocks.

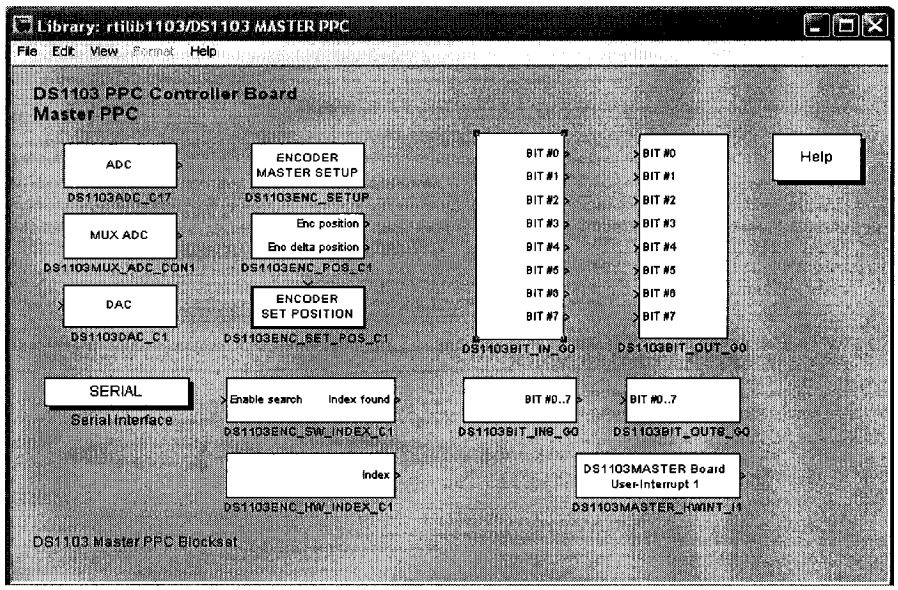

Fig.4.33 Master Processor block library for Simulink

The slave DSP library, shown in Fig.4.34, offers frequently used functions of the TMS320F240, such as single-phase and three-phase PWM signal generation, frequency measurement, A/D conversion, and digital I/O. Because the real-time simulation is executed in the master PPC board, it is wished to employ the functions provided by the slave DSP as much as possible to save the computation time on the Master PPC board.

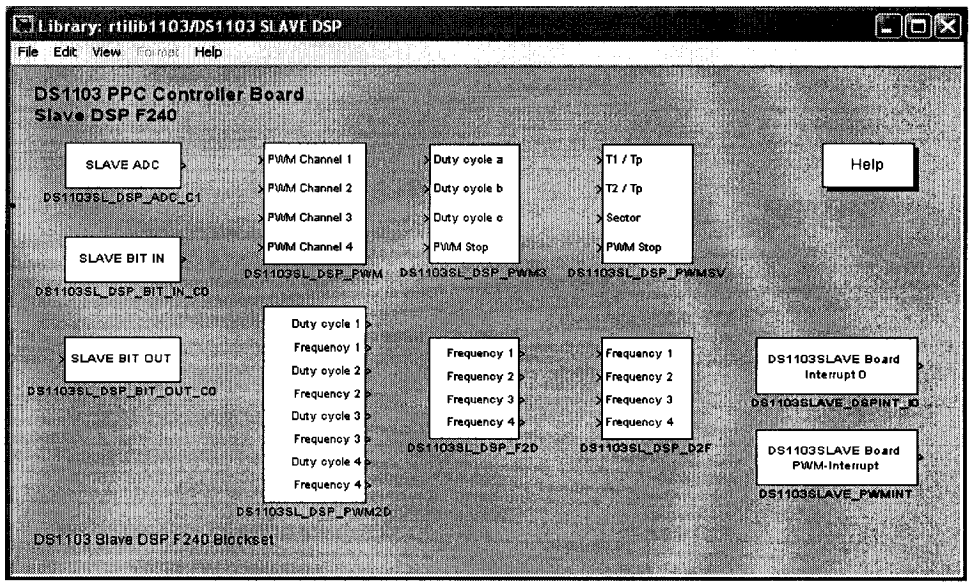

Fig. 4.34 Slave DSP block library for Simulilnk

4.5 PRACTICAL LIMITATION OF dSPACE SYSTEM

In the dSPACE system, PWM waveform can be generated by the PWM generator block in the Slave DSP F240 library. The PWM frequency is set in advance ranging from 1.25Hz to 5MHz. The duty ratio of the PWM waveform is given to the PWM generator block by the MASTER PPC controller board. The real time simulation operates in a fixed simulation step size, which means the simulation program of the control system designed in Simulink and downloaded to the dSPACE system is executed in the time period determined by the fixed simulation step size. So the duty ratio of the PWM waveform is given to the PWM generator block every simulation time period.

However, Peak Current Control scheme is employed as the controller of the MPPT control system of the thesis, which is achieved by the comparison of I_{ref} and i_{PV}. The PWM generator block in the Slave DSP F240 library PWM waveform cannot be utilized. The operation of the comparison of I_{ref} and I_{PV} is only executed in the MASTER PPC controller board and in fixed simulation step size, which is 10us. So the switching on time in each PWM pulse is always adjusted by a multiple of 10us. Because the resolution of the duty ratio is obtained by the minimum variation of the switching on time of the PWM pulse divided by switching time period, the switching time period has to be increased to make the resolution of the duty ratio and the control error small. For example, if the MPPT converter needs duty ratio of 0.636 for perfect control and the resolution of the duty ratio is 0.01, then 0.64 of duty ratio has to be used for the minimum control error of (0.64-0.636)/0.636 ≈ 0.63%. If the resolution of the duty ratio is 0.1, then 0.6 of duty ratio has to be used for the minimum control error of (0.636-0.6)/0.636 ≈

5.7%, which is much larger than the former one. So the smaller the resolution of the duty ratio, the better it is for control precision. However, because the minimum variation of the switching on time of the PWM pulse here is fixed, the smaller resolution of the duty ratio means larger switching time period and lower switching frequency, which is not expected for the MPPT converter. So a trade-off has to be made between control precision and switching frequency.

In this thesis, a switching frequency of 10 KHz is chosen, which means the resolution of the duty ratio is 0.1 and the duty ratio can be only the values of 0.1, 0.2, ... It can not fall into the values between any consecutive two values above, which make the control not very precise and results in lower performance. The limitation of dSPACE system mentioned above can be overcome by FPGA system.

4.6 EXPERIMENTAL SETUP

The diagram of the MPPT system is shown in Fig. 4.35. From the diagram we can see that the system is comprised of three parts, PV Panels, boost converter, and the MPPT controller.

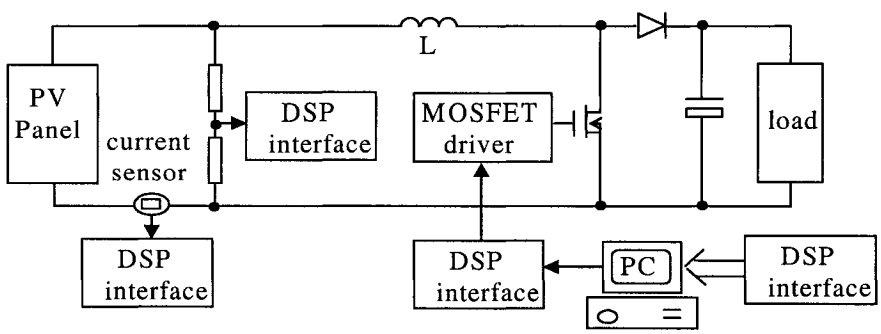

Fig. 4.35 The diagram of the MPPT system in the experiment

4.6.1 PV Panels

Both PV panel simulator and real PV panels are used to test the MPPT system in the experimental set-up.

1. PV panel simulator

The Agilent E4350B Solar Array Simulator (SAS) is employed as the PV panel simulator. It is a dc power source that simulates the output characteristics of a solar array. The Agilent SAS is primarily a current source with very low output capacitance. It is capable of simulating the *i-v* curve of a solar array under different conditions such as temperature and age. The *i-v* curve is programmable over the IEEE-488.2 bus and is automatically generated within the Agilent SAS. The Agilent SAS has three operating modes:

Fixed Mode: This is the default mode that occurs when the unit is first powered up. The i x v output has the rectangular characteristics of a standard power supply, but with excellent high speed constant current characteristics and low output capacitance.

Simulator Mode: An internal algorithm is used to simulate a i x v curve. One can easily approximate the curve through four input parameters: open circuit voltage (V_{OC}), short-circuit current (I_{SC}), current at the approximate maximum power point on the curve (I_{MPP}), and voltage at the approximate maximum power point on the curve (V_{MPP}).

Table Mode: The Agilent SAS provides a table mode for a more accurate i x v simulation of solar arrays. In this mode, a table of i x v points, often provided by the solar array manufacturer, specifies the curve.

In the experiment the Simulator Mode is used and the program to put the i x v curve in SAS is shown Appendix A2.

2. Real PV Panels

A PV panel manufactured by Siemens Solar Industries is used in the experiment. The model No. is SM110-P, which is comprised of two modules that can be used separately, in series for high output voltage, or in parallel for low output voltage and large current. Each module has the following parameters under standard test conditions of 1000W/m^2, 25°C cell temperature. In the experiment, only one module is employed to verify the proposed implementation of the P&O MPPT algorithm.

The open circuit voltage (V_{OC}) is 21.7V.

The short-circuit current (I_{SC}) is 3.45A.

The voltage at the MPP (V_{MPP}) is 17.5V.

The current at the MPP (I_{MPP}) is 3.15A.

4.6.2 The MPPT Converter

In the MPPT system implemented, the load was not a 24V battery as assumed in the simulation, but a variable resistor load for simplicity. As in section 3.3.5, the *calculation of the power components* in the MPPT converter, the rated voltage of MOSFET and Diode is 1.5 times output voltage, which is 24 x 1.5 = 36V, and the rated current is 1.2 times short-circuit current of the PV panels, that is 3.45 x 1.2 = 4.14 A. Diode MBR1645 and HEXFET L2505S are used here.

From Eq. 3.19, the perturbation step size I_{step} should be determined as following:

$$2\ times\ the\ resulution\ of\ A/D\ convterter < I_{step} < 0.6 \times (3.45 - 3.15) \quad (4.12)$$

So $I_{step} = 0.1$A.

The inductor is determined according to Eq 3.26:

$$\frac{17.5}{\frac{1}{2}\times 0.1+0.9(3.45-3.15)}\times 0.75\times 100\times 10^{-6} < L < \frac{17.5}{0.1}\times 100\times 10^{-6}$$

$$4.1mH < L < 17.5mH \tag{4.13}$$

For the rated current of the circuit (3.15A), the largest inductor available in the laboratory was 600uH. 4 inductors were connected in series yielding 2.4mH. It is below the minimum value calculated. However, since the duty cycle under normal conditions is smaller than the value used for the calculation of the minimum inductor, the actual ripple for normal operating conditions was very close to the design specification (0.32A).

The output capacitor was chosen just large enough for small output voltage ripple.

4.6.3 The Controller

The control circuit implemented in dSPACE system is shown in Fig. 4.36. We can see that the dSPACE system just samples the PV panels output current i_{PV} and voltage v_{PV} by A/D converters, then processes them and outputs the PWM signals to the driving circuit of the boost converter by the I/O unit. The gains of the PV output voltage and current channel are chosen in terms of the following considerations.

First, the scaling between the analog input voltage and the output of the A/D blocks is as follows:

Input voltage range	Simulink output
-10V...+10V	-1...+1

For the PV output voltage channel, because the maximum input voltage of the A/D converter is 10V and the open circuit voltage of the PV panels is 21.7V, which is

maximum voltage of the PV panels, a voltage divider is used to limit the input voltage of the A/D converter to 10 V with the maximum PV output voltage (21.7V). To restore the PV output voltage in the Simulink, the gain used in PV output voltage channel is computed as follows:

$$\frac{21.7}{10} \times Gain\, V_c = 21.7,\ \text{Gain } V_c = 10 \tag{4.14}$$

Similarly, for the PV output current channel, because the maximum input voltage of the A/D converter is 10V and the short-circuit voltage of the PV panels is 3.45A, which is maximum output current of the PV panels, the output resistor of the current sensor (LA 55-P with input to output ratio of 1000:1) is calculated to limit the input voltage of the A/D converter to 10 V with the maximum PV output current (3.45A). The value of the output resistor and the gain used in PV output current channel are computed as follows:

$$\frac{10}{3.45 \times 10^{-3}} = 2.9K\Omega \tag{4.15}$$

$$Gain\, I_c = \frac{1}{2.9 \times 10^{3} \times 10^{-3}} \times 10 = 3.45 \tag{4.16}$$

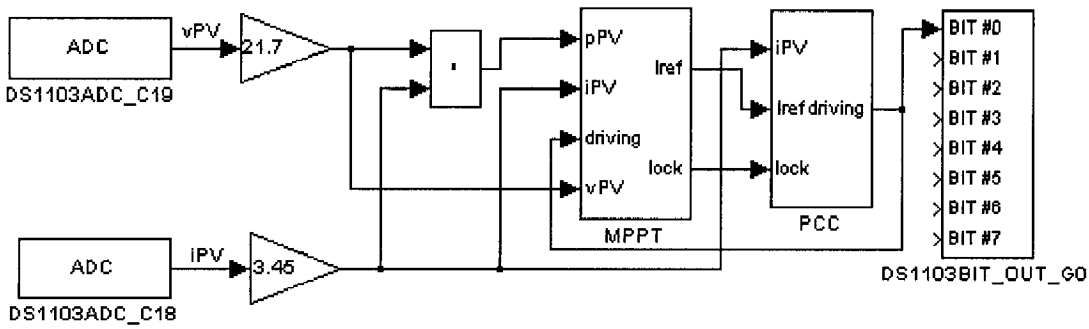

Fig.4.36 The control circuit in DSP system

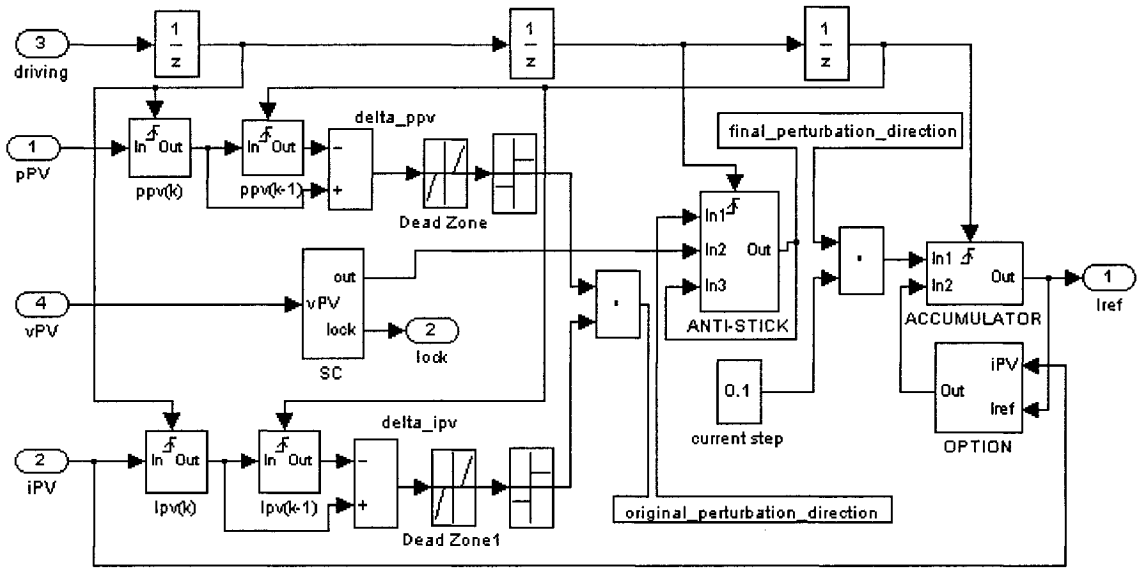

Fig.4.37 The MPPT model in dSPACE system

The contents of the MPPT block in the experiment, shown in Fig.4.37, are almost the same as of the MPPT block in the simulation. Two more blocks were added: An ANTI-STICK block and DEAD-ZONE unit, as explained below.

In practical implementations, the difference between the present PV output power $P_{PV}(k)$ and previous one $P_{PV}(k-1)$ or the present PV output current $I_{PV}(k)$ and previous one $I_{PV}(k-1)$, ΔP_{PV} or ΔI_{PV}, can be zero when the differences are too small to be distinguished by the A/D converters. Then the perturbation direction, which is the product of ΔP_{PV} and ΔI_{PV}, is zero and I_{ref} will not be perturbed. This may cause the differences of power and current of two consecutive sampling points, ΔP_{PV} and ΔI_{PV}, to be zero and I_{ref} will not be perturbed again. So the operating point may "stick" there and the MPPT function fails. To prevent the situation above from happening, the ANTI-STICK block, shown in Fig. 4.38, is added. The idea is that when the original perturbation direction in Fig. 4.37 is zero, the final perturbation direction of the next cycle is kept the same as the perturbation

direction of the previous cycle. In Fig. 4.38, when In1 is not zero, which means the product of the differences of i_{PV} and p_{PV} is not zero, the SWITCH unit outputs In1. The original non-zero perturbation direction is kept at the output of the SWITCH unit. If In1 is zero, SWITCH outputs In3, which is the output of the ANTI-STICK block. So the present perturbation direction is held. If the operating point is close to or beyond the short-circuit PV output current, In2 is -2, which comes from the SC block and sets the output of ANTI-STICK block -1, irrespective of the output of the SWITCH unit. I_{ref} always decreases until In2 is zero.

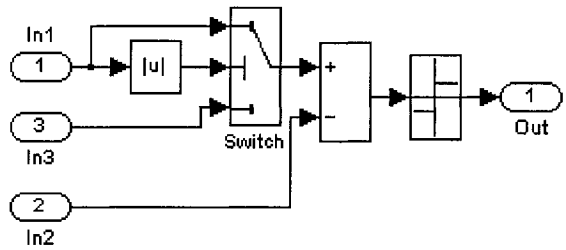

Fig.4.38 The ANTI-STICK block in dSPACE system

The DEAD_ZONE units are added after the difference of p_{PV} and i_{PV}, ΔP_{PV} and ΔI_{PV}. When real ΔP_{PV} and ΔI_{PV} are small, they cannot be computed correctly because of the noise. So when ΔP_{PV} and ΔI_{PV} fall into the set ranges, the DEAD_ZONE units output zero.

There are three UNIT_DELAY units in implemented MPPT block. The first DELAY unit is used to avoid the switching on noise while sampling p_{PV} and i_{PV} after a delay of the rising-edge of the driving signals.

The second DELAY unit gives p_{PV} and i_{PV} channels some time to process the sampled values and obtain the original perturbation direction. Then the ANTI-STICK block is

triggered to output the final perturbation direction in terms of the original perturbation direction.

Now the third DELAY unit shifts the present p_{PV} and i_{PV} samples to the P_{PV}(k-1) and I_{PV}(k-1) blocks to prepare for the next cycle, and trigger the ACCUMULATOR block to update I_{ref}.

4.7 Experimental Results and Analysis

4.7.1 MPPT System with Solar Array Simulator (SAS)

1. Sampling at the switching on time instant

Fig. 4.39 shows the start up process of the MPPT system connected to the Solar Array Simulator (SAS). At the beginning, the SAS is disconnected from the MPPT system and the MPPT system is working. It can be seen from the Fig. 4.39 that I_{ref} increases because of ΔP_{PV} and ΔI_{PV} are both zero and the initial output value of the ANTI-STICK block is 1. When the difference between I_{ref} and i_{PV}, which is zero because of the disconnected SAS, exceeds the limit set by OPTION block, the OPTION block outputs i_{PV} to ACCUMULATOR block. The new I_{ref} is pulled down to i_{PV} = 0A and then it increases again. So I_{ref} looks like a sawtooth waveform before the SAS is connected to the MPPT system. Here the limit between I_{ref} and i_{PV} in the OPTION block is 1A, which is the maximum possible current increment in one switching cycle. That may happen at the beginning of the start up process with the PV open circuit voltage (V_{OC}) and maximum duty ratio. As an approximate calculation, the maximum possible current increment in one switching cycle should be less than

$$\frac{V_{OC}}{L} \times T_{SW} = \frac{21.7}{2.4 \times 10^{-3}} \times 100 \times 10^{-6} \approx 1A \tag{4.17}$$

Once the SAS is connected to the MPPT system, i_{PV} increases much faster than I_{ref} because of the minimum duty ratio and low output voltage of the converter with a capacitive resistive load at the beginning. I_{ref} steps up two times because the difference between I_{ref} and i_{PV} exceeds the limit. If the load of the MPPT system is a battery, i_{PV} cannot increase as fast as that in the MPPT system with a capacitive/resistive load because i_{PV} increases during the switching on interval and decreases during the switching off interval of each switching cycle even in the start up process.

The start up process is about 6 ms, which is relatively long if compared to the simulation results. This is because the output capacitor of the converter needs to be charged.

One can also see from Fig. 4.39 that v_{PV} decreases from V_{OC} = 21.7V to about 4V at the beginning of the SAS connecting to the converter and i_{PV} increases rapidly. However, it is known from p_{PV} curve that the MPP in transient process is lower than the MPP in the steady-state. This shows the dynamic output characteristic of the SAS is not very good. Ideally the p x i curve of the PV panels under unchanged ambient conditions should be fixed, and there is one and only one output power value for a PV output current i_{PV}. There should be also only one MPP for given ambient conditions.

Fig. 4.40 shows the waveforms in the steady-state. It can be seen that i_{PV} operates around 3.15A, but the averaged value of i_{PV} is a little higher than 3.15A because of the sampling at switching on time instant. The output averaged power of PV panels is about 52W, which is close to the maximum PV output power (55W). From the Fig. 4.39, it can

be seen that the oscillation range of I_{ref} in the steady-state is very large, which has many steps, and it is also irregular. This is also because of the poor p x i output characteristic of the SAS for high operation frequency. For example, if the current and power of two consecutive sampling points "A" and "B" are $I_{PV}(A)$, $I_{PV}(B)$, and $P_{PV}(A)$, $P_{PV}(B)$, respectively; i_{PV} is increasing and $I_{PV}(A) < I_{PV}(B)$, and $P_{PV}(A) < P_{PV}(B)$, I_{ref} is increased. However, assuming that i_{PV} decreases and the two consecutive sampling points are also "A" and "B" after a period of time; "A" is the present sampling point and "B" is the previous sampling point, and $I_{PV}(A) < I_{PV}(B)$ again. Now $P_{PV}(A)$ is less than $P_{PV}(B)$ because that SAS can not output the same power for the same current, then I_{ref} is decreased. So on the same position of p x i curve I_{ref} is increased with increasing i_{PV} and decreased with decreasing i_{PV} which makes the oscillation range of I_{ref} larger. The fact that I_{ref} may be increased or decreased for the same position on the p x i curve also makes the oscillation of I_{ref} in the steady-state irregular. From the experimental waveforms of the MPPT system with real PV panels shown in Fig. 4.46, one sees that the oscillation range of I_{ref} is smaller and more regular.

Fig. 4.41 shows the system response to the stepping down and ramping up of I_{SC}. Fig. 4.42 shows the system response to the stepping up and ramping down I_{SC}. Fig. 4.43 and 44 show the detailed waveforms of system response to the stepping down and stepping up of I_{SC} between 1.7A and 3.45A, respectively. The MPPT system responses to the ramping up and down of I_{SC} in Fig. 4.41 and 42 seem very well.

It is shown in Fig. 4.43 that the system response time to the stepping down of I_{SC} is about 1.5 ms, which seems very fast. However, it should be faster than 1.5 ms because of the OPTION block making I_{ref} step down. The cause of the slow response to the stepping

down is the relatively poor p x i output characteristics of the Solar Array Simulator (SAS), making the system response to the stepping down of I_{SC} longer. In Fig. 4.43, when I_{SC} steps down, v_{PV}, p_{PV}, and I_{ref} also step down. Then i_{PV} decreases and v_{PV} increases. However, because SAS can not completely simulate the p x i output characteristics of the PV panels during the transient process, v_{PV} increases too much. Comparing the PV output voltage of the two points on the two vertical dashed lines with identical PV output current, the voltage in transient process is larger than the voltage in the steady-state. Then SAS modifies its output voltage, which makes the transient process longer. The fact that the SAS can not completely simulate the p x i output characteristics of the PV panels during the transient process is demonstrated by that. In Fig. 4.41, when I_{SC} steps down to 1.7A the current at the MPP is set to 1.55A. Because the voltage at the MPP just changes a little with variation of the irradiation level, it is assumed the same with different solar irradiation levels in SAS, which is set as 17.5V. So the power at the MPP is 1.55 x 17.5 ≈ 27W for I_{SC} = 1.7A solar irradiation level. However, from the waveforms in Fig. 4.43 the power at some points is larger than 30W before the system response settles down.

In Fig. 4.44 the time of response to the stepping up of I_{SC} is about 1.6 ms. The theoretical time from I_{SC} = 1.7A to 3.45A is

$$\frac{3.15-1.55}{0.1A}\times 0.1ms = 1.6ms \tag{4.18}$$

in which, 3.15A is the current at MPP with I_{SC} = 3.45A; 1.55A is the current at MPP with I_{SC} = 1.7A; 0.1A is the perturbation step size; 0.1 ms is the tracking time period (also the switching time period).

So it can be seen from the calculation above that the practical system response time matches the theoretical time for the system response to the stepping up of I_{SC}.

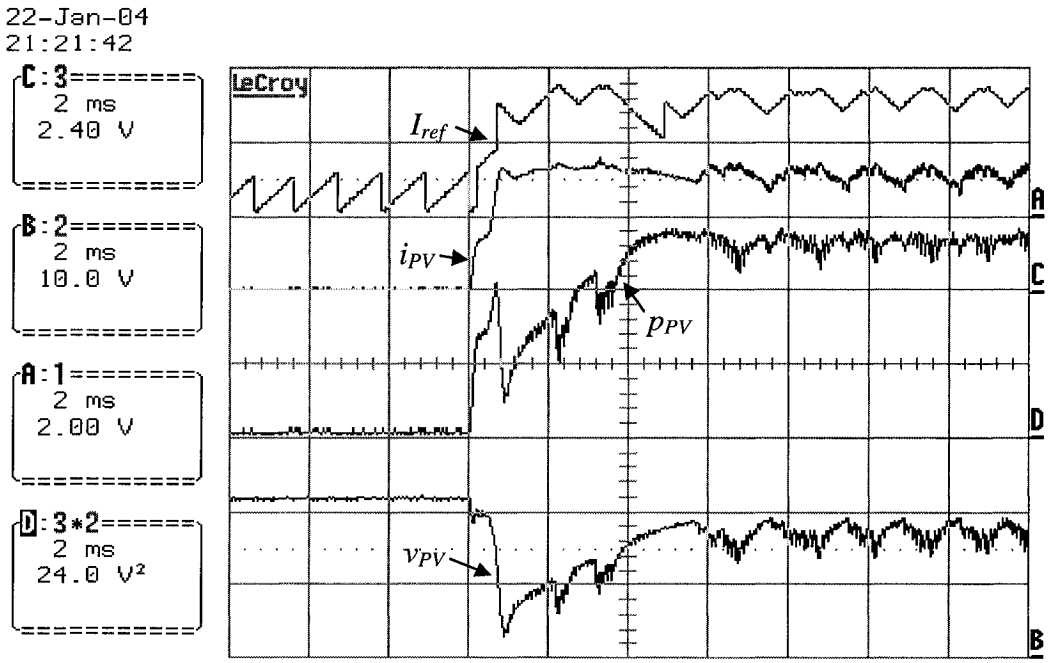

Channel A: I_{ref}, 2A/div, B: v_{PV}, 10V/div, C: i_{PV}, 2A/div, D: p_{PV}, 20W/div

Fig. 4.39 Start up process with SAS as the input of the MPPT system

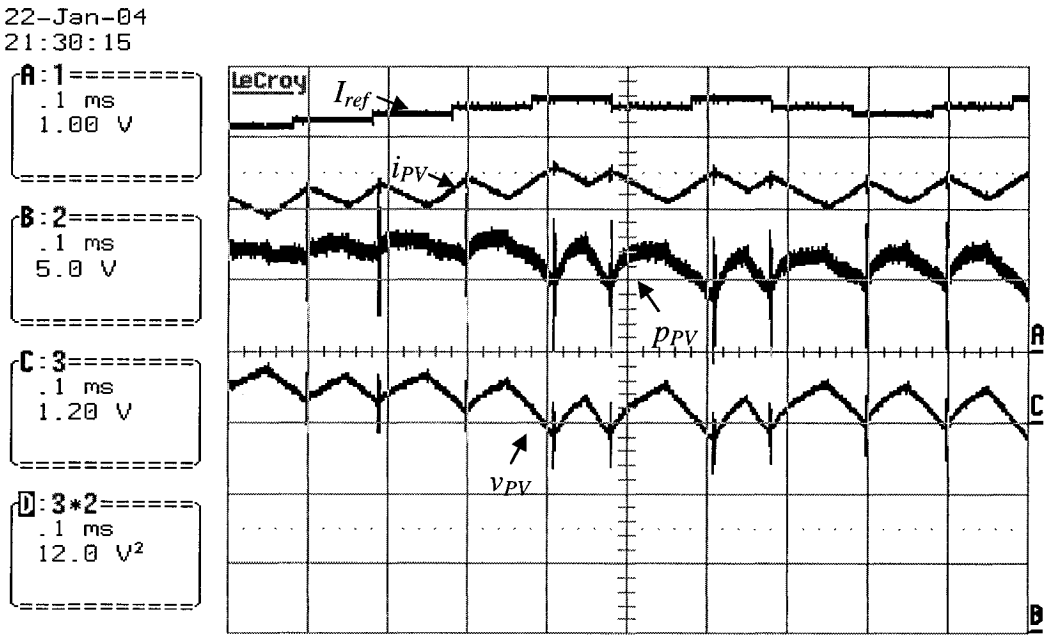

Channel A: I_{ref}, 1A/div, B: v_{PV}, 5V/div, C: i_{PV}, 1A/div, D: p_{PV}, 10W/div

B and D are on the same reference.

Fig. 4.40 steady-state waveforms with SAS as the input of the MPPT system

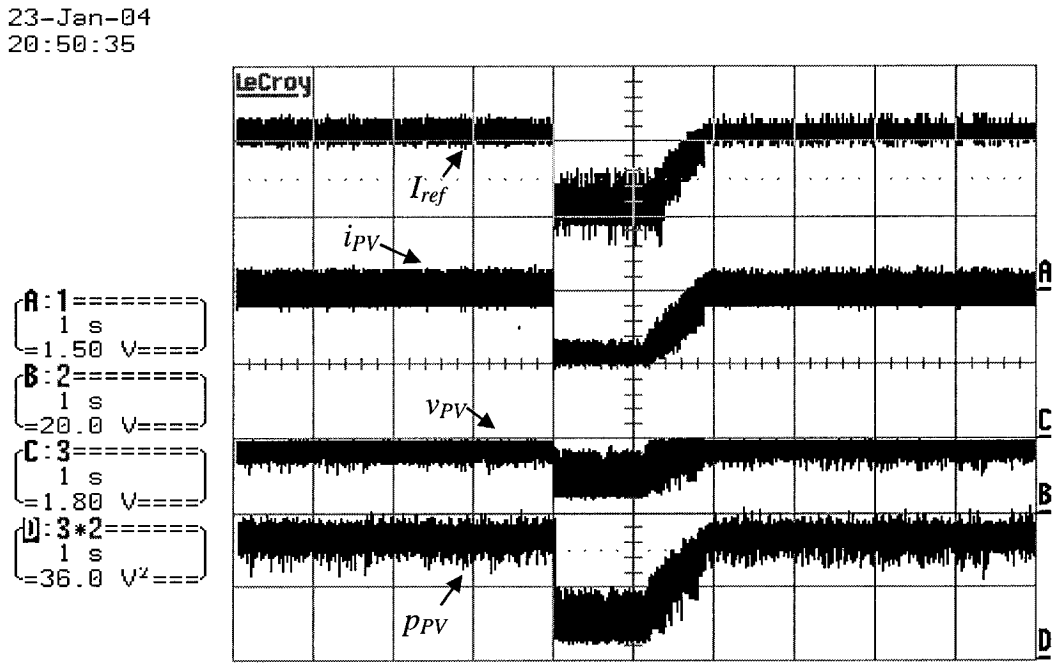

Channel A: I_{ref}, 1.5A/div, B: v_{PV}, 20V/div, C: i_{PV}, 1.5A/div, D: p_{PV}, 30W/div

Fig. 4.41 system response to the stepping down and ramping up of I_{SC}

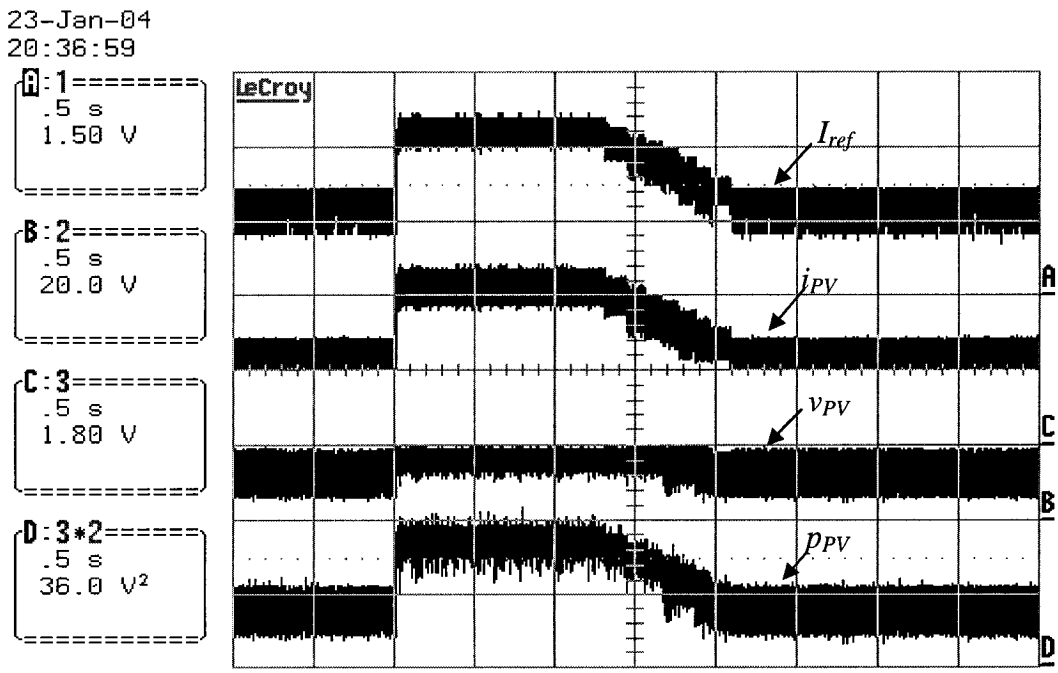

Channel A: I_{ref}, 1.5A/div, B: v_{PV}, 20V/div, C: i_{PV}, 1.5A/div, D: p_{PV}, 30W/div

Fig. 4.42 System response to the stepping up and ramping down of I_{SC}

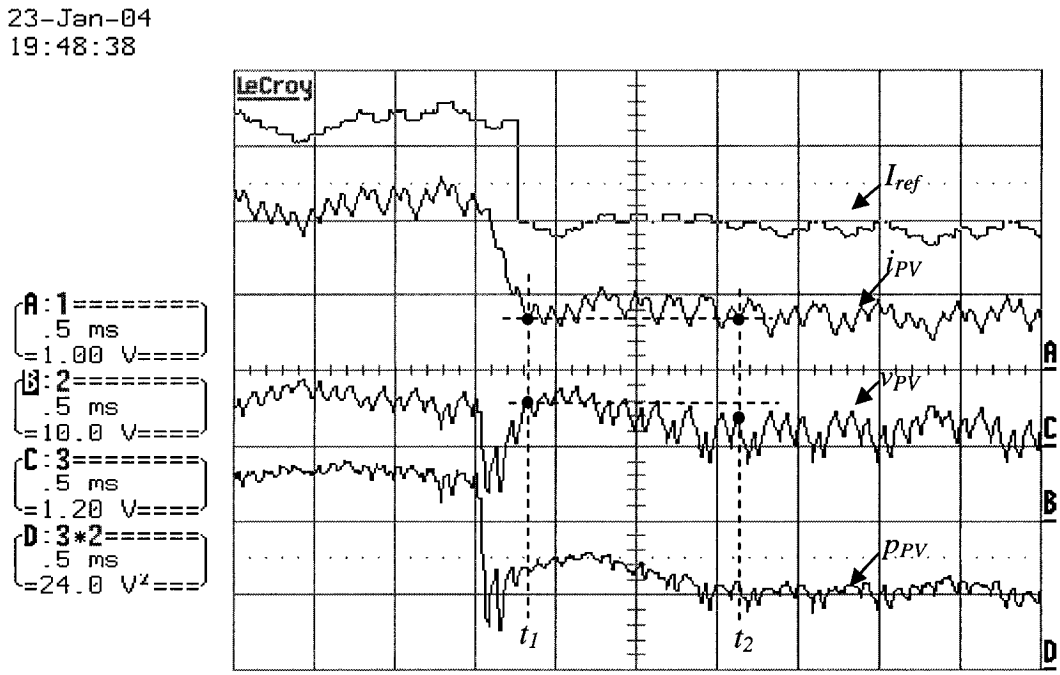

Channel A: I_{ref}, 1A/div, B: v_{PV}, 10V/div, C: i_{PV}, 1A/div, D: p_{PV}, 20W/div

Fig. 4.43 The detailed waveforms of system response to the stepping down of I_{SC}

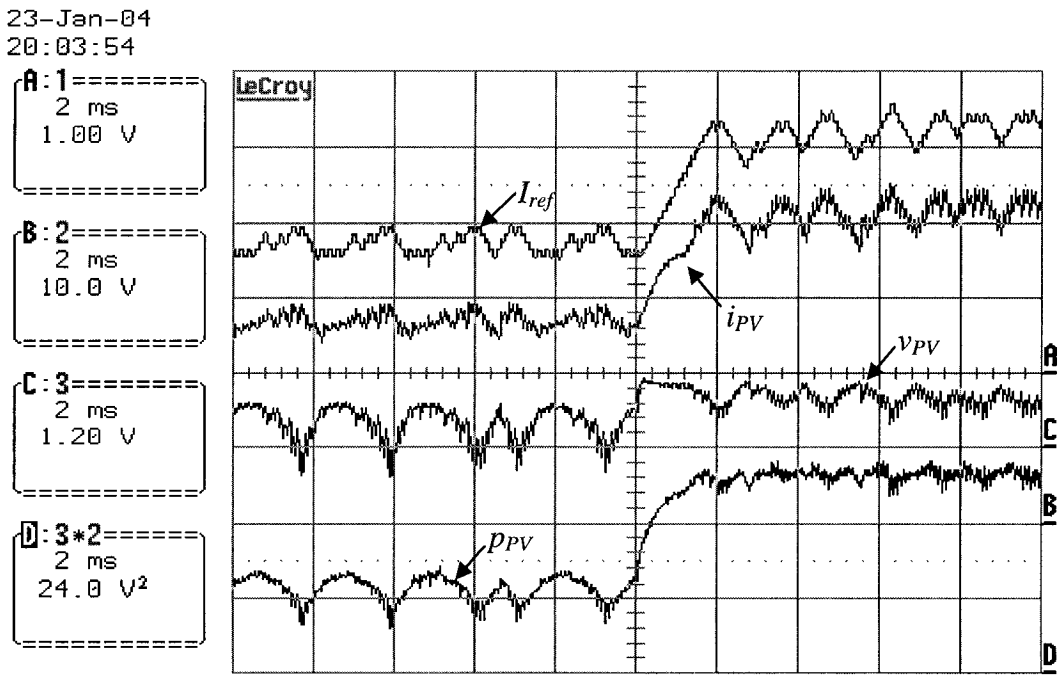

Channel A: I_{ref}, 1A/div, B: v_{PV}, 10V/div, C: i_{PV}, 1A/div, D: p_{PV}, 20W/div

Fig. 4.44 The detailed waveforms of system response to the stepping up of I_{SC}

2. Sampling at the switching off time instant

Fig. 4.45 shows the waveforms of the MPPT system with sampling at the switching off point in the steady-state. Comparing Fig. 4.45 with 4.40, I_{ref} of the system with sampling at off point is 0.1A less than I_{ref} for the system with sampling at switching on point. It is hard to say from the comparison of Fig. 4.45 and 4.40 that the PV output power in the system with sampling at off point is higher than the counterpart in the system with sampling at switching on point. However, the PV output power in the two cases can be estimated by comparing the voltage across the resistive load, since $P_{out} = V_{out}^2 / R$. Under the same conditions, the output voltage of the MPPT converter (V_{out}) with sampling at switching on point is 24V while the output voltage with sampling at off point is 24.3V. This confirms the validity of the analysis presented in section 4.3.2.

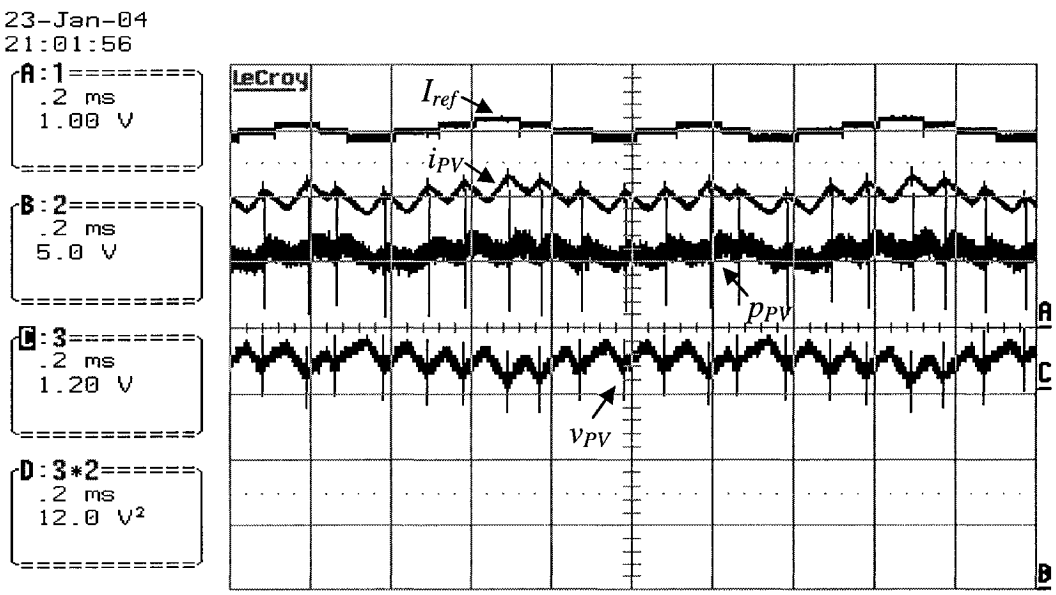

Channel A: I_{ref}, 1A/div, B: v_{PV}, 5V/div, C: i_{PV}, 1A/div, D: p_{PV}, 10W/div
B and D are on the same reference.

Fig. 4.45 Steady-state waveforms with SAS and sampling at off instant

4.7.2 MPPT System with Real PV Panels

Fig. 4.46 and 47 show the waveforms of system in the steady-state with sampling at switching on point and off point, respectively. For the sake of better visualizing the top part of the curves, and verifying the operation of the MPPT algorithm, the reference levels, 0A and 0V points of the curves, are pushed well below the bottom part of the window. It can be seen that when p_{PV} decreases with increasing I_{ref} and i_{PV}, the perturbation direction reverses and p_{PV} increases; the perturbation direction is kept until p_{PV} decreases and the perturbation direction reverses again. So the MPPT system operates around the MPP. By comparing Fig. 4.46, 47 with 4.40 and 45, the oscillation range of the MPPT system with real PV panels around the MPP in the steady-state is smaller and more regular because of the output p x i characteristics of real PV panels is fixed under certain unchanged ambient conditions. There is only one PV output power p_{PV} with the same PV output current i_{PV}.

The PV output power decreases significantly when i_{PV} becomes a little bigger than I_{MPP} (dashed-line oval of Fig. 4.46) and very little when it becomes a little smaller than I_{MPP} (dashed-line oval of Fig. 4.47). The first case is common for systems with sampling at switching on point since the evaluation of power and current variations is performed before the PV current ramps up, what can result in the system operating for a full switching cycle at the right side of the MPP. Conversely, systems with sampling on the off time compare values of PV power obtained with the largest values of current for each switching cycle. Therefore, when a decrease in the output power due to an increased current has been detected, the reference current is decreased and the operating point of the system is driven to the left side of the MPP.

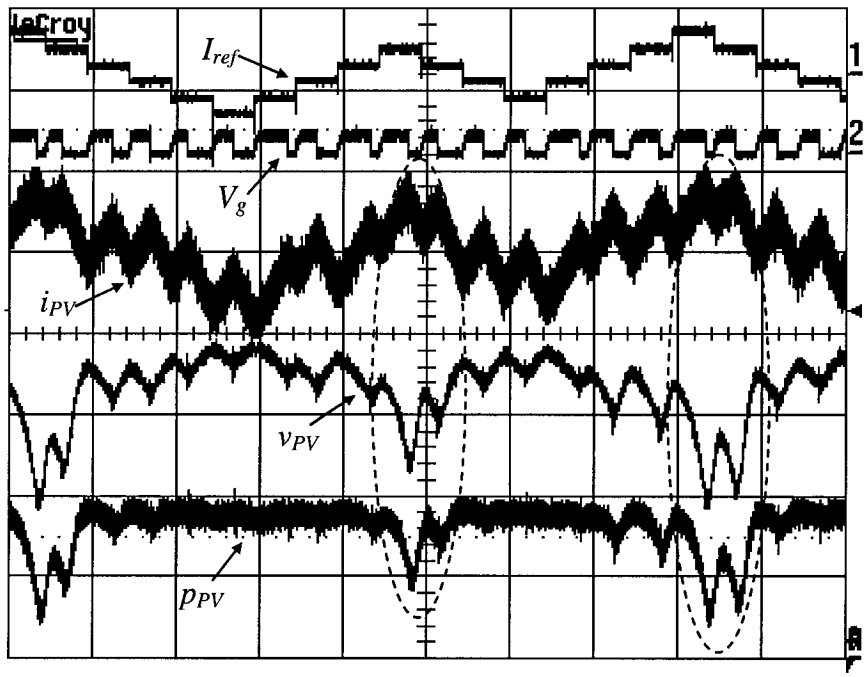

Fig. 4.46 steady-state waveforms with real PV panels and sampling at on instant, V_g is gate driving signal of the power switch in MPPT converter.

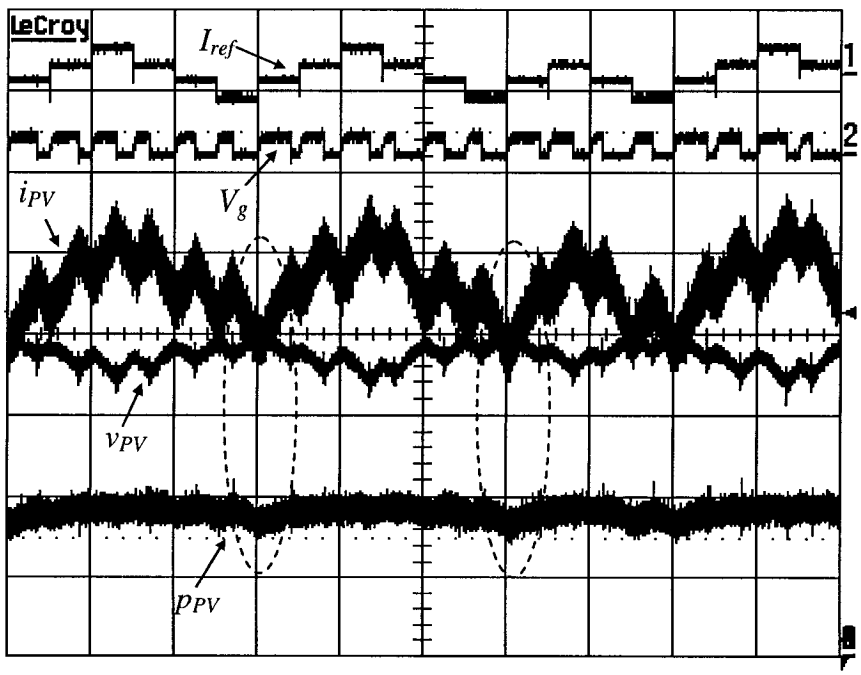

Fig. 4.47 Steady-state waveforms with real PV panels as the input of the MPPT system and sampling at off instant.

4.8 CONCLUSIONS

In this Chapter, simulations and experiments with an SAS and a real PV panels are conducted to verify the proposed Instantaneous Sampling method. Two extra blocks are added to guarantee the MPPT system operates properly.

All results of simulations and experiments with SAS and real PV panels show that the MPPT system works very well. In the steady-state, the system operates around the MPP. The experimental results with SAS also show very good dynamic responses for ramping up down, stepping up, and down of solar irradiation level. The experimental results with real PV panels are much better that those results with the SAS, because the SAS cannot fully emulate the dynamic response of the real PV panels and it is not adequate for the analysis of fast tracking speed of the MPPT system.

The experimental results also confirm the analysis that MPPT systems with sampling at the switching off point can draw more power from the PV panels than systems with sampling at the switching on point.

CHAPTER 5

CONCLUSIONS

5.1 SUMMARY

The work carried out in this thesis consists of three main parts presented in Chapters 2, 3, and 4, respectively. Chapter 2 is devoted to the comparison of the MPPT algorithms, which are often employed in MPPT systems; Chapter 3 presents a detailed analysis of the proposed approach for implementing a P&O algorithm and the design of the MPPT system. Finally, Chapter 4 shows the simulation and the experimental results, and analyzes them in details.

P&O algorithms are used in most PV generation systems for their simplicity and easy to implement. However, they have some problems such as oscillation around the MPP, slow response speed, and tracking in wrong direction under rapidly changing atmospheric conditions as discussed in Chapter 2. So in Chapter 3, Instantaneous Sampling and peak current control are proposed as a means to reduce these drawbacks. The feasibility of the Instantaneous Sampling approach is analyzed and discussed. The reasons that Instantaneous Sampling can reduce the drawbacks of the P&O algorithms are illustrated and the determination of the sampling point in each cycle is also discussed. A single instantaneous sampling per switching cycle permits that the perturbation cycle be equal to the switching period of MPPT converter that is very small and leads to fast tracking and

response speed of the MPPT system which reduces the drawback of the traditional P&O MPPT algorithm that tracks in wrong direction under rapidly changing atmospheric conditions. A smaller perturbation cycle permits smaller perturbation step size, which implies smaller power loss when operating point oscillates around the MPP.

The simulation and experimental results demonstrate that the P&O algorithm with Instantaneous Sampling operates very well and has very fast dynamic response. The results also show that the MPPT system with sampling at switching off point can draw more power from the PV panels than the MPPT system with sampling at switching on point. This is due to the inherent $p\ x\ i$ characteristics of PV panels, where the output power decreases significantly when the system operates with currents higher than the one at the maximum power point.

5.2 CONTRIBUTIONS

The major contributions of this thesis are:

(1) Proposed a new implementation for P&O MPPT algorithms where instantaneous samplings along with peak current control are used to mitigate /reduce the main drawbacks commonly related to the P&O method.

(2) Identified that sampling at the switching off point can draw more power from the PV panels and discussed the reasons of this phenomenon.

(3) A laboratory prototype was built and experimental results verified the theoretical analysis and computer simulation.

5.3 SUGGESTIONS FOR FUTURE WORK

(1) Implement the proposed algorithm with FPGA to be able to operate the power converter with higher switching frequency, what should reduce the size of the passive components and further increase the speed of response of the MPPT system.

(2) Utilize the switching ripple of the PV current to replace the perturbation and avoid the oscillation of the reference variable around the MPP in the steady-state. The locus of the switching ripple on the p x i or p x v curves can be used to determine if the locus is on the left or right side of the MPP. Once the locus works around the MPP, the reference variable is held to avoid the oscillation.

(3) Compare the performance of P&O and IncCond MPPT algorithms implemented with the same system (DSP or FPGA).

REFERENCES

[1] Roger Messenger and Jerry Ventre, "PHOTOVOLTAIC SYSTEMS ENGINEERING", CRC Press LLC New York, 2000.

[2] K. H. Hussein, I. Muta, T. Hoshino, and M. Osakada, "Maximum photovoltaic power tracking: An algorithm for rapidly changing atmospheric conditions", *Proc. IEE-Generation, Transmission, Distribution,* vol. 142, No. 1, Jan. 1995, pp. 59-64.

[3] Z. Salameh and D. Tayolor, "Step-Up Maximum Power Point Tracker For Photovoltaic Arrays", *Solar Energy*, Vol. 44, No.1, 1990, pp. 57-67.

[4] C. Hua and C. Shen, "Comparative Study of Peak Power Tracking Techniques for Solar Storage System", *APEC'98 13th Annual Applied Power Electronics Conference and Exposition,* 1998, Vol. 2, pp.679-685.

[5] Y. M. Chen, Y. C. Liu, F. Y. Wu, and Y. E. Wu, "Multi-Input Converter with Power Factor Correction and Maximum Power Point Tracking Features", *APEC'02, 17th Annual IEEE*, Vol. 1, 10-14 Mar. 2002, pp.490-496.

[6] T. F. Wu, C. H. Chang and Y. K. Chen, "A Fuzzy-Logic-Controlled Single-stage Converter for PV-Powered Lighting System Applications", *IEEE Transactions on Industrial Electronics*, Vol. 47, No.2, Apr. 2000, pp.287-296.

[7] C. Hua, J. Lin, and C. Shen, "Implementation of a DSP-Controlled Photovoltaic System with Peak Power Tracking", *IEEE Transactions on Industrial Electronics*, Vol. 45, Feb. 1998, pp. 99-107.

[8] Chihchiang Hua and Chihming Shen, "Control of DC/DC Converters for Solar Energy System with Maximum Power Tracking", *Industrial Electronics, Control and Instrumentation, 1997, IECON 97*, Vol. 2, Nov. 1997, pp. 827-832.

[9] E. Koutroulis, K. Kalaitzakis and N. C. Voulgaris, "Development of a Microcontroller-Based, Photovoltaic Maximum Power Point Tracking Control System", *IEEE Transactions on Power Electronics*, Vol. 16, No.1, Jan. 2001, pp.46-54.

[10] P. Huynh and B. H. Cho, "Design and Analysis of a Microprocessor- Controlled Peak-Power-Tracking System", *IEEE Transactions on Aerospace and Electronic Systems*, Vol. 32, No.1, Jan. 1996, pp. 182-189.

[11] A. Brambilla, M. Gambarara, A. Garutti, and F. Ronchi, "NEW APPROACH TO PHOTOVOLTAIC ARRAYS MAXIMUM POWER POINT TRACKING", *PESC 99, 30th Annual IEEE*, Vol. 2, 27 June-01 July 1999, pp. 632-637.

[12] P. Midya, P. T. krein, R. J. Turnbull, R. Reppa, J. Kimball, "Dynamic Maximum Power Point Tracker for Photovoltaic Applications", *Proc. PESC*, Baveno, Italy, 24-27 June 1996, pp.1710-1716.

[13] K. Irisawa, T. Saito, I. Takano, and Y. Sawada, "MAXIMUM POWER POINT TRACKING CONTROL OF PHOTOVOLTAIC GENERATION SYSTEM UNDER NON-UNIFORM INSOLATION BY MEANS OF MONITORING CELLS", *Photovoltaic Specialists Conference, 2000, 28th Conference. Record, IEEE*, Sep. 2000, pp.1707-1710.

[14] Y. C. Kuo, T. J. Liang and J. F. Chen, "Novel Maximum-Power-Point-Tracking Controller for Photovoltaic Energy Conversion System", *IEEE Transactions on Industrial Electronics*, Vol. 48, No. 3, June 2001, pp.594-601.

[15] M. Andersen and B. Alvsten, "200W Low Cost Module Integrated Utility Interface for Modular Photovoltaic Energy Systems", *Proc. 95, IEEE IECON, 21st Conf.* Vol. 1, Nov. 1995, pp. 572-577.

[16] J. H. R. Enslin, M. S. Wolf, D. B. Snyman, and W. Sweigers, "Integrated Photovoltaic Maximum Power Point Tracking Converter", *IEEE Transactions on Industrial Electronics*, Vol. 44, no. 6, Dec. 1997, pp.769-773.

[17] T. Noguchi, S. Togashi and R. Nakamoto, "Short-Current Pulse-Based Maximum-Power-Point Tracking Method for Multiple Photovoltaic-and-Converter Module System", *IEEE Transactions on Industrial Electronics*, Vol. 49, No.1, Feb. 2002, pp.217-223.

[18] T. F. Wu, C. H. Chang, and Y. J. Wu, "Single-Stage Converters for PV Lighting Systems with MPPT and Energy backup", *IEEE Transactions on Aerospace and Electronic Systems*, Vol. 35, No.4, Oct. 1999, pp. 1306-1317.

[19] Y. C. Kuo, T. J. Liang, and J. F. Chen, "A High-Efficiency Single-Phase Three-Wire Photovoltaic Energy Conversion System", *IEEE Transactions on Industrial Electronics*, Vol. 50, No.1, Feb. 2003, pp. 116-122.

[20] M. A. S. Masoum, H. Dehbonei, and E. F. Fuchs, "Theoretical and Experimental Analyses of Photovoltaic Systems With Voltage- and Current-Based Maximum Power-Point Tracking", *IEEE Transactions on Energy Conversion*, Vol. 17, No.4, Dec. 2002, pp. 514-522.

[21] C. T. Pan, J. Y. Chen, C. P. Chu, and Y. S. Huang, "A FAST MAXIMUM POWER POINT TRACKER FOR PHOTOVOLTAIC POWER SYSTEMS", *Industrial Electronics Society, 1999, IECON'99 proceedings. The 25th Annual Conference of the IEEE*, Vol. 1, 29 Nov.–3 Dec. 1999, pp. 390-393.

[22] M. Matsui, T. Kitano, D. H. Xu, and Z. Q. Yang, "A New Maximum Photovoltaic Power Tracking Control Scheme Based on Power Equilibrium at DC Link", *Industry Applications Conference, 1999, conference record of the 1999 IEEE*, Vol.2, Oct. 1999, pp. 804-809.

[23] Keyue M. Smedley, and Slobodan Ćuk, "One-Cycle Control of Switching Converters", *IEEE Transactions on Power Electronics*, Vol. 10, No. 6, Nov. 1995, pp. 625-633.

[24] Philip T. Krein, "Elements of Power Electronics", New York: *Oxford University Press*, 1998.

[25] Ned Mohan, Tore M. Undeland, and William P. Robbins, "POWER ELECTRONICS: Converters, Applications, and Design", 2nd ed., *John Wiley & Sons, Inc.* New York, 1995.

[26] Luiz A. C. Lopes and Anne-Marie Lienhardt, "A SIMPLIFIED NONLINEAR POWER SOURCE FOR SIMULAING PV PANELS", *PESC03, 34th Annual IEEE*, Vol. 4, 15 - 19 June 2003, pp. 1729-1734.

[27] DS1103 PPC Controller Board RTI Reference.

[28] "OPERATION GUIDE for SOLAR ARRAY SIMULATOR AGILENT MODELS E4350B, E4351B".

[29] Specifications of Siemens Solar photovoltaic modules.

APPENDIX

A1. The Calculation of the Output Characteristics of PV Panels

The program to compute the output characteristics of the PV panels is written in MATLAB language. The following program can draw the *v-i*, *p-v*, and *p-i* output characteristics of PV panels.

```
q=1.60e-19;        %Electron Charge(c)
k=1.38e-23;        %Boltzmann's Constant (eV/K)
A=1;               %Ideality Factor
Tr=25+273;         %Cell Reference Temperature (K)
ns=200;            %Cells in Series
np=10;             %Panels in Parallel
Iscr=0.546;        %Cell Short-circuit current
Ki=5.46e-4         %Short-circuit Temperature Coefficient
Irr= 2.54e-09      %Reverse Saturation Current at Tr
T1=28+273          %Cell Temperature (K)
T2=56+273
S1=100             %Solar irradiation Intensity(mW/cm^2))
S2=80
S3=60
S4=40
S5=20
EG=1.13            %Energy Gap(eV)
```

```
Iph11=[Iscr+Ki*(T1-Tr)]*S1/100;

Iph12=[Iscr+Ki*(T1-Tr)]*S2/100;

Iph13=[Iscr+Ki*(T1-Tr)]*S3/100;

Iph14=[Iscr+Ki*(T1-Tr)]*S4/100;

Iph15=[Iscr+Ki*(T1-Tr)]*S5/100;

Iph21=[Iscr+Ki*(T2-Tr)]*S1/100;

Iph22=[Iscr+Ki*(T2-Tr)]*S2/100;

Iph23=[Iscr+Ki*(T2-Tr)]*S3/100;

Iph24=[Iscr+Ki*(T2-Tr)]*S4/100;

Iph25=[Iscr+Ki*(T2-Tr)]*S5/100;

Irs1=Irr*(T1/Tr)*(T1/Tr)*(T1/Tr)*exp(q*EG/(k*A)*(1/Tr-1/T1));

Irs2=Irr*(T2/Tr)*(T2/Tr)*(T2/Tr)*exp(q*EG/(k*A)*(1/Tr-1/T2));

V11=0:0.01:97.2;

I11=np*Iph11-np*Irs1*(exp(q*V11/(k*T1*A*ns))-1);

P11=V11.*I11;

V12=0:0.01:96.04;

I12=np*Iph12-np*Irs1*(exp(q*V12/(k*T1*A*ns))-1);

P12=V12.*I12;

V13=0:0.01:94.55;

I13=np*Iph13-np*Irs1*(exp(q*V13/(k*T1*A*ns))-1);

P13=V13.*I13;
```

```
V14=0:0.01:92.44;
I14=np*Iph14-np*Irs1*(exp(q*V14/(k*T1*A*ns))-1);
P14=V14.*I14;

V15=0:0.01:88.84;
I15=np*Iph15-np*Irs1*(exp(q*V15/(k*T1*A*ns))-1);
P15=V15.*I15;
V21=0:0.01:83.86;
I21=np*Iph21-np*Irs2*(exp(q*V21/(k*T2*A*ns))-1);
P21=V21.*I21;

V22=0:0.01:82.59;
I22=np*Iph22-np*Irs2*(exp(q*V22/(k*T2*A*ns))-1);
P22=V22.*I22;

V23=0:0.01:80.96;
I23=np*Iph23-np*Irs2*(exp(q*V23/(k*T2*A*ns))-1);
P23=V23.*I23;

V24=0:0.01:78.66;
I24=np*Iph24-np*Irs2*(exp(q*V24/(k*T2*A*ns))-1);
P24=V24.*I24;

V25=0:0.01:74.72;
I25=np*Iph25-np*Irs2*(exp(q*V25/(k*T2*A*ns))-1);
P25=V25.*I25;
```

```
plot(V11,I11,'k',V12,I12,'k',V13,I13,'k',V14,I14,'k',V15,I15,'k',V21,I21,'--
    k',V22,I22,'--k',V23,I23,'--k',V24,I24,'--k',V25,I25,'--k');
figure
plot(V11,P11,'k',V12,P12,'k',V13,P13,'k',V14,P14,'k',V15,P15,'k',V21,P21,'--
    k',V22,P22,'--k',V23,P23,'--k',V24,P24,'--k',V25,P25,'--k');
figure
plot(I11,P11,'k',I12,P12,'k',I13,P13,'k',I14,P14,'k',I15,P15,'k',I21,P21,'--k',I22,P22,'--
    k',I23,P23,'--k',I24,P24,'--k',I25,P25,'--k');
```

A2. The programs to set SAS Simulating the Solar Panels behavior with different ambient changing

All programs to access the Agilent Solar Array Simulator (SAS) are written in Visual Basic.

1. The program to turn on the SAS in Simulator mode with I_{SC} = 3.45A, V_{OC} = 21.7V, I_{MPP} = 3.15A, and V_{MPP} = 17.5V is shown as follows:

```
Option Explicit

Sub Main()
  Dim defrm As Long
  Dim vi As Long

  Call viOpenDefaultRM(defrm)
  Call viOpen(defrm, "GPIB0::5::INSTR", 0, 0, vi)

  Call viVPrintf(vi, "CURR:SAS:ISC 3.45;IMP 3.15;:VOLT:SAS:VMP 17.5;VOC
            21.7" + Chr$(10), 0)

  Call viVPrintf(vi, "CURR:MODE SAS" + Chr$(10), 0)

  Call viVPrintf(vi, "Output on" + Chr$(10), 0)

  Call viClose(vi)
  Call viClose(defrm)

End Sub
```

2. The program to turn off the SAS is shown as follows:

```
Option Explicit
Sub Main()
  Dim defrm As Long
  Dim vi As Long

  Call viOpenDefaultRM(defrm)

  Call viOpen(defrm, "GPIB0::5::INSTR", 0, 0, vi)
```

```
  Call viVPrintf(vi, "*RST" + Chr$(10), 0)

  Call viClose(vi)

  Call viClose(defrm)

End Sub
```

3. The program setting I_{SC} of the SAS to ramp up from 1.7A to 3.45A is shown as follows:

```
Private Sub Command1_Click()

  Dim defrm As Long
  Dim vi As Long

  Dim ISC1, ISC2, ISC3, ISC4, IM1, IM2, IM3, IM4 As Long
  Dim X, Y As Long
  Dim i, J As Long

  Call viOpenDefaultRM(defrm)
  Call viOpen(defrm, "GPIB0::5::INSTR", 0, 0, vi)

  Call viVPrintf(vi, "CURR:SAS:ISC 1.7;IMP 1.55;:VOLT:SAS:VMP 17.5;VOC
21.7" + Chr$(10), 0)

  Call viVPrintf(vi, "CURR:MODE SAS" + Chr$(10), 0)

  Call viVPrintf(vi, "Output on" + Chr$(10), 0)

For J = 1 To 100000000#
  Next
  ISC = 1.7
For i = 1 To 9

  ISC = ISC + 0.2
  If ISC > 3.5 Then GoTo WRONG
  IM = ISC * 0.913
  X = Int(ISC * 1000 + 0.5)
  Y = Int(IM * 1000 + 0.5)

 ISC1 = X \ 1000
 ISC2 = (X - ISC1 * 1000) \ 100
 ISC3 = (X - ISC1 * 1000 - ISC2 * 100) \ 10
```

```
ISC4 = X - ISC1 * 1000 - ISC2 * 100 - ISC3 * 10

IM1 = Y \ 1000
IM2 = (Y - IM1 * 1000) \ 100
IM3 = (Y - IM1 * 1000 - IM2 * 100) \ 10
IM4 = Y - IM1 * 1000 - IM2 * 100 - IM3 * 10

Call viVPrintf(vi, "CURR:SAS:ISC " + Chr$(48 + ISC1) + Chr$(46) + Chr$(48 +
          ISC2) + Chr$(48 + ISC3) + Chr$(48 + ISC4) + ";IMP " + Chr$(48 +
          IM1) + Chr$(46) + Chr$(48 + IM2) + Chr$(48 + IM3) + Chr$(48 +
          IM4) + ";:VOLT:SAS:VMP 17.5;VOC 21.7" + Chr$(10), 0)
Call viVPrintf(vi, "CURR:MODE SAS" + Chr$(10), 0)
Call viVPrintf(vi, "Output on" + Chr$(10), 0)

Next

WRONG:  Call viClose(vi)
        Call viClose(defrm)
End Sub
```

4. The program setting I_{SC} of the SAS to ramp down from3.45A to 1.7A is shown as follows:

```
Private Sub Command1_Click()
  Dim defrm As Long
  Dim vi As Long

  Dim ISC1, ISC2, ISC3, ISC4, IM1, IM2, IM3, IM4 As Long
  Dim X, Y As Long
  Dim i, J As Long


  Call viOpenDefaultRM(defrm)
  Call viOpen(defrm, "GPIB0::5::INSTR", 0, 0, vi)

  Call viVPrintf(vi, "CURR:SAS:ISC 3.45;IMP 3.15;:VOLT:SAS:VMP 17.5;VOC
          21.7" + Chr$(10), 0)

  Call viVPrintf(vi, "CURR:MODE SAS" + Chr$(10), 0)

  Call viVPrintf(vi, "Output on" + Chr$(10), 0)

For J = 1 To 100000000#
  Next
```

```
  ISC = 3.65
  For i = 1 To 9
  ISC = ISC - 0.2
  If ISC > 3.45 Then GoTo WRONG
  IM = ISC * 0.913

  X = Int(ISC * 1000 + 0.5)
  Y = Int(IM * 1000 + 0.5)

  ISC1 = X \ 1000
  ISC2 = (X - ISC1 * 1000) \ 100
  ISC3 = (X - ISC1 * 1000 - ISC2 * 100) \ 10
  ISC4 = X - ISC1 * 1000 - ISC2 * 100 - ISC3 * 10

  IM1 = Y \ 1000
  IM2 = (Y - IM1 * 1000) \ 100
  IM3 = (Y - IM1 * 1000 - IM2 * 100) \ 10
  IM4 = Y - IM1 * 1000 - IM2 * 100 - IM3 * 10

  Call viVPrintf(vi, "CURR:SAS:ISC " + Chr$(48 + ISC1) + Chr$(46) + Chr$(48 +
                  ISC2) + Chr$(48 + ISC3) + Chr$(48 + ISC4) + ";IMP " + Chr$(48 +
                  IM1) + Chr$(46) + Chr$(48 + IM2) + Chr$(48 + IM3) + Chr$(48 +
                  IM4) + ";:VOLT:SAS:VMP 17.5;VOC 21.7" + Chr$(10), 0)
  Call viVPrintf(vi, "CURR:MODE SAS" + Chr$(10), 0)
  Call viVPrintf(vi, "Output on" + Chr$(10), 0)
Next

WRONG:  Call viClose(vi)
        Call viClose(defrm)
End Sub
```

5. The program setting I_{SC} of the SAS to step up from 1.7A to 3.45A is shown as follows:

```
Private Sub Command1_Click()

  Dim defrm As Long
  Dim vi As Long
  Dim ISC1, ISC2, ISC3, ISC4, IM1, IM2, IM3, IM4 As Long
  Dim X, Y As Long
  Dim i, J As Long

  Call viOpenDefaultRM(defrm)
  Call viOpen(defrm, "GPIB0::5::INSTR", 0, 0, vi)
  Call viVPrintf(vi, "CURR:SAS:ISC 1.7;IMP 1.55;:VOLT:SAS:VMP 17.5;VOC
21.7" + Chr$(10), 0)
```

```
  Call viVPrintf(vi, "CURR:MODE SAS" + Chr$(10), 0)
  Call viVPrintf(vi, "Output on" + Chr$(10), 0)

For J = 1 To 100000000#
  Next
  Call viVPrintf(vi, "CURR:SAS:ISC 3.45;IMP 3.15;:VOLT:SAS:VMP 17.5;VOC
          21.7" + Chr$(10), 0)
  Call viVPrintf(vi, "CURR:MODE SAS" + Chr$(10), 0)
  Call viVPrintf(vi, "Output on" + Chr$(10), 0)
  Call viClose(vi)
  Call viClose(defrm)
End Sub
```

6. The program setting I_{SC} of the SAS to step down from3.45A to 1.7A is shown as follows:

```
Private Sub Command1_Click()
  Dim defrm As Long
  Dim vi As Long

  Dim ISC1, ISC2, ISC3, ISC4, IM1, IM2, IM3, IM4 As Long
  Dim X, Y As Long
  Dim i, J As Long

  Call viOpenDefaultRM(defrm)
  Call viOpen(defrm, "GPIB0::5::INSTR", 0, 0, vi)
  Call viVPrintf(vi, "CURR:SAS:ISC 3.455;IMP 3.15;:VOLT:SAS:VMP 17.5;VOC
          21.7" + Chr$(10), 0)
  Call viVPrintf(vi, "CURR:MODE SAS" + Chr$(10), 0)
  Call viVPrintf(vi, "Output on" + Chr$(10), 0)

For J = 1 To 1000000000#
  Next

  Call viVPrintf(vi, "CURR:SAS:ISC 1.7;IMP 1.55;:VOLT:SAS:VMP 17.5;VOC
21.7" + Chr$(10), 0)
  Call viVPrintf(vi, "CURR:MODE SAS" + Chr$(10), 0)
  Call viVPrintf(vi, "Output on" + Chr$(10), 0)
  Call viClose(vi)
  Call viClose(defrm)
End Sub
```